SZENT ISTVÁN UNIVERSITY

Performance enhancement of solar air collectors applied for drying processes

PhD dissertation

By

Maytham Ali Jasim Al-Neama

Gödöllő
2018

Doctoral school denomination: Engineering Sciences Doctoral School

Science: Solar Energy Applications

Leader: Prof. Dr. Farkas István
Dr. of Technical Sciences
Faculty of Mechanical Engineering
Szent István University, Gödöllő, Hungary

Supervisor: Prof. Dr. Farkas István
Dr. of Technical Sciences
Faculty of Mechanical Engineering
Szent István University, Gödöllő, Hungary

....

Affirmation of head of school Affirmation of supervisor

CONTENTS

NOMENCLATURE AND ABBREVIATIONS…….. 5
1. INTRODUCTION AND OBJECTIVES……... 8
1.1. Introduction …… 8
1.2. Research objectives …… 9
2. LITERATURE REVIEW……. 10
2.1. Concept and classification of solar drying systems …… 10
2.1.1. Drying concept..... 10
2.1.2. Classification of solar dryers……. 12
2.1.3. Indirect-passive solar drying systems..... 13
2.1.4. Indirect-active solar drying systems……. 15
2.2. Solar air collectors…….. 16
2.3. Air movement methods…… 21
2.3.1. Passive movement systems……... 21
2.3.2. Active movement systems…… 24
2.4. Modelling and simulation of solar collectors and dryers……..…… 27
2.5. Timeline of the previous researches …….. 29
2.6. Summary of litreture review evaluation……... 32
3. MATERIALS AND METHODS……. 33
3.1. Solar radiation componenets and orientation anaylsis …… 33
3.2. Thermal analysis of solar collectors……...…… 35
3.2.1. Thermal analysis of single air pass solar collector…… 35
3.2.2. Thermal analysis of double air pass solar collector…….. 39
3.3. Thermal analysis of drying chamber…….…… 40
3.4. Solar collectors location and orientation…….. 41
3.5. Design and structure of solar collectors ……..…….. 43
3.6. Design and structure of drying chambers ……..…….. 49
3.7. Chimney design and structure ……...…..…….. 50
3.8. Solar drying system accessories……..…….…….. 51
3.8.1. Inline air blower…….…… 51
3.8.2. Photovoltaic modules……...…….. 52
3.8.3. Power supply controller…….…… 52
3.8.4. Air ducts…….…… 52
3.9. Installation and measurments……..…..…….…….. 53
3.9.1. Thermocouples and thermometers……..…… 55
3.9.2. Solar power meter……..…….. 55
3.9.3. Anemometer ……..…….…… 55
3.9.4. Relative humidity meters……...…….…… 56
3.9.5. Weight scale…… 57
4. RESULTS…… 58
4.1. Parameters and calculations ……..……...……...… 58
4.2. Effect of air passes number…….……..……...… 59
4.2.1. Single air pass solar collector experimantal analysis……..……..…. 59
4.2.2. Double air pass solar collector experimantal analysis……..…….. 64
4.3. Effect of direction and shape of extended surfaces …… 69
4.3.1. Horizontally finned plate solar air collector experimantal analysis…… 69

4.3.2. Inclined by 45^o finned plate solar air collector experimantal analysis…..…. 74
4.3.3. Vertically finned plate solar air collector experimantal analysis……...… 78
4.3.4. Helically finned plate solar air collector experimantal analysis……..…. 82
4.4. Daily efficiency analysis ……..…… 86
4.5. Effect of air mass flow rate……..……..…… 88
4.5.1. Forced air movement……...……... 88
4.5.2. Natural air movement by chimney effect……. 89
4.6. Final weight analysis of dried product……..……..…… 92
4.7. New scientific results……... 96
5. CONCLUSIONS AND SUGGESTIONS…… 99
6. SUMMARY…….…… 100
7. ÖSSZEFOGLALÁS (SUMMARY IN HUNGARIAN)…….. 101
8. APPENDICES……..... 102
A1. Bibliography…….…... 102
A2. Publications related to the dissertation…… 108
9. ACKNOWLEDGEMENTS…….. 110

NOMENCLATURE AND ABBREVIATIONS

A_c	Area of collector's absorbing surface (m^2)
A_{duct}	Area of air duct (m^2)
B	Atmospheric extinction coefficient
C	The ratio of diffuse radiation on a horizontal surface to the direct normal irradiation
c_p	Air specific heat at constant pressure (kJ/kg K)
CR	Concentration ratio
D	Hydraulic diameter of the chimney (m)
D_h	Hydraulic diameter of air channel (m)
f	Friction coefficient
F_{sg}	Angle factor between the surface and earth
F_{ss}	Angle factor between the surface and sky
g	Gravitational acceleration (m/s^2)
G_b	Beam solar radiation intensity component (irradiance) (W/m^2)
G_{bn}	Normal bean solar radiation intensity (W/m^2)
G_d	Diffuse solar radiation intensity component (W/m^2)
G_h	Total horizontal solar radiation intensity (W/m^2)
G_o	Apparent extraterrestrial solar radiation intensity (W/m^2)
G_r	Ground-reflected solar radiation intensity (W/m^2)
G_T	Total solar radiation intensity (W/m^2)
H	Height of chimney (m)
h_{cag}	Ambient-glass cover convection heat transfer coefficient (W/m^2K)
h_{cpa}	Absorbing plate-air convection heat transfer coefficient (W/m^2K)
h_{rgs}	Sky-glass cover radiative heat transfer coefficient (W/m^2K)
h_{rpg}	Absorbing surface-glass cover radiative heat transfer coefficient (W/m^2K)
h_w	Wind heat transfer coefficient (W/m^2K)
I	Hourly solar radiation (J)
K_a	Air thermal conductivity (W/m K)
K_b	Back insulation thermal conductivity (W/m K)
k_d	Drying process constant
L	Solar collector length (m)
l	Length (m)
L_v	Latent heat energy of vaporization (J)
$\dot{m}$	Air mass flow rate (kg/s)
m_i	Initial mass of product (kg)
MR	Moisture ratio
n	Number of day in year
Nu	Nusselt's number
p	Perimeter (m)
P_E	Electric power (W)
Pr	Prandtl number
Qu	Useful gained heat (W/m^2)
R	Reflectivity of earth's surface
Re	Reynold's number

RH	Relative humidity (%)
Sc	Solar constant (1367 W/m^2)
t	Time (s, h)
T_a	Ambient temperature (^{o}C)
T_{av}	Average air temperature (^{o}C)
$T_{c1,i}$	First-pass collector inlet temperature (^{o}C)
$T_{c2,i}$	Second pass collector inlet temperature (^{o}C)
T_{ch}	Chimney temperature (^{o}C)
$T_{ch,i}$	Chimney inlet temperature (^{o}C)
$T_{ch,o}$	Chimney outlet temperature (^{o}C)
$T_{c,o}$	Collector outlet temperature (^{o}C)
T_{di}	Dryer inlet temperature (^{o}C)
T_{do}	Dryer outlet temperature (^{o}C)
T_g	Glass transparent cover temperature (^{o}C)
T_i	Fluid inlet temperature (^{o}C)
T_o	Fluid outlet temperature (^{o}C)
T_p	Plate temperature (^{o}C)
$T_{s,av}$	Absorbing surface average temperature (^{o}C)
T_{sky}	Sky temperature (^{o}C)
U	Overall heat loss coefficient (W/m^{2}K)
U_b	Back heat loss coefficient (W/m^{2}K)
U_T	Top heat loss coefficient (W/m^{2}K)
v	Air velocity (m/s)
V_w	Wind velocity (m/s)
w	Width of absorbing surface (m)
w_e	Equilibrium mass (kg)
w_f	Final moisture content of product (%)
w_i	Initial moisture content of product (%)
w_v	Mass of evaporated water from product (kg)
X_b	Back insulation thickness (m)

Greek symbols

α_g	Glass cover absorptivity
α_p	Absorbing surface absorptivity
α_s	Solar altitude angle (^{o})
β	Collector tilt angle (^{o})
λ	Wave length (μm)
ψ	Fins angle (^{o})
ε_g	Glass cover emissivity
ε_p	Absorbing plate emissivity
δ	Declination angle (^{o})
φ	Latitude angle (^{o})
η	Efficiency (%)
γ_s	Solar azimuth angle (^{o})

ρ	Density (kg/m^3)
ρ'	Average density of fluid (kg/m^3)
τ_g	Glass cover transmissivity
σ	Stephan-Boltzmann constant (5.67×10^{-8} J/s m^2 K^4)
μ	Air viscosity (kg/m s)
μ_w	Air viscosity at channel wall (kg/m s)
θ	Incidence angle (^{o})
ω	Solar hour angle (^{o})

Abbreviations

AC	Alternating current
ASHRAE	American Society for Heating, Refrigeration and Air conditioning Engineering.
CFD	Computational fluid dynamics
CPC	Compound parabolic concentrator
DC	Direct current
EES	Engineering equation solver
EPS	Extended polystyrene insulation
PCM	Phase change material
PV	Photovoltaic
PVT	Photovoltaic-thermal
TW	Tera Watt

1. INTRODUCTION AND OBJECTIVES

In this chapter, the importance of the research topic is presented along with the objectives of this research.

1.1. Introduction

Energy is the most critical issue for human development and is a key in international politics and the economy. To reduce the impact of conventional energy sources on the environment should be paid to develop new sources of energy. According to this, the development of renewable energies has become one of the essential tasks in the field of modern science and engineering. Fig. 1.1. compares the current annual energy consumption of the world to the known reserves (finite fossil and nuclear resources) and the yearly potential of the renewable alternatives (solar, wind, geothermal, biomass, ... etc.). The volume of each sphere represents the total amount of energy recoverable from the finite reserves and the power recoverable in terawatt (TW) per year from renewable sources. Solar energy can be recognized as one of the most promising energy forms of renewable energy sources (Perez and Marc, 2009).

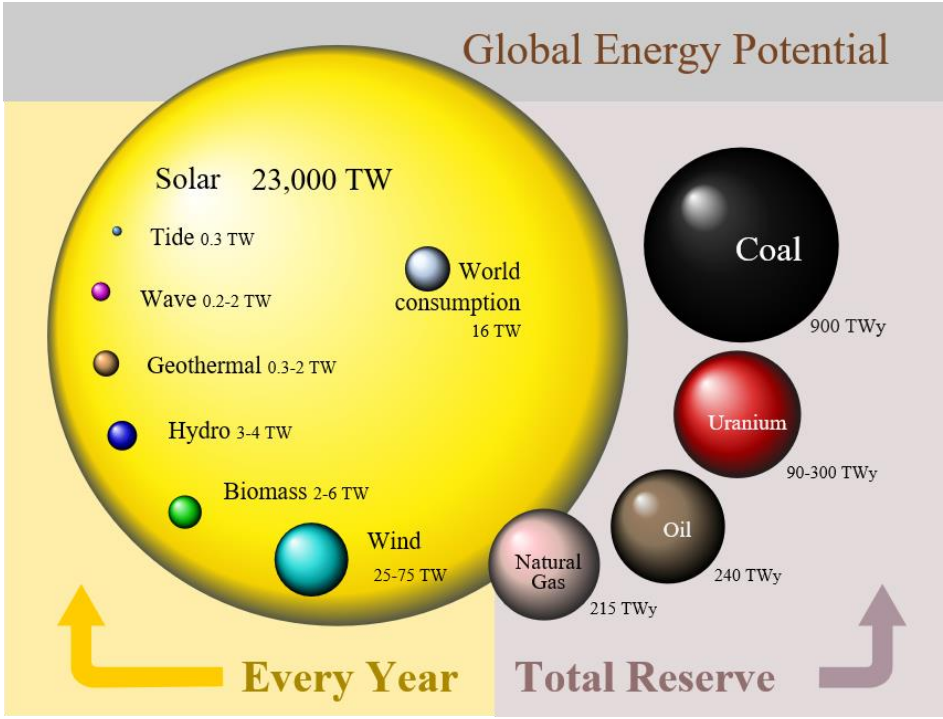

Fig. 1.1. Comparing finite and renewable energy reserves (Perez and Marc, 2009)

One of the most common and important components of solar thermal energy system is the solar collector or solar heater. There are two main types of solar collectors based on method of solar radiation receiving; concentrating solar collector and non-concentrating solar collector (flat plate solar collector). Flat plate solar collectors are classified into two types based on working fluid which flows through the collector; water and solar air collectors. Solar air collectors are low cost and most widely used collection devices because of their simple construction. There are a lot of studies on solar air collectors been done to use them in space heating, solar cooking, agricultural products drying and different industrial process.

Solar drying is one among the common applications of solar energy utilization. Solar drying is one of the oldest methods of preservation of agricultural products and it is utilized everywhere. Solar

drying is a dual process of heat transfer to the product items from the heat source (solar collector) and mass transfer in the form of moisture content from the product to product's surface and then to the surrounding air. Solar drying systems are available in the different design and sizes according to dried products capacity (Chauhan et al., 2015). According to many studies, the performance of drying process depends mainly on the performance of solar collector. The improvement of solar collector leads to improve the dryer work also. But, some products do not need for high air temperature because it will damage such as fish, meats, etc. So, the control of the process parameters, air temperature, moister content for air and product and airspeed critical (Al-Neama and Farkas, 2016).

1.2. Research objectives

In this research, comprehensive evaluation of different designs of solar collector integrated with drying chamber will be performed according to heat transfer basses to enhance the thermal performance of the total system. Additionally, to show the effect of each parameter on system behaviour under Gödöllő city climatic conditions. The objectives of this research can be described as follow:

- Comparison of single-pass solar air collector thermal performance for drying process with the double-pass solar air collector performance experimentally.
- Investigation of solar air collector thermal behaviour experimentally by using five shapes of absorbers: un-finned absorber, absorber with horizontal rectangular fines, absorber with vertical rectangular fines, absorber with 45^{o} inclined rectangular fines and absorber with aluminium helical fines.
- Test the performance of drying chamber experimentally by integrating it with five shapes of absorbers: un-finned absorber, absorber with horizontal rectangular fines, absorber with vertical rectangular fines, absorber with 45^{o} rectangular fines and absorber with aluminium helical fines.
- Estimation of thermal daily efficiency of the tested solar air collectors.
- Investigation the effect of air movement method and air velocity on the thermal daily efficiency of solar air collector with forced and natural mode by using a circular chimney.
- Estimation the weight loss of dried product items by using different tested types of solar air collectors.

2. LITERATURE REVIEW

Solar energy can be recognized as one of the most promising renewable energy sources. Along with other forms of renewable energy sources, i.e. biomass energy, geothermal energy, wind energy, fuel cell, ocean energy, it has a great potential for a wide variety of applications because of its abundance and accessibility.

The importance of solar energy using in the drying technology field has increased due to changes of traditional energy sources price, such as fossil fuel, environmental concerns and expectations of conventional fossil fuel depletion. In this chapter, scientific entrance and the critical literature which related to the research topic going to be reviewed.

2.1. Concept and classification of solar drying systems

Drying process is the most energy-intensive operation of the industrial processes. In a lot of industrialized countries, about 7 to 15% of industrial consumption energy for drying process. For example, according to a report that energy consumption for drying processes are ranging from 10 to 15% for United States, Canada, France, and United Kingdome and about 20 to 25% for Germany and Denmark. Most of drying energy consumption is used for paper and pulp industry, it is about 35% (Bennamoun, 2012).

The use of solar dryers in the drying of different products can significantly reduce or eliminate product wastage, food poisoning and sometimes improve productivity of the farmers towards better revenue derived (Toshniwal and Karale, 2013). In the present chapter, an extensive review of the literature has been done on solar heaters performance and energy analyses of different solar dryers systems.

2.1.1. Drying concept

Drying is defined as a process of moisture removal due to simultaneous heat and mass transfer. It is also a classical method of food preservation, which provides longer life, lighter weight for transportation and smaller space for storage. Natural or open sun drying is practiced widely in the world, but has some problems related to the contamination by dirt and dust and infestation by insects, rodents and other animals. Therefore, the drying process should be undertaken in closed equipment, to improve the quality of the final product (Ertekin and Yaldiz, 2004).

Drying of different crops dates back to the beginning of the civilization. The need for drying was increased by the rapid increase in mechanization with high productivity (Hall, 1980). Drying is applied to a wide variety of food products, from cereals to finished goods, from raw materials to by-products. Many processes are used, according to the type and quantity of product to dry, the amount of water to remove, the final desired quality or functionality of the dried product (Bimbenet et al., 2002).

Drying process takes place in two stages. In the first stage of drying, the system is considered as a pure material and drying takes place at surface of the drying material at a constant rate. It is similar to the vaporization of water in the ambient. Mass of the vaporized water depends mainly on external conditions and it is not much affected by the condition of the material. In the second stage, drying takes place with decreasing drying rate and this type of drying follows constant rate drying. The condition of the second stage is determined by the properties of the material being dried (Can, 2000).

As mentioned before, drying process depends on two types of conditions or parameters; external and internal ones. These conditions and parameters have been explained in details by Mahendra et al. (1987). Table 2.1 shows external and internal parameters briefly with their descriptions as follow:

Table 2.1. Drying parameters

External parameters (properties of moist air)		
Psychrometric chart	Dry bulb temperature	The temperature of moist air indicated by an ordinary thermometer.
	Wet bulb temperature	The temperature of moist air indicated by a thermometer, the bulb of which is covered with a wet wick
	Dewpoint temperature	The temperature at which the condensation of water vapour begins if a mixture of air and water is cooled.
	Relative humidity	The ratio of water vapour pressure in the air to water vapour pressure of the saturated air.
	Humidity ratio	The weight of water vapour which is associated with unit weight of dry air.
	Enthalpy	The specific heat of air with water vapour content in it is known as the enthalpy of moist air.
Internal parameters (properties product)		
Moisture content		It is expressed as a percentage of moisture based on wet weight or dry matter.
Equilibrium moisture content		The rate at which the product loses moisture to the surrounding environment is identical to the rate at which it absorbs moisture from the surrounding air, the product is said to be in equilibrium.
Drying ratio		It is a dimensionless number representing the ratio of the weight of wet material entering a dryer to the weight of the same material leaving the dryer.
Latent heat		This property is required to estimate the energy required for evaporation of the desired amount of water from the wet product.

The use of the solar energy is getting a greater importance in the agricultural drying. At the same time the quality control and quality preservation become also more and more important items for processing of agricultural products than before. In the systems which used solar energy to dry different agricultural products, the moisture content is removed by air which heated by sun arrays energy with a temperature range of 50 ^{o}C to 60 ^{o}C. The percentage of moisture content varies from product to product (Kumar et al., 2016).

2.1.2. Classification of solar dryers

Generally, the drying systems are classified into low and high temperature operated drying systems. In low-temperature systems, the moisture of the product is brought into equilibrium level by heated air using proper ventilation. For high-temperature systems, usually used for fast drying rate, especially for high moisture contents products (Kumar et al., 2016). For solar drying systems, different types of dryers are used with different sizes and designs, which depends on the application and requirements. Usually, solar dryers are classified according to many factors: (Toshniwal and Karale, 2013):

1. Air movement method.
2. Solar contribution.
3. Air movement direction.
4. Type of product items to be dried.
5. Assembly insulation.

Also, solar dryers are broadly classified into three categories according to the solar radiation receiving; direct, indirect and mixed solar dryers. Or according to the air movement mode through the system, solar dryers can be classified into active, passive or hybrid dryers. Fig. 2.1. shows the classification of solar dryers with more details.

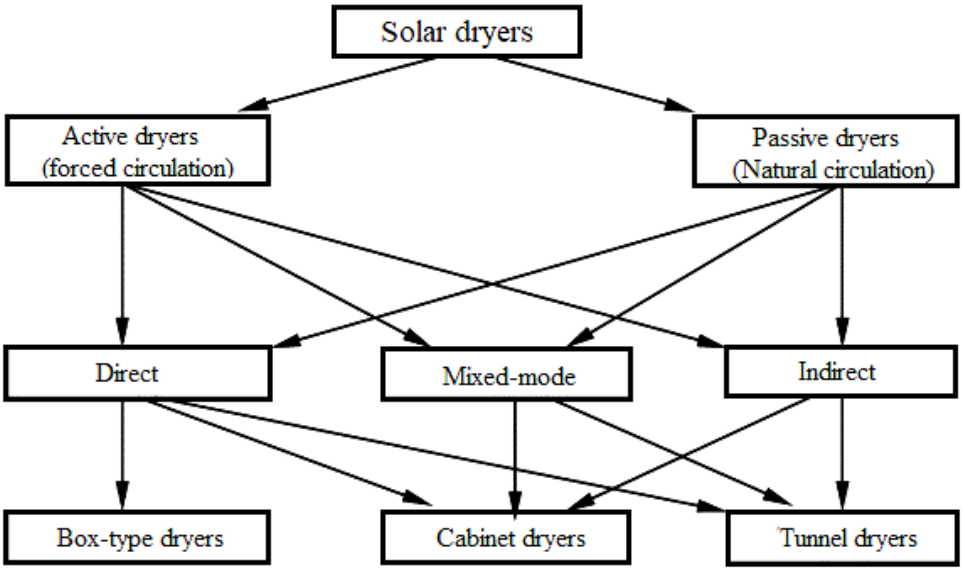

Fig. 2.1. Classification of solar dryers (Leon et al., 2002)

In forced convection solar dryers (active solar dryers), the air required for product drying is forced through the solar collector to the dryer chamber using a fan or a blower. In natural convection solar dryers (or passives solar dryers), the flow of the air required for product drying is due to natural or buoyancy force action (Ekechukwu and Norton, 1999). In a direct solar dryer, the moisture content of the product to be dried is taken away by the direct exposing of solar radiation on the product itself with or without the natural air circulation (Ekechukwu and Norton, 1999). A schematic view of the simple direct solar dryer is shown in Fig. 2.2. Direct solar dryers have a drying chamber which is an insulated box covered by a transparent cover made of glass or plastic and having air holes to allow air to enter and exit the chamber (Ghazanfari et al., 2003) and (Seveda and Jhajharia, 2012).

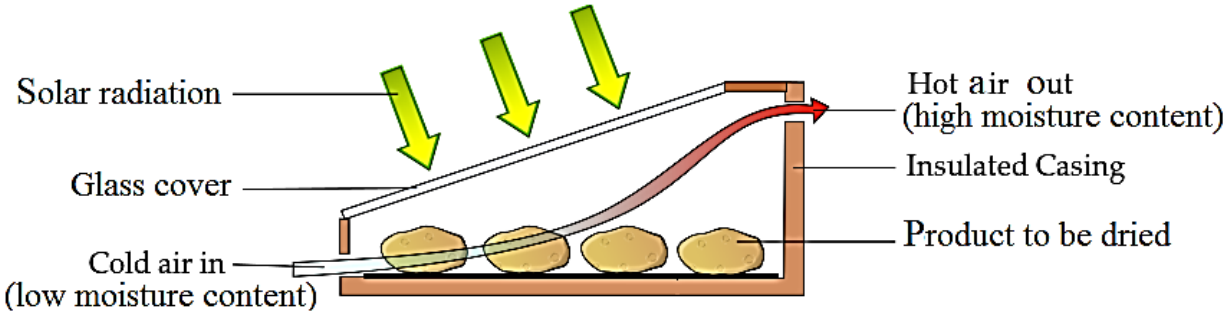

Fig. 2.2. Direct solar dryer (Wikipedia: Solar dryer, 2017)

When the solar radiation hits the glass cover, the air heats up and circulates either naturally or by wind pressure using external source (fan, blower,… etc.) or combination of both. A part of impinged solar radiation will reflect back to the atmosphere whereas the other part will get transmitted inside the dryer cabinet. This transmitted part is again reflected back from the product surface and rest is absorbed by it which increases the product temperature and reduces its moisture content by evaporation (Sharma et al., 2009). The features of the direct solar dryer, it has a simple and cheaper construction which protects the drying product from dust, rain, debris, dews, etc. But direct solar dryers also have some drawbacks in their functioning like product overheating, undesirable product quality, and limited drying capacity (Hii et al., 2012).

From many last the literature, it has been observed that direct solar dryers are the most commonly used devices for drying agricultural and food products. The average drying efficiency of these dryers is varying from 20 to 40% depending on the product types, air flow rate, and the location. The quality of product obtained by direct solar dryers is acceptable and can be improved or enhanced by using some chemical treatments processes.

2.1.3. Indirect-passive solar drying systems

Farkas et al. (1999) developed a modular solar dryer having energy saving feature. The effect of various drying parameters especially air flow rate was studied along with the calculation efficiency. The dryer had three main parts: drying cabin, solar collector and chimney and PV module, as shown in Fig. 2.3. The modular construction of this system operated with different modes; natural air circulation, a chimney was planned to strengthen the air flow with the height of 2 m with cross-section area of 0.2×0.2 m which is installed in the top of the drying cabin to help this operating mode, artificial circulation of ambient air when the photovoltaic module is applied, artificial circulation of the drying air preheated by a solar air collector and also can be combined the above modes.

Madhlopa et al. (2002) developed a solar drying system which had a solar air heater, constitute of two absorber systems in a single flat plate solar collector, was designed according to the principles of psychometry. The system consists of a flat plate solar collector, wire mesh absorber, glass transparent cover, chimney and drying chamber. Results showed that the thermal efficiency of flat plate collector and wire mesh absorber were approximately 21% and 17% respectively with flow rate 0.0083 kg/s. Also, the dryer reduced the moisture content of sliced fresh mangoes from about 85% to 13% on a wet basis and retained 74% of ascorbic acid. Simate (2003) studied and tested two different types of dryers; mixed and indirect-mode natural convection solar dryers. In the mixed-mode operation, the drying chamber cover was glass whereas in the indirect mode it was

plywood. Buoyancy pressure drives air movement through the unit. The researcher concluded that the drying cost of the mixed-mode dryer is 12.76 USD/tons and is about 26% lower than the indirect-mode; the quantity of dry grain obtained from the mixed-mode for the whole year is about 2.81 tons and it was less than that from the indirect dryer by 15%.

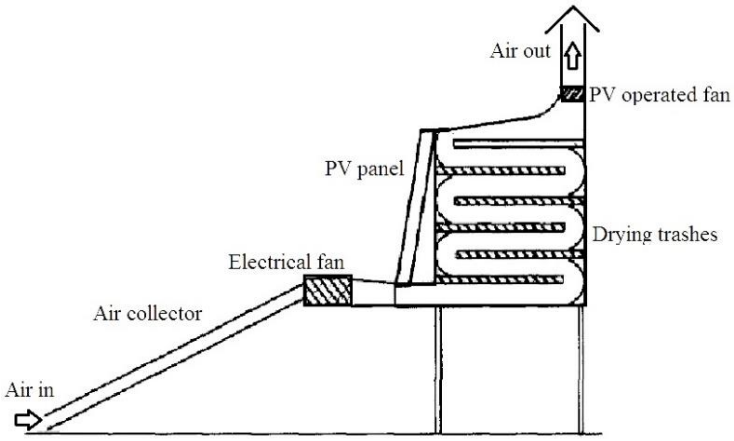

Fig. 2.3. The modular solar dryer (Farkas et al., 1999)

Bolaji (2005) developed and evaluated the performance of a box type absorber solar air collector used for crops drying. The dryer as shown in Fig. 2.4 consists of a solar air collector, drying chamber, and a chimney. The box-type absorber collector made of a glass transparent cover and black absorber plate was installed with 17.5^{o} tilt angle to the horizontal to get maximum solar radiation at experiments location and to allow the heated air to raise in the unit with little flow resistance. The researcher reported that the heating temperature inside the dryer was higher than the ambient temperature by an average of 15.3 ^{o}C throughout the daylight. Also, the efficiency can be enhanced by using box-type absorber solar air collector because the maximum efficiency that obtained was about 60% while those of flat plate absorber and fin type absorber were 21 and 36% respectively. Also, he measured the maximum average temperature inside the solar collector and drying chamber were 64 and 57 ^{o}C respectively, while the maximum ambient temperature observed was 33.6 ^{o}C.

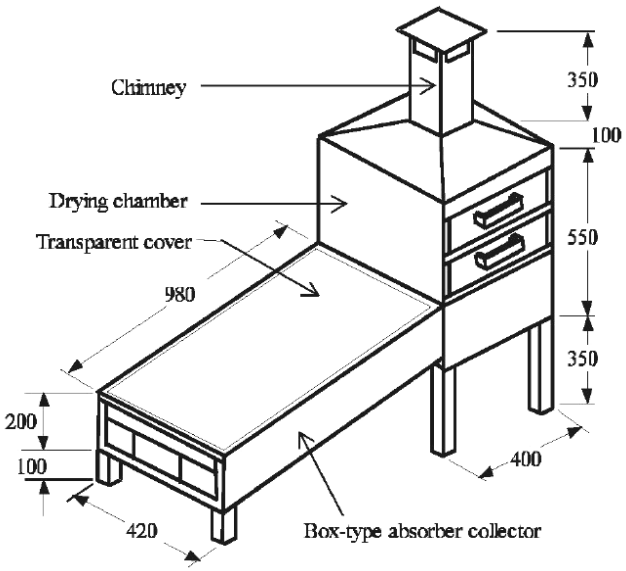

Fig. 2.4. Indirect passive solar dryer (Bolaji, 2005)

Umogbai and Iorter (2013) designed, constructed and evaluated the performance of a passive solar dryer for maize cobs at the University of Agriculture, Makurdi. The side walls of dryer cabin were made of plywood and coated with white emulsion paint, with an inner drying tray made of wire mesh. A Zinc roofing sheet painted black served as the absorber plate with dimensions of (0.5 mm) thickness and (100 cm× 70 cm) area. The results with using about 5 kg of maize cobs reported that the savings in time were achieved as against sun drying as it took 3 days to dry the maize cobs to a moisture content of 13.3 % from 30.3 % by using the passive solar dryer while it took 6 days to dry the cobs to 13.4 % under sun drying. Tashtosh et al. (2014) developed and designed a mathematical model of indirect solar drying system for drying one of the famous dairy product in Jordan called Jameed. The dryer consists of many components; a flat plate solar collector with dimensions of 0.1 m height, 0.8 m width and 1.2 m length, drying chamber consisting of four trays separated from each other equally with a distance of 0.2 m. The chamber made of wood with 1 m long. The total solar radiation on the solar collector surface and drying chamber walls at each hour of the day was estimated at the 21st of May in Jordan. The mathematical modeling for this simple solar dryer was explained and solved by using engineering equation solver software (EES).

2.1.4. Indirect-active solar drying systems

An indirect solar drying system of potato studied by Ali and Desmons (2005) with two different mathematical models. The two models are developed separately; the first allows the estimation of the thermal performances of the solar collector with offset rectangular plate fin absorber plate and the second, allows determining the kinetics of drying for the data input of the air at the exit of the collector. Experimental results of the solar drying system thermal performances, using sunlight in the north of France are compared with the results that obtained by the theoretical model, and the predicted and experimental results were in good agreement. Also, an indirect-mode forced solar dryer to dry the fruit and vegetable in Iraq has constructed and tested by Al-Juamily et al. (2007). The drying system consisted of three main parts are: solar air collector, blower, and a solar drying chamber. Two air solar V-groove absorption plate collectors were used; two air passes and a single glass cover. The cabinet is divided into six separated trays by five shelves. The effect of speed variation of air inside the drying chamber was small and can be neglected. Also, the relative humidity of air exit from the chamber was low between (25 and 30%), and therefore there is no need for high-velocity air inside the chamber.

Mohanraj and Chandrasekar (2009) developed an indirect forced convection solar drier integrated with different sensible heat storage material for copra drying. The drier consists of a solar flat plate air heater integrated with a heat storage unit, a drying chamber and a centrifugal blower as shown in Fig. 2.5. The experiments have done with and without the integration of heat storage materials. Sand mixed with aluminium scrap was used as a heat storage material for solar air collector. The results also proved, the time to reduce the moisture content of copra from about 52% to about 8% with heat storage materials was about 80 hour that is mean faster than without using storage materials with 104 hours. The average thermal efficiency of the solar drying system with both drying modes was estimated to be about 23%. Sundari et al. (2013) designed and developed a forced convection solar dryer having an evacuated tube collector to estimate its performance on the bitter gourd. The solar drying system mainly consists of a drying chamber, evacuated tube solar collector, a blower, and a chimney. The results showed that the moisture removal is high initially and then gets reduced exponentially, that is because of the removal of moisture content

from the surface first followed by the movement of moisture from the internal part of the product to its surface. Also, the moisture content of bitter gourd reduced from 91% to 6.25% in 6 h compared to natural direct sun drying.

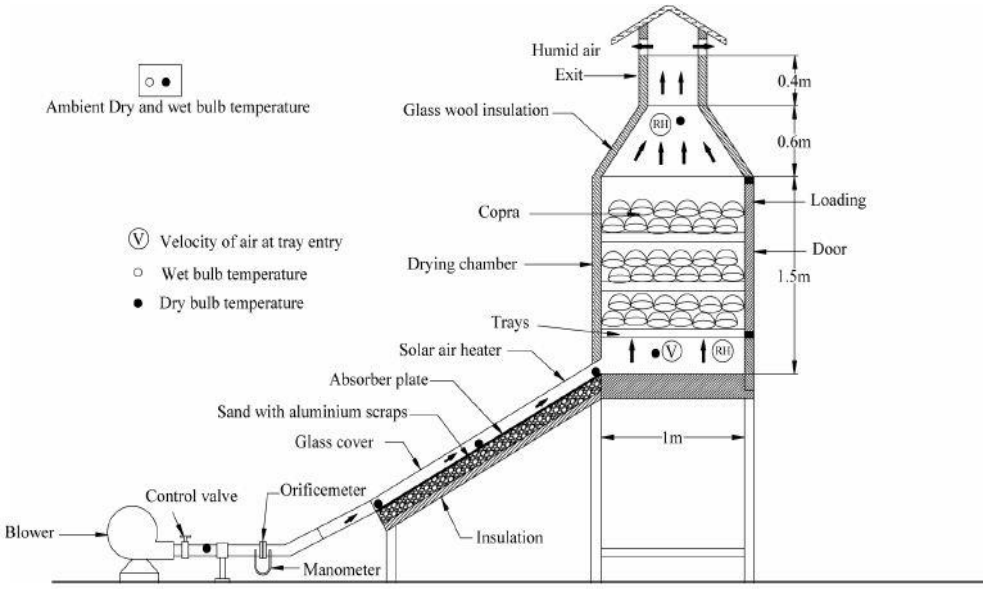

Fig. 2.5. Indirect passive solar dryer (Mohanraj and Chandrasekar, 2009)

Aissa et al. (2014) studied the drying behaviour of sponge cotton by using an indirect solar dryer forced convection for different temperatures and air flow rates. A solar dryer chamber designed and operated for five days of July 2008 for this purpose. A painted black cylindrical chimney, made from galvanized iron, with 0.4 m height and 0.1 m diameter connected to the top of the drying chamber to increase the speed of air flow. The results showed that the temperature of the drying air inside the chamber decreases as it flows horizontally and vertically along the dryer chamber. Additionally, many empirical correlations of temperature lapse and moisture ratio in the drying chamber are found to describe the drying curves of this product according to the basis for the development of solar dryer design charts.

2.2. Solar air collectors

Solar drying system performance and especially indirect dryers are depending on the performance of solar air heater. Several studies and literature have been published and discussed how to improve and enhance heat performance of this important part. Many parameters are playing a main factor to increase or improve the performance of these units.

Ekechukwu and Norton (1999) classified the solar air heaters broadly into two categories: bare plate and cover plate solar air heaters. The bare plate solar air heaters consist simply of an air duct, the upper surface of which operates as the solar-energy absorber plate and the back surface insulated. Bare-plate solar collectors are used widely in crop drying process (for both types passive and active drying systems). For covered-plate solar air-heating collectors to reduce upward heat losses from solar air heaters transparent cover materials above and usually parallel to the absorber plate are used of one or more. Common cover materials used are glass, Plexiglas, and transparent plastics. The cover material prevents convection heat losses from the absorbing plate to the surrounding, reduces long-wave radiation heat losses and protects the absorber plate against cooling by occasional rainfall and against the dust.

Aboul-Enein et al. (2000) studied a flat plate solar air heater with and without thermal storage material under the absorber surface for drying applications. The performance of the solar air heater estimated by simulation software according to the climatic conditions of Tanta (Lat. 30º, 47' N, Egypt). Effects of design parameters of the solar heater such as length, width, gap spacing between the absorber plate and glass cover, mass flow rate and thickness and type of the storage material (sand, granite, and water) on the outlet and average temperatures of the flowing air are studied. The study obtained that the thermal performance of the solar air heater with using storage materials was higher than that without storage. The optimum thickness of the storage material layer was about 12 cm and found to be convenient for drying different agriculture products. Also, the outlet temperature of flowing air decreased with the increasing the gap spacing and mass flow rate. Öztürk and Demirel (2004) investigated experimentally the thermal performance of a solar air heater having its flow channel packed with Raschig rings based on the energy and exergy analyses. The dimensions of the solar heater are 0.9 m width and 1.9 m length. The aluminium-made absorber plate was coated with ordinary black paint.

Fig. 2.6. shows a section view of the packed-bed solar air heater with its dimensions. The results showed that the average daily net energy and exergy efficiencies were found to be 17.51 and 0.91%, respectively. Also, the energy and exergy efficiencies 17 of the packed-bed solar air heater increased as the outlet temperature of heat transfer fluid increased.

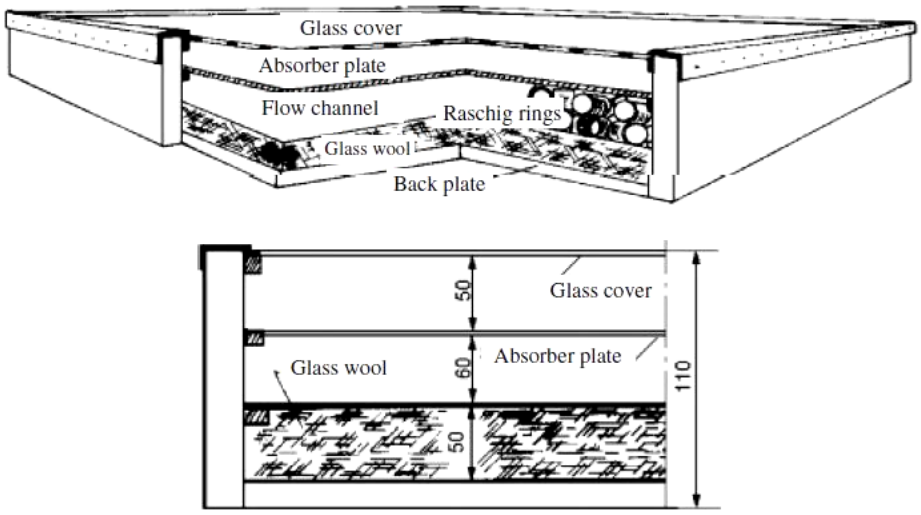

Fig. 2.6. Section view of the packed-bed solar air heater (Öztürk and Demirel, 2004)

Kurtbas and Turgut (2006) investigated the solar air heater performance with fixed and free fins. The solar air heater provides many rectangular shape fins located in flow area to increases the heat transfer coefficient and output temperature of the air. The system operated with two cases. In the first case, the fins were located on the absorber plate in a way that the fins can move freely, while in the second case model fins were fixed to the absorber surface. The absorber surface had an area 1.64 m^2 and the fixed and free fins with 8 and 32 items had surface areas 0.048 and 0.012 m^2 respectively. The results showed there is a reverse relationship between exergy loss ratio and collector efficiency as well as a temperature difference of fluid. In case pressure drop increases, both heat transfer and exergy loss also increase. They obtained that the Fins located on the absorber increase heat transfer and pressure drop. The results found the fixed fin collector is more effective than free fin collector.

A flat-plate solar collector with phase change material (PCM) studied by Koca et al. (2008) by using energy and exergy analyses, $CaCl_2$. $6H_2O$ has been used as phase change material in thermal energy storage system. The designed system combined the solar collector and storage in a single unit as shown in Fig. 2.7. The experiments were carried out for three different days on October. The study showed there is a significant difference between the results of energy and exergy. The net energy efficiency was higher than that of exergy efficiency. The obtained experimental data and calculations showed that exergy efficiencies of latent heat storage systems with PCM were very low.

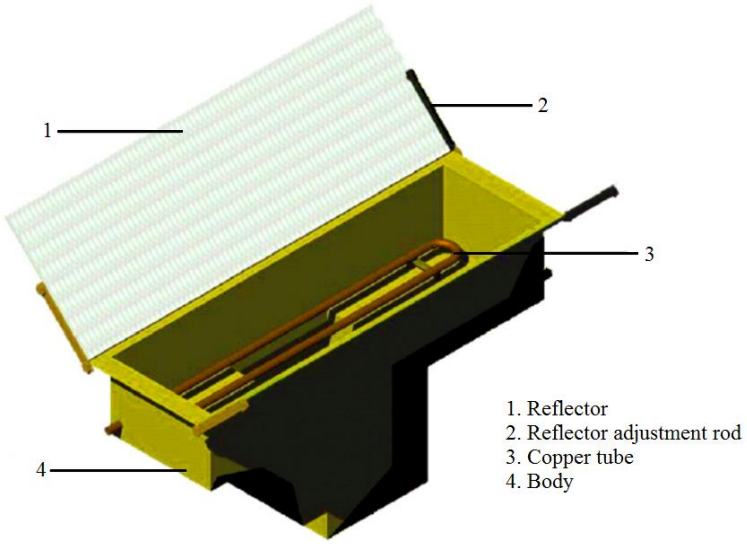

Fig. 2.7. Flat-plate solar collector with the phase change material storage unit (Koca et al., 2008)

Akpinar and Koçyiğit (2010) designed, analysed and experimentally investigated a flat-plate solar air heater having different obstacles on absorber plates. The experiments were carried out at two different air mass flow rates of 0.0074 and 0.0052 kg/s. It was found that the efficiency of the solar air collectors depends on various parameters such as solar radiation, the surface geometry of the collectors and extension of the air flow line. The efficiency of the collector has been found to be increasing function of mass flow rate. The energy efficiency was found to be varied between 20% and 82% while those of exergy efficiency changed from 8.32% to 44% at the mentioned mass flow rates. The highest efficiency was found to be for the solar air heater with an absorbent plate in flow channel duct for all operating conditions.

After two years, the performance and the cost of double duct air solar collector studied and analysed by Yousef and Adam (2012). They developed a model to estimate the effect of mass flow, channel depth and length of the collector on the thermal performance and cost ratio for two types of solar air heaters in double flow mode, flat plate collector with porous media and V-groove absorber plate. The study has been made under many considerations such as; heat transfer is steady and one dimensional, the temperatures of the glass, absorber and bottom plates vary only along the x-direction of the air flow, there is no leakage from the flow channels, the absorption of solar radiation in the cover is neglected and the heat losses through the front and back of collector are to the same ambient temperature. For these models and under these considerations the results showed that the increase of the air mass flow rate leads to increase the thermal efficiency of the solar collector and decreasing the outlet temperature at the same time. The decreasing of the flow depth causes increasing the collector thermal efficiency and increasing the outlet temperature.

They found that increasing the collector length results decreasing the collector thermal efficiency. The study also showed the effect of porous media using, the using of porous media leads to increasing the collector thermal efficiency and increasing the outlet temperature. Collins and Abulkhair (2014) analysed and studied the performance of heat transfer and effectiveness for unglazed transpired solar air collector because it is one of the most effective methods of reducing thermal loads in buildings. A three-dimensional CFD model created to evaluate the effectiveness and heat loss of an unglazed transpired solar collector with a trapezoidal groove. The numerical development was successful, and the model was validated by comparison to the experiments and correlations.

At the same year, Yang et al. (2014) designed and tested a solar air heater with offset trip finned absorber surface (see Fig 2.8.), Single-layer glass used as the transparent cover to maximize the heat loss from the air heater could also be minimized by adding thermal insulation on the side and back plates, as well as the stagnant air layer between the glazing and the absorber plate. Based on the empirical data results , the instantaneous thermal efficiency could exceed 40% under the typical heating condition even at the low airflow rate 100 m^3/h , where the solar radiation on the collecting area was about 600W/m^2, indoor air temperature 14 ^oC, outdoor air temperature -5 ^oC and incident angle 0-30^o . Also the required power to operate the fan was as low as 20 W.

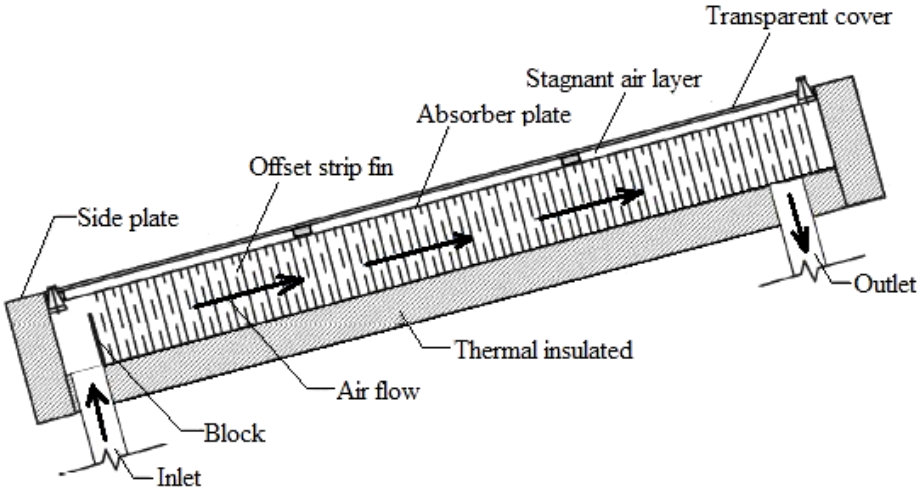

Fig. 2.8. View of the solar air heater with offset strip fin attached (Yang et al., 2014)

A parabolic trough collector was tested under the climatic condition of Aliero Town, Kebbi State, Nigeria to see the effect of meteorological parameters on the performance of the system. The experimental results obtained lowest daily average ambient temperature of 37.2 ^oC was recorded at 1.30 m/s daily average wind speed while efficiency has its peak value of 8.36%. It is, therefore, indicates that efficiency and wind speed has a positive correlation and negatively correlated with ambient temperature. The results obtained that wind speed is inversely proportional to the direct solar radiation and it had also shown that a maximum daily average wind speed of 1.39 m/s was observed when the ambient temperature reached its lowest value. (Umar et al., 2014). Also, wind flow around a cylindrical trough solar collector had been investigated numerically. Ambient temperature was assumed to be constant at 300 K, and for specific geometries, different meshing methods and boundary conditions were used in various runs. Validation was done by comparing the simulation results for a horizontal collector with empirical data. At medium angles (15^o to 45^o) the flow crosses the receiver pipe with a higher velocity which increases the heat loss. For angles

more than 45^o the collector covers the receiver pipe. Therefore, the Nusselt number is reduced (Shojaee et al., 2015).

Hematian and Bakhtiari (2015) analysed an air solar flat plate heater worked with different convection modes. The absorber plate was made from steel with thickness of 0.5 mm and painting by black. A standard glass with a thickness of 4 mm used as a transparent collector cover. The experiments were done with two convection modes; natural and forced convection and the data was collected from 18 to 24 June when the atmospheric conditions were almost uniform for the day. The results showed that the average airspeed in the forced convection case was about 21% higher than natural convection case. It has been found that the solar collector operated with natural convection gave high efficiency compared to the solar collector with forced convection. Mahboub et al. (2016) experimentally studied a new design on solar air heater. Test design consists of a curved smooth flow channel with an absorber plate of convex shape as shown in Fig. 2.9. A prototype of a curved solar air heater with 1.28 m^2 collector area built and tested under summer conditions in Biskra, Algeria. This design improved the performance of the solar air heater due to taking advantages of the centrifugal forces effect on the airflow structure inside the duct of the heater. The flow vortices that formed in the cross-sectional of the curved duct allowed to enhance heat transfer between the absorber surface and air. From the cost side, this collector made or constructed with the same amount of materials that used to fabricate the conventional flat plate collectors, then there will be no additional manufacturing cost or construction weight.

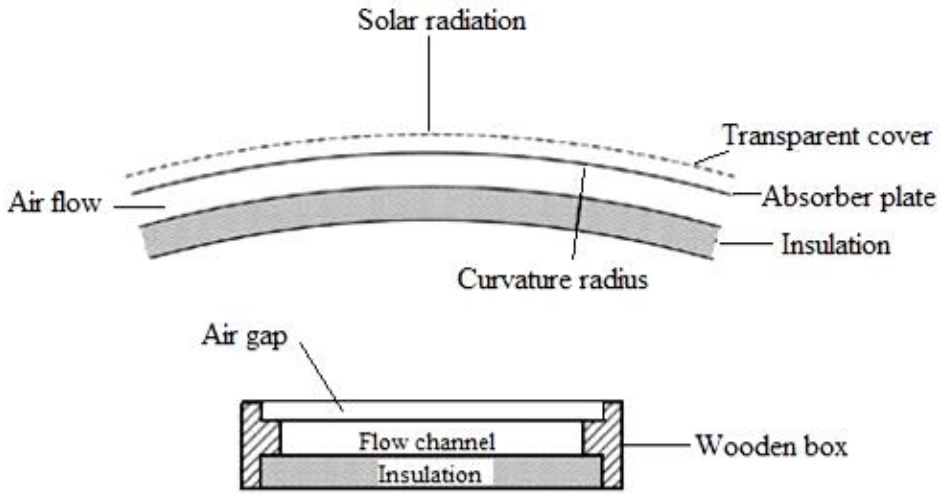

Fig. 2.9. Flat plate collector with curved flow channel (Mahboub et al., 2016)

The effect of the cross-sectional configurations on the thermal performance of the plastic solar air heater is examined by Abdullah et al. (2017). The tested shapes are circular, semi-circular and half-circle plus isosceles triangle. The mass flow rate of air was changed from 0.05 to 0.25 kg/s. Results indicated that the highest efficiencies were accomplished for the circular configuration and reached to about 80% at a mass flow rate of 0.18 kg/s and average solar radiation of 925 W/m^2. On the other hand, for the same conditions, the thermal efficiency reached about 64% and 48% for half-circle plus isosceles triangle and semi-circular shapes, respectively. In the same years, an analytical investigation on the thermal and thermohydraulic performance of offset finned solar air heater has been evaluated by Rai et al. (2017). Study was done to investigate the effect of variation of system and operating parameters such as fin spacing, fin height, air mass flow rate and insolation on the thermal efficiencies. The solar radiation incident on solar collector has little effect on

efficiency of the collector, although it has a significant effect on the ambient air temperature around the collector. The outlet air temperature in flow channel increases almost linearly with insolation. It is also found that the maximum percentage enhancement in thermal efficiencies increases to 114.1% with a decrease in fin spacing and increase in fin height.

2.3. Air movement methods

2.3.1. Passive movement systems

One of the most common problems in passive solar drying systems is operating with low air velocity. The best solution for this problem is the chimney. A chimney is a structure which increases the speed of flow or provides ventilation for hot gases from any thermal system such as solar system, drying system, boiler, furnace, … etc. to the outside atmosphere. Zambrano and Alvarado (1984) designed and tested a chimney to reduce the danger of high temperatures in the solar drying system. Theoretical and experimental comparison between the cylindrical shape and conical chimney at the same height and base diameter has been done. The velocity of air at the basal section of the conical chimney was approximately twice that of a cylindrical chimney.

In (1989) Zahed and Elsayed modeled a solar kiln was utilized for solar drying purposes. The governing equations for the temperatures through the system are derived together with their boundary conditions. The finite difference technique used to solve these governing equations with their boundary conditions. An implicit method was used with the Gauss-Seidel iterative technique. A FORTRAN software program has been prepared to solve the finite difference equations. Ekechukwu and Norton (1997) designed and measured the performance of solar chimney integrated with natural convection solar dryer (passive dryer).

The experimental test rig consists of a 5.3 m height and 1.64 m diameter cylindrical vertical chamber, supported structurally by steel framework and draped internally with a selectively absorbing surface (see Fig. 2.10). The greenhouse effect of the system was expected to keep air temperatures in the chimney higher than ambient temperatures consistently. The tests taken with and without the selective surface in place to study the effectiveness of the design parameters. Theoretically, by the deriving they found that the relation between air velocity and temperature difference in the chimney as written below:

$$v = 0.453 \left[\frac{D\ g}{\rho}\ \Delta T_{ch}\right]^{\frac{1}{2}}, \tag{2.1}$$

where (D) is the hydraulic diameter of the chimney in (m), (g) is the gravitational acceleration in (m/s^2) and ρ is the average density of the fluid in the chimney in (kg/m^3). The results obtained that the solar chimney if appropriately designed can maintain chimney air temperatures consistently above the ambient temperature which would enhance the desired buoyancy-induced air flow through the chimney. The desired performance of the system was achieved by integrated the solar "greenhouse" chimney. A solar drying system integrated with a solar chimney was designed and tested by Vlachos et al. (2002). The design based on energy balances and an hourly-averaged radiation data reduction procedure for tilted surfaces. The chimney which used consists of two main parts; a trapezoid base connected with the top of the drying chamber and the chimney duct that has the shape of a narrow pipe. The trapezoid section insulated from internal side, and chimney duct insulated from external sides. Chimney duct was capable of being at various inclinations

between 90^o and 30^o. Chen et al. (2003) studied a solar chimney model with uniform heat flux experimentally. The experiments has been done on a chimney model has a uniform heat flux on one wall with a variable chimney gap to height ratios were between 1:15 and 2:5 and different heat flux values and inclination angles. The experimental solar chimney had internal dimensions of 1.5 m high, 0.62 m wide and a variable chimney gap from 100 to 600 mm. The inlet of the chimney was 1 m above the floor. The results showed that the air flow rate reached a maximum at an inclination angle of around 45^o with 200 mm gap and 1.5 m high chimney. The flow rate with inclination angle 45^o was about 45% higher than that for a vertical chimney under otherwise identical conditions.

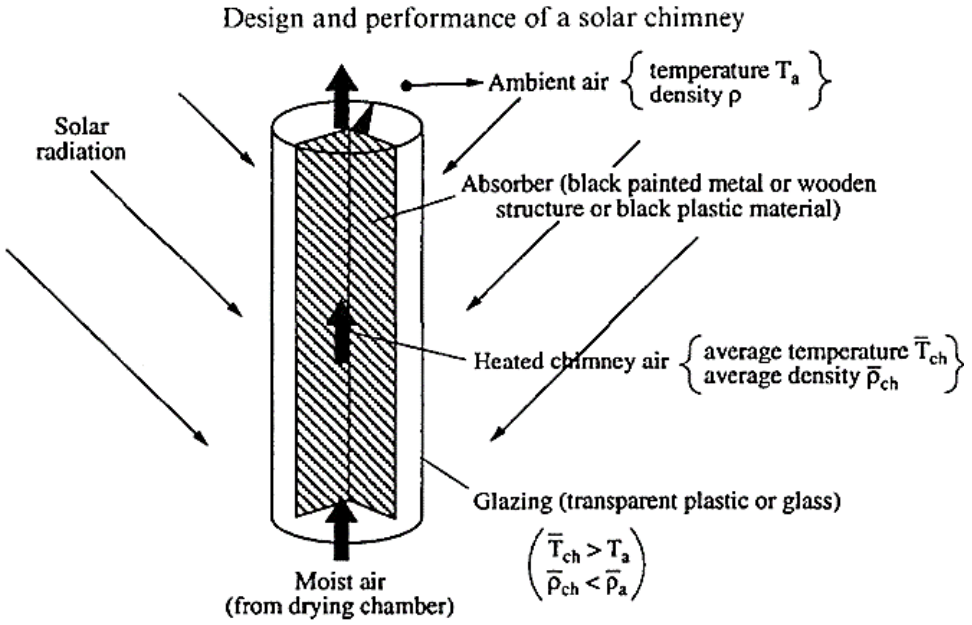

Fig. 2.10. Greenhouse type solar chimney (Ekechukwu and Norton, 1997)

Ferreira et al. (2008) showed the feasibility to use the solar chimney for solar agriculture products drying. A prototype solar chimney was built specifically in Belo Horizonte (Brazil) as shown in Fig. 2.11. Sheets of wood constructed a tower with 12.3 m in height and diameter of 1.0 m and covered by fiberglass. According to the thermal behaviour of the flow obtained that the drying products must be placed at the centre of the device and close to the ground. Drying tests on bananas support this idea and suggest that drying on wire mesh is more efficient than drying on plastic canvas. The low thermal efficiency which observed was because of the heat diffusion through the ground, by the low transmittance of solar radiation and by the high transmittance of infrared radiation from the plastic cover. These thermal losses can be minimized by providing thermal insulation in the ground and replacing the material of the cover.

Afriyie et al. (2009) investigated the performance of chimney-dependent solar crop dryer experimentally. A rectangular cross-section chimney was built with a dimension of (440×80×625 mm) width, uniform gap, and height respectively. The chimney was all-rounded with glass with the dryer chamber. Also, an additional replaceable back wall has been constructed from wood with the black painted inner surface, was used to replace the transparent back wall to transform the normal chimney into a solar chimney where necessary, as shown in Fig. 2.12. The tests have been done in four cases; the first on the dryer with roof angle 81^o with using the normal chimney, the second by repeating the first with the solar chimney, third test was by using the roof angle of 64^o

and still with the solar chimney and the last test was with roof angle 51^o still with the solar chimney. The results showed that the solar chimney could increase the airflow rate of a solar direct-mode dryer especially when it is well designed with the appropriate angle of the drying-chamber roof. However, if the flow rate increased the drying rate will also increase when the relative humidity (RH) of the ambient air is below a certain mark.

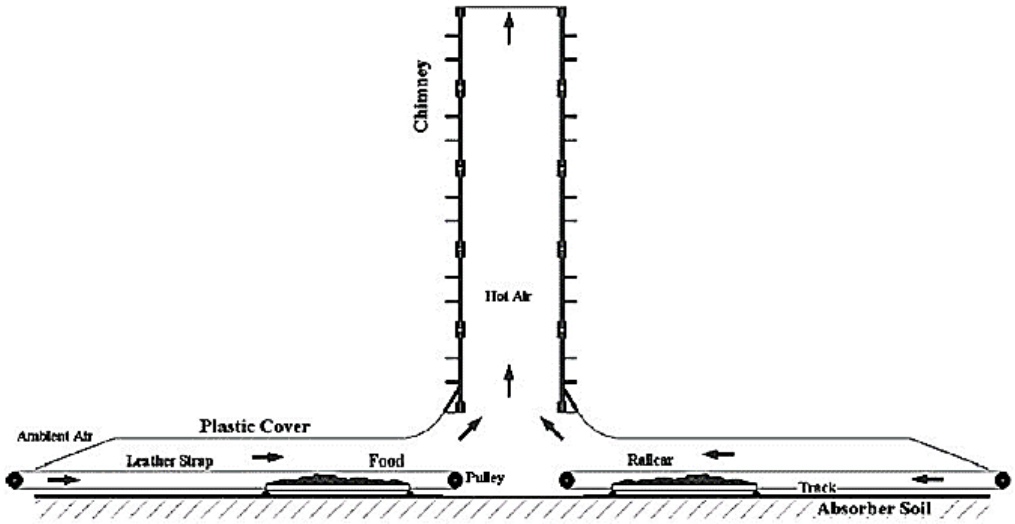

Fig. 2.11. Solar chimney prototype for solar drying (Ferreira et al., 2008)

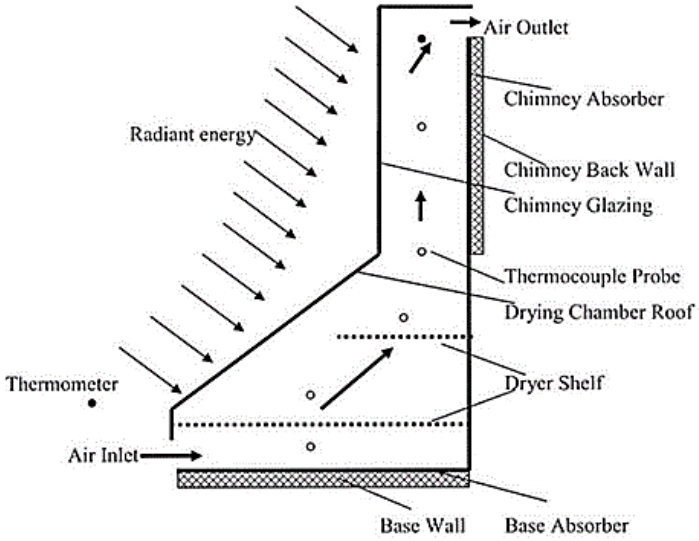

Fig. 2.12. Chimney-dependent direct-mode solar crop dryer (Afriyie et al., 2009)

Afriyie and Plange (2012) described the performance of a direct-mode solar crop dryer with a solar chimney for different inlet areas with a fixed outlet area. The same cases that studied with the chimney-dependent direct-mode solar dryer in Fig. 2.12. has been done, but with three different inlet designs were also constructed with inlet gaps 70 mm, 50 mm, and 30 mm, respectively. Each inlet had a width of 390 mm. The tests were grouped in three sets based on the roof angle, and different inlet gaps (different inlet areas); the first on the dryer with roof angle 81^o with inlet gaps 30 mm, 50 mm, and 70 mm, the second and third used the roof angles 64^o and 51^o respectively with the same different inlet gaps for the first case. The experimental tests showed that inlet area of the direct dryer could be set appropriately together with the use of a solar chimney and a suitable angle of the roof of drying chamber to improve the ventilation through the dryer. This combination

only effective for improving the drying performance of the direct mode dryer in areas of low relative humidity, because the direct dryers are highly sensitive to the relative environmental humidity. The results showed that the dryer with roof angle 51^{o} and inlet gap 70 mm had the best performance, from the combination of low ambient RH and high mass flow rate.

Tan and Wong (2013) explained the effect of the solar chimney's stack height, depth, width and inlet position on the interior performance as well as proposes an optimal tropical solar chimney design. According to the four parameters (height, depth, width and inlet position) as input parameters as well as physical and computational models have been developed, 300 cases of employing the solar chimney in the tropics are generated, of which 139 cases are simulated. All simulations showed that output air temperature of the chimney remains constant. Also, the results showed that the solar chimney's width was the most significant factor influencing the output air speed. The ratio of solar chimney's length to hydraulic diameter should be greater than 15 to ensure developed flow, and the ratio of solar chimney's stack height to width should be less than seven if airflow within the solar chimney is to be two-dimensional. For chimney position found it had limited influence on the output airspeed, although the region near to the solar chimney's inlet shows an increase in airspeed but is damped when the airspeed is averaged across the plane. Ghaffari and Mehdipour (2015) are improved and modeled solar dryer integrated with a solar chimney by using computational fluid dynamics. Chimney model was a part from this study, and based on the kinetic energy balance for a chimney element with a length of (dy) and the distance of (y) from the chimney's inlet, the outlet air chimney temperature equation was obtained as follows:

$$T_{cho} = T_{am} + (T_{chi} - T_{am})\, e^{-U\, p\, l / m\, Cp}, \tag{2.2}$$

where (T_{chi}) and (T_{cho}) are the chimney inlet and outlet air temperatures respectively, (p) is the chimney's base perimeter, (U) is the chimney's overall heat transfer coefficient, (T_{am}) is the ambient temperature, (m) is air mass flow rate and (l) is the length.

2.3.2. Active movements systems

Photovoltaic technology (PV), which utilizes sunlight to generate electrical energy, is an attractive alternative energy source because it is renewable, harmless, and domestically secure. Because photovoltaic technology basic component is the cell which produces less than three watts on average, cells must be bundled in series/parallel configurations known as modules or solar cells to achieve high powered tasks. PV arrays produce power only when illuminated, and it is, therefore, standard to employ a large energy storage mechanism, most commonly a series of rechargeable batteries. To prevent harmful battery overcharge and over discharge conditions and to drive AC loads, a charge controller and an AC to DC converter must be implemented (Messenger and Ventre, 2004).

Photovoltaic-thermal solar drying system was successfully tested and performance estimated under the conditions of University Kebangsaan Malaysia by Othman et al. (2008) to obtain the high-quality product. The collector was tilted at 14^{o} from the horizontal and facing south. The array consisted of two type of solar collectors, photovoltaic-thermal collector and flat plate solar thermal collector in series. It consisted of 72 solar cells, compound parabolic concentrator CPC with 1.86 concentration ratio and series of fins attached to the back of the absorber surface, as shown in Fig. 2.13. The dimension of the dryer chamber was 1.10 m×0.60 m×0.80 m (length×

width×height). It consisted of many wire mesh strays and four small DC fans powered by PV/T collector located on the rooftop of the device. The fans were installed at the inlet duct of the dryer to ensure continuous ventilation by sucking the hot air from the collector into the dryer. The performance parameters of the hybrid PV/T collector were collected in term of the electrical and thermal efficiency for the period from t_1 and t_2:

$$\eta_{PVT} = \frac{\dot{m}\, Cp \int_{t_1}^{t2}(T_o - T_i)\, dt + \int_{t_1}^{t2} P_E\, dt}{CR\ A_c \int_{t_1}^{t2} I\, dt}, \tag{2.3}$$

where (ṁ) is the mass flow rate (kg/s), (Cp) is the fluid specific heat (J/kg K), (I) is the incident solar radiation (W/m^2), (A_c) is the collector absorber area (m^2), (P_E) is the electric power generated by the PV module (W), (T_i) and (T_o) is the fluid inlet, and outlet temperature (C^o) and (CR) is the concentration ratio of the CPC.

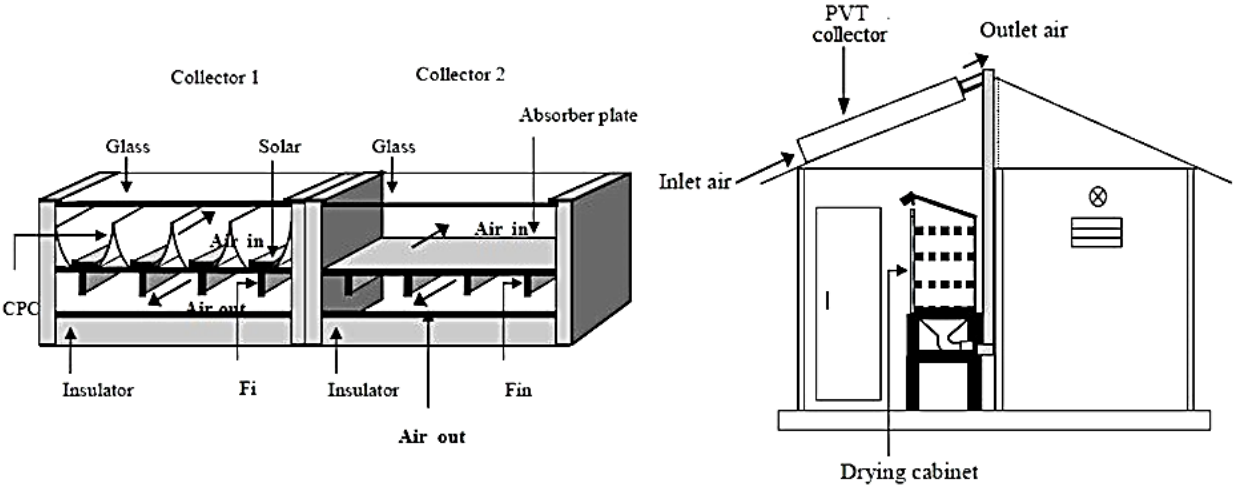

Fig. 2.13. Photovoltaic-thermal solar collector (Othman et al., 2008)

Adelaja et al. (2009) developed a forced convection solar dryer (active dryer) that powered by a solar photovoltaic module. The PV solar dryer consisted of the drying chamber, the solar collector, the blower and PV module. The motion of air through the dryer and collector by a fan. The fan has been connected with photovoltaic module rated 11 Wp powered DC blower rated 12 V to facilitate air flow and evacuation of moisturized air within the drying chamber. He concluded that PV powered solar dryer offers a good solution to the many problems encountered by farmers in the rural communities of Africa, particularly, the preservation and commercialization of their farm produce which quality do not meet either or both national and international standards.

Anyanwu et al. (2012) tested and investigated the performance of a photovoltaic powered solar dryer. Solar collector consisted of a black painted absorber plate made of 1.5 mm thick mild steel, encased in glazing formed out of 4-mm-thick silicon glass panels. The absorber plate was insulated with glass wool and sawdust insulators. The blower mounted facing the air channel of a solar collector with a rated power of 90 W (positive draft). The supply power to the fan was provided by 2×80 W photovoltaic modules connected in series. The collector was connected to the drying chamber with polyethylene pipes of 80mm internal diameter, which are usually flexible insulators. The major advantages of the system derive from its independence from grid electricity also the overall cost could be reduced by using a DC blower. Ceylan et al. (2013) analysed and evaluated the energy performance of a new design of a photovoltaic cell-assisted solar dryer. The system included many parts; solar heat pipe collector, a fan, an air regulating damper, halogen lamps,

batteries, photovoltaic cells, a load cell, and a drying chamber. The solar heat pipe collector contains a sealed copper pipe. This pipe attached to a black copper fin, which fills the tube (absorber plate). When the sun shines on the black surface of the fin, the alcohol was heated and hot vapor rises to the top of the pipe. Water, or glycol, flows through the manifold and picks up the heat from the tubes. The heated liquid circulated through another heat exchanger and loosed its heat to the drying air. The system had two photovoltaic cells. The first used to operate circulation fan during the day. The other cell used to charge the batteries. The researchers concluded from the obtained results, the period of drying with halogen lamps was a short period because of low charged batteries with photovoltaic cells. Also, they obtained, when the solar radiation increases, the batteries charge will increase.

Many kinds of literature reviewed by Bennamoun (2013) which explained that the PV cell could be used inside the solar collector to increase the total efficiency of the solar drying system. According to the different studies, efficiencies as high as 70% were obtained. On the other hand, PV cells can be used to provide electrical energy that can be consumed by the other components of the solar drying system such as the circulation fans. Also, electrical energy can be stored by using batteries to use it during low sun radiation periods. This makes the drying systems self-sufficient and independent of any another external source of energy.

Also, Ahn et al. (2015) studied the performance of photovoltaic/thermal (PV/T) solar air collector coupled with heat recovery ventilation. From the results, it was obtained that thermal and electrical efficiencies of PV/T collector were 23% and 15%, respectively. Therefore, the overall efficiency of the PV/T collector system is the summation of two efficiencies and equal 38%. Also, heat transfer efficiency of heat recovery ventilation was improved to about 20% with pre-heat air from PV/T collector.

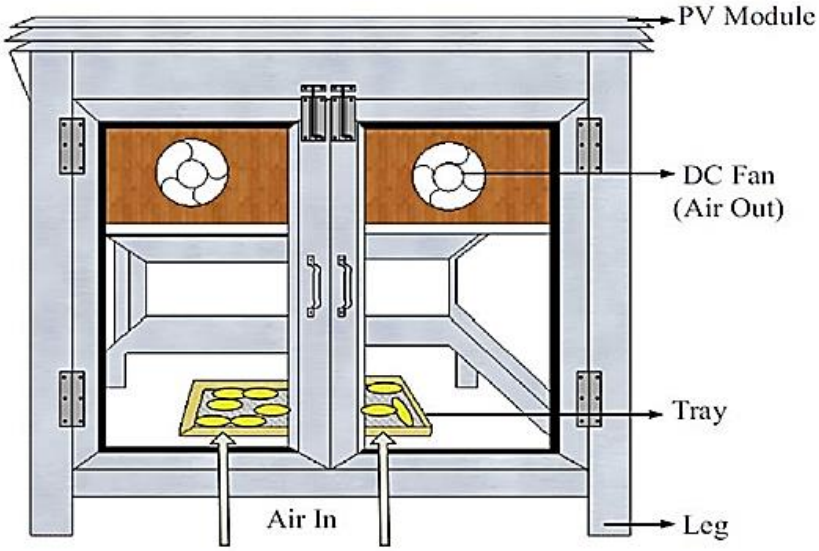

Fig. 2.14. Photovoltaic integrated greenhouse dryer (Tiwari et al., 2016)

The performance of photovoltaic–thermal (PVT) integrated with a mixed mode solar dryer have been analysed by Tiwari et al. (2016). The device consisted of three PV modules, two DC fan and a drying chamber as shown in Fig. 2.14. The dimensions of each semi-transparent PV module is 1 m×0.4 m which have 36 circular shape cell of 35 W power. The rating of DC fan was 12 V and 1 A. The structure of dryer was made of 3 mm thick glass which fitted in an aluminum frame with

the help of rubber gasket. Numerical computations have been done with the using a MATLAB software, and the results are validated with experimental values. The results showed that the quality of the dried product was increased and the problem of discoloration has been minimized. Also, the solar cell efficiency decreases as cell temperature increases. In the same year of this study, Elbreki et al. (2016) were reviewed many literatures which related to the parameters of climatic, design and operational factors was carried out to evaluate their effect on the thermal, electrical and overall efficiency of photovoltaic-thermal systems.

2.4. Modelling and simulation of solar collectors and dryers

Based on the last studies, there is various computer software which used to design, optimize, describe and estimate the performance of different drying systems and especially solar drying systems. Different types of software such as MATLAB, FORTRAN, ANSYS, TRNSYS or different CFD techniques have been applied for thermal analysis for solar drying systems. The advantages of software using are to save the time, to get more accurate results and to give more clear description of the performance.

A physical-mathematical model has been developed by Mahapatra et al. (1994) to simulate the performance of an integral direct solar dryer. Under operation conditions and based on the heat and mass balance equations, the models have been solved by computer, using numerical time-stepping scheme. The simulation predicted results had been verified by experiments for drying chamomile. The simulated and experimental results showed good qualitative and quantitative agreement such as moisture content percent during drying time. Modeling and validation of a natural convection greenhouse drying system done by Kumar and Tiwari (2006).

To calculate product temperature, the greenhouse air temperature and the moisture evaporated, a computer program was developed with MATLAB software for this purpose. The software program was also used to predict the thermal performance of the greenhouse on the basis of solar intensity and ambient temperature. The developed software was experimentally validated. The results are showed that the analytical (simulated) and experimental results for drying were in good agreement. Jain (2007) was presented an analytical model to study the new concept of a crop dryer integrated with the reversed absorber plate type solar collector and thermal storage with natural airflow. A 30^{o} inclined absorber plate with thermal storage and 0.12 m width of airflow channel induced the mass flow rate varied in the range of 0.032-0.046 kg/s during the drying process.

The thermal model was developed based on the basic energy balance equations (mass and heat) on the various components of the solar crop drying system. The mathematical model was solved for Delhi city with latitude $28^{o}35'$ N, longitude $77^{o}170'$ E and altitude 216 m from mean sea level. A MATLAB 6.1 software program has been prepared to solve the mathematical model. The results obtained that absorber plate with 1 m length and 1 m breadth with 0.15 m packed bed could dry 95 kg of onion from a moisture content of 6.14 to 0.27 kg water/kg of dry matter in a 24 h drying period.

A thin layer indirect solar drying system has been simulated and validated experimentally by Dissa et al. (2009). This system used to dry mango slices. The prototype of the indirect solar dryer consisted of many parts as shown in Fig. 2.15. The products items were put in the dryer on four rectangular trays. The experiments were done for three days during harvest period of mangoes. It was observed that on the first day there was a very less constant drying rate period and on the

second day it becomes negligible. For the three days, the drying rates were reached a maximum value of 0.18 g/kg s on the first day, 0.13 g/kg s on the second day and 0.04 g/kg s on the third day. Authors were used MATLAB version 7.0.1 software for simulation drying process with many assumptions has been taken. MATLAB version 7.0.1 has been used for estimation of drying rate at regular interval of time by derivation of the moisture content dry basis with respect to time using a derivation program.

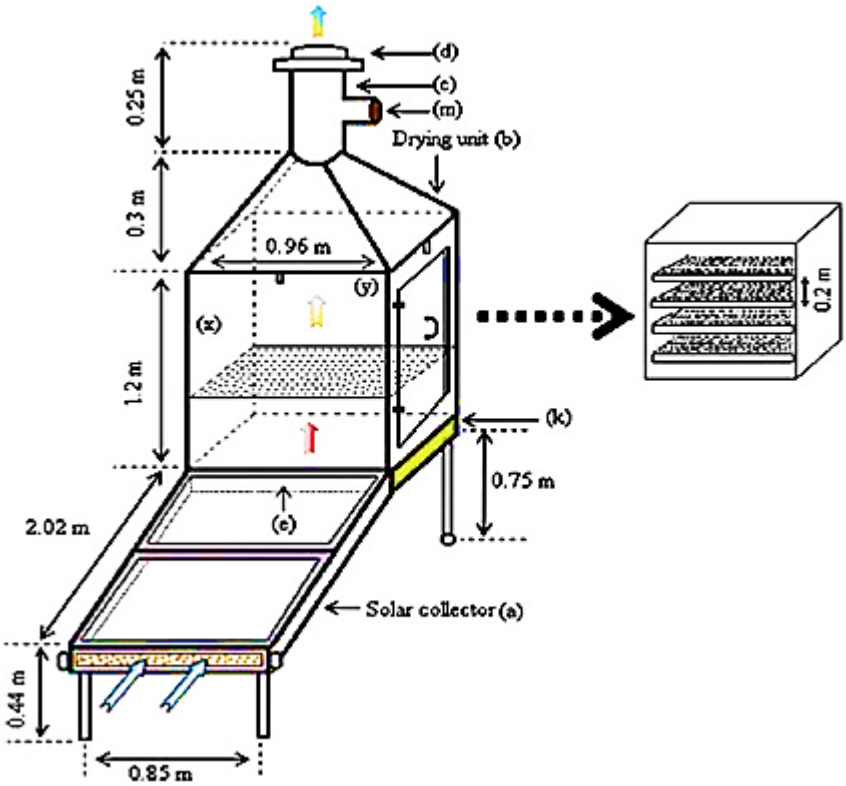

Fig. 2.15. The prototype of indirect solar dryer (Dissa et al., 2009)

Marathe et al. (2013) Solved mathematical models representing solar air heating systems. Results from the developed model such as efficiency of the collector for specific flow rate, inlet and an outlet temperature of air or temperature lift of the collector are compared with experimental data available in the literature. The simulation program was run for location-specific condition, Chennai (13.08° N, 80.27° E). This result is closely matching with results recorded in literature for the same type of collector.

Romero et al. (2014) used CFD fluent program to simulate drying process by indirect solar dryer prototype. The simulated model has been validated with experimental results. Drying system consisted from flat solar collector with dimensions (2.0 m×1.0 m×0.1 m), drying cabinet with dimensions (1.0m × 0.80 × 1.2m) and 1.2m chimney with diameter 0.2 m. Solar dryer geometry was made with ANSYS design modeler program with 21° tilt angle of with respect to the horizontal plane was considered for the months from January to March. Comparison between CFD simulated and thermal measured results showed that at solar collector outlet there was a good degree of similarity between measured and calculated temperatures.

Aghbashlo et al. (2015) modeled and simulated a deep-bed solar greenhouse drying system used for chamomile flowers drying. For this purpose, a new model containing a phenomenological for the deep-bed drying process of materials has been developed which effectively permits users of

the TRNSYS program to design, simulate, and optimize the solar greenhouse drying system. The model was validated by using previous field trial data for solar greenhouse drying of chamomile in Serbia. The validated TRNSYS model was suitable to simulate the performance of solar drying systems in different locations, predict system performance under different weather conditions and operating conditions, to optimize solar drying system size to match different load profiles and to develop effective control methods.

2.5. Timeline of the previous researches

Table 2.2 shows the timeline of the previous researches in details. The solar collectors, drying systems, air movement methods, modelling and simulations of solar system are showed.

Table 2.2. Summarize the literature

Authors	Year	Highlight
Aboul-Enein et al.	2000	The outlet temperature of flowing air decreases with the increasing of solar air heater gap spacing and mass flow rate.
Adelaja et al.	2009	PV powered solar dryer offers a good solution to the many problems encountered by farmers in the rural communities.
Afriyie et al.	2009	Solar chimney can increase the airflow rate of a solar direct-mode dryer especially when it is well designed with the appropriate angle of the drying-chamber roof.
Aghbashlo et al.	2015	Validated a suitable TRNSYS model to simulate the performance of solar drying systems in different locations, predict system performance under various weather and operating conditions.
Ahn et al.	2015	The overall efficiency of the PV/T collector system is the summation of two efficiencies; thermal and electric. Heat transfer efficiency of heat recovery ventilation was improved to about 20% with pre-heat air from PV/T collector.
Aissa et al.	2014	The temperature of air inside drying chamber decreases as it flows horizontally and vertically along the dryer chamber.
Akpinar and Koçyiğit	2010	The energy efficiency was found to be varied between 20% and 82% while those of exergy efficiency changed from 8.32% to 44% at the mass flow rates 0.0074 and 0.0052 kg/s.
Ali and Desmons	2005	The results of solar drying system performances have compared with the results that obtained by the theoretical model, and the predicted and experimental results were in good agreement.
Al-Juamily et al.	2007	The effect of speed variation of air inside the drying chamber was small and can be neglected.
Bennamoun	2013	Electrical energy can be stored by using batteries to use it during low sun radiation periods. This makes the drying systems self-sufficient and independent of any another external source.

Bimbenet et al.	2002	Many processes are used, according to the type and quantity of product to dry, the amount of water to remove, the final desired quality or functionality of the dried product.
Bolaji	2005	The average temperature inside drying chamber higher than ambient by an average of 15.3^{o} throughout the daylight.
Can	2000	Drying process takes place in two stages. In the first stage of drying, the system is considered as a pure material, and drying takes place at the surface of the drying material at a constant rate. In the second stage, drying takes place with decreasing drying rate and this type of drying follows constant rate drying.
Ceylan et al.	2013	The period of drying with halogen lamps was a short period because of low charged batteries with photovoltaic cells.
Chen et al.	2003	The flow rate with inclination angle 45^{o} was about 45% higher than that for a vertical chimney under otherwise identical conditions.
Ekechukwu and Norton	1994	Solar chimney if designed properly can maintain chimney air temperatures consistently above the ambient which would enhance the desired buoyancy-induced air flow through it.
Ekechukwu and Norton	1999	The solar air heaters classified broadly into two categories: bare plate and cover plate solar air heaters.
Ferreira et al.	2008	The drying on wire mesh is more efficient than drying on plastic canvas.
Ghaffari and Mehdipour	2015	Improved and modelled solar dryer integrated with a solar chimney by using computational fluid dynamics.
Hematian and Bakhtiari	2015	It has been found that the solar collector operated with natural convection gave high efficiency compared to solar collector with the forced convection.
Hii et al.	2009	Direct solar dryers have simple and cheap construction which protects product items from dust, rain, debris, dews…. etc.
Koca et al.	2008	The experimental data and calculations showed that exergy efficiencies of latent heat storage systems with phase change material were very low.
Kumar and Tiwari	2006	A computer program was developed with MATLAB software to predict the thermal performance of the greenhouse on the basis of solar intensity and ambient temperature.
Kurtbas and Turgut	2006	The Fins located on the absorber increase heat transfer and pressure drop. The results found the fixed fin collector is more effective than free fin collector.

Madhlopa et al.	2002	Moisture content of mangoes reduced from 85% to 13% by using solar dryer integrated with collector having wire mesh absorber.
Mahboub et al.	2016	The flow vortices that formed in the cross sectional of the curved duct solar collector allowed to enhance heat transfer between the absorber surface and air.
Messenger and Ventre	2004	To prevent harmful battery overcharge and over discharge conditions and to drive AC loads, a charge controller and an AC to DC converter must be implemented.
Mohanraj and Chandrasekar	2009	The time to reduce moisture content of copra from 52% to 8%with heat storage materials was about 80 hour that is mean faster than without using storage materials with 104 hours.
Rai et al.	2017	The outlet air temperature in flow channel increases almost linearly with insolation. It is also found that the maximum percentage enhancement in thermal efficiencies increases to 114.1% with a decrease in fin spacing and increase in fin height.
Romero et al.	2014	Comparison between CFD simulated and measured thermal results showed that at collector outlet there was a good degree of similarity between measured and calculated temperatures.
Shojaee et al.	2015	At medium angles (15^o to 45^o) of cylindrical trough solar collector, the flow crosses the receiver pipe with a higher velocity which increases the heat loss.
Simate	2003	Drying cost of mixed-mode dryer lower than indirect mode dryer.
Tan and Wong	2013	Solar chimney's width was the most significant factor influencing the output air speed. For chimney position found it had limited influence on the output air speed.
Tiwari et al.	2016	The solar cell efficiency decreases as cell temperature increases.
Toshniwal and Karale	2013	The use of solar dryers can significantly reduce or eliminate product wastage, food poisoning.
Umogbai and Iorter	2013	The savings in time were achieved as against sun drying as it took three days to dry the maize cobs to a moisture content of 13.3% from 30.3% by using the passive solar dryer while it took six days to dry the cobs to 13.4 % under sun drying.
Yousef and Adam	2012	Increasing of collector length results decreasing the collector thermal efficiency. The using of porous media leads to increasing the collector efficiency and increasing the outlet temperature.
Yang et al.	2014	The instantaneous thermal efficiency could exceed 40% under the typical heating condition even at the low airflow rate 100 m^3/h, the solar radiation on area was about 600 W/m^2, indoor air temperature 14 ^oC, outdoor air temperature -5 ^oC.

Zambrano and Alvarado	1984	The velocity of air at the basal section of the conical chimney was approximately twice that of a cylindrical chimney.

2.6. Summary of literature review evaluation

A comprehensive literature review of solar drying systems including different solar dryers, solar air heaters, chimney effect, photovoltaic thermal systems and applications of software in solar drying have been carried out. These studies were showed the importance of solar air heaters and drying by solar energy. A different solar dryers designs have been showed and the effects of various parameters on drying process performance, the quality of dried products and drying time. The literature proved that the improvement of solar collecting performance would enhance the performance of drying process. The results of solar drying system performances have compared with the results that obtained by the theoretical model, and the predicted and experimental results were in good agreement. The fins located on the absorber increase heat transfer and pressure drop. The results found the fixed fin collector is more effective than free fin collector. The dimensions and design of solar air collectors plays a main aspect to improve the performance of solar drying systems.

The effects of solar chimney and photovoltaic cells have been studied experimentally and theoretically from many authors. PV powered solar dryer offers a good solution to the many problems encountered by farmers in the rural communities. The overall efficiency of the PV/T collector system is the summation of two efficiencies; thermal and electric. The solar photovoltaic cell efficiency decreases as cell temperature increases. Software applications have been used widely with a solar collector and drying applications such as MATLAB, FORTRAN, ANSYS and CFD techniques. Comparison between CFD simulated and measured thermal results showed that at collector outlet there was a good degree of similarity between measured and calculated temperatures.

Based on the results achieved so far in the studied previous works, during the forming of the aims of the recent PhD work, it was a strong initiation for an experimental improvement for the solar air collectors carried out to enhance the process of drying. The shape and dimensions of absorbing surfaces are tested under the conditions of Gödöllő city in Hungary. The different methods of air movements are investigated to show the effect of air speed on solar drying system.

3. MATERIALS AND METHODS

Solar drying refers to a technique that utilizes incident solar radiation to convert it into thermal energy required for drying purposes. Most solar dryers use solar air collectors, and the heated air is then passed through the drying cabin to be dried. The air transfers its energy to the material (product items) causing evaporation of moisture of the material. In order to achieve the goals of this research, the thermal performance of different types of flat plate solar collectors for drying processes will be enhanced and estimated in Szent István University laboratory, Gödöllő city, Hungary.

In this chapter, the used materials and methods for experimental investigation and theoretical analysis are discussed concerning to the solar test rig consists of many principal components to achieve study objectives. Solar drying system consists mainly of solar air collector, drying chamber, chimney, photovoltaic module and inline air blower.

3.1. Solar radiation components and orientation analysis

Radiation is a composition of many wavelengths. 98% of solar radiation is carried by a wave of length $0.3 \leq \lambda \leq 2$ μm. The flux of the solar radiation reaching the earth's outside atmosphere surface is 1367 W/m². This quantity is named the solar constant (Sc).

The total solar radiation on an orientated inclined is the sum of three components: A beam component (direct), a diffuse component (indirect) and a ground-reflected component (see Fig. 3.1). Beam radiation is radiation that arrives at the earth's surface in a straight line from the sun without scattering by water vapor, dust, gases or air pollutant in the atmosphere. On the other hand, diffuse radiation is the rays that reach the earth's surface after scattering by molecules and particles in the atmosphere (gases and moisture). While, the ground-reflected radiation describes sun rays that have been reflected off of non-atmospheric things such as the ground, buildings, and trees. Ground-reflected radiation depends mainly on the reflectivity of the Earth's surface (R), it varies between 0.1 for dark, wet soil or forest to more than 0.9 for fresh snow.

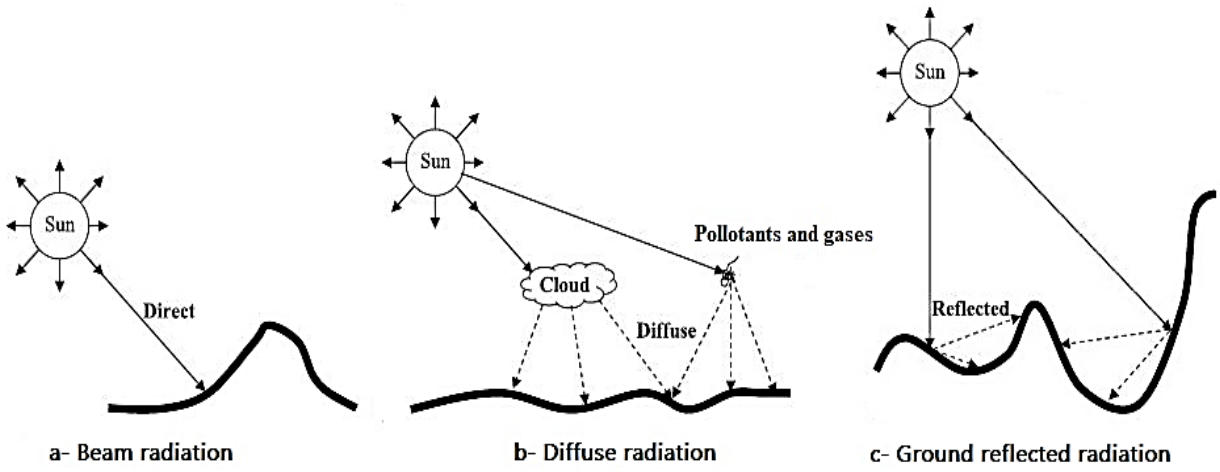

Fig. 3.1. Solar radiation components

The angular relationship between any plane (collector) and the beam radiation line is the most critical issue to have efficient solar collection process. Many angles contribute to beam radiation estimation: (Duffie and Beckman, 2013):

1. Latitude (φ) is the angular location north or south of the equator, for experiments location (Gödöllő) is 47.59° N.
2. Declination (δ) is the angle between the sun ray and the equator plane at noon on the earth's equator. The declination can be estimated for the number of the day in the year (n) from the following equation:

$$\delta = 23.45\ sin\left(360\frac{284+n}{365}\right). \tag{3.1}$$

3. Incidence angle (θ) is the angle between beam radiation on the plane and the perpendicular line to that plane. The following formula can calculate incidence angle:

$$cos\,\theta = sin\,\delta\,sin\,\varphi\,cos\,\beta - sin\,\delta\,cos\,\varphi\,sin\,\beta\,cos\,\gamma + cos\,\delta\,cos\,\varphi\,cos\,\beta\,cos\,\omega + cos\,\delta\,sin\,\varphi\,sin\,\beta\,cos\,\gamma\,cos\,\omega + cos\,\delta\,sin\,\beta\,sin\,\gamma\,sin\,\omega. \tag{3.2}$$

4. Solar hour angle (ω) is the angular displacement of the sun east or west of the local meridian (1-hour corresponding to 15° of angular movement of longitude, with morning positive and afternoon negative)
5. Tilt angle (β) is the angle between the plane and the horizontal.

The sun is constrained by two degrees of freedom in the celestial sphere. As a result, the location of the sun can be specified by two angles. The first is the angle between the horizontal and the line to the sun; it is called solar altitude angle (α_s). While the second is the displacement from south of the projection of beam radiation on the horizontal plane, it is called the solar azimuth angle (γ_s). Solar altitude and azimuth angles can be calculated as follows: (Duffie and Beckman, 2013):

$$sin\,\alpha_s = cos\,\varphi\,cos\,\delta\,cos\,\omega + sin\,\varphi\,sin\,\delta. \tag{3.3}$$

For γ_s in the below equation, the sign is equal to +1 if ω is positive and equals -1 if ω is negative.

$$\gamma_s = \pm\left|cos^{-1}\left(\frac{sin\,\alpha_s\,sin\,\varphi - sin\,\delta}{cos\,\alpha_s\,cos\,\varphi}\right)\right|. \tag{3.4}$$

The intensity of the normal beam irradiation (G_{bn}) at the earth's surface on a bright day can be estimated by the following method (ASHRAE, 1999):

$$G_{bn} = G_o\,e^{\frac{-B}{sin\,\alpha_s}}, \tag{3.5}$$

where (G_o), the apparent extraterrestrial irradiation at air mass zero, and B, the atmospheric extinction coefficient, are functions of the date. The values of the parameters G_o and B given in table 3.1. The Beam radiation component (G_b) on a tilt surface can be determined to incidence angle (θ):

$$G_b = G_{bn}\ \cos\theta\ . \tag{3.6}$$

The diffuse radiation (G_d) component is difficult to estimate because of its non-directional nature and its wide variations. The following equation may be used to evaluate the amount of diffuse radiation that reaches a tilted or vertical surface:

$$G_d = G_{bn}\,C\,F_{ss}, \tag{3.7}$$

where (C), the ratio of the diffuse radiation on a horizontal surface to the direct normal irradiation, given in table 3.1. (F_{ss}) is the angle factor between the surface and the sky, it can be calculated from the following relation:

$$F_{ss} = \frac{1+\cos\beta}{2}. \quad (3.8)$$

The ground-reflected radiation (G_r) from the foreground is given by the following equation:

$$G_r = G_h\, R\, F_{sg}, \quad (3.9)$$

where (G_h), the total horizontal radiation at specified latitude and day. (F_{sg}) is the angle factor between the surface and the earth, calculated from:

$$F_{sg} = \frac{1-\cos\beta}{2}. \quad (3.10)$$

The reflected radiation that reaches any surface depends on the nature of the reflecting surface and the incident angle between the beam radiation and the surface. Fresh snow has the highest reflectance (R=0.87).

Table 3.1. The parameters G_o and B for the 21st day of each month (ASHRAE, 1999)

	Jan	Feb	Mar	Apr	May	June	July	Aug	Sept	Oct	Nov	Dec
G_o (W/m^2)	1230	1215	1186	1136	1104	1088	1085	1107	1152	1193	1221	1234
B	0.142	0.144	0.156	0.180	0.196	0.205	0.207	0.201	0.177	0.160	0.149	0.142
C	0.058	0.060	0.071	0.097	0.121	0.134	0.136	0.122	0.092	0.073	0.063	0.057

The total solar radiation (G_T) of a terrestrial surface of any orientation and tilt with an incident angle (θ) is the sum of the beam component (G_b) plus the diffuse component (G_d) coming from the sky plus whatever amount of reflected radiation (G_r) may reach the surface from the earth or adjacent surfaces:

$$G_T = G_b + G_d + G_r. \quad (3.11)$$

3.2. Thermal analysis of solar collectors

In this section two kinds of flat-plate solar air collector are discussed and analysed with single and double air passes. In order to calculate the heat transfer and overall heat loss coefficients, a detailed thermal analysis of all components of the collector is required. To avoid some difficulties, many assumptions are considered as follows:

1. Steady state heat transfer.
2. One dimensional heat transfer.
3. Wind speed approximately constant.
4. Homogenous air flow through collectors.
5. No dust and dirt on the cover of the collector.
6. No leakages are in airflow section.
7. No mass transfer in the collectors.
8. Thermal properties of absorbers are constant.

3.2.1. Thermal analysis of single air pass solar collector

Fig. 3.2 shows the heat transfer coefficients network of single air pass solar collector.

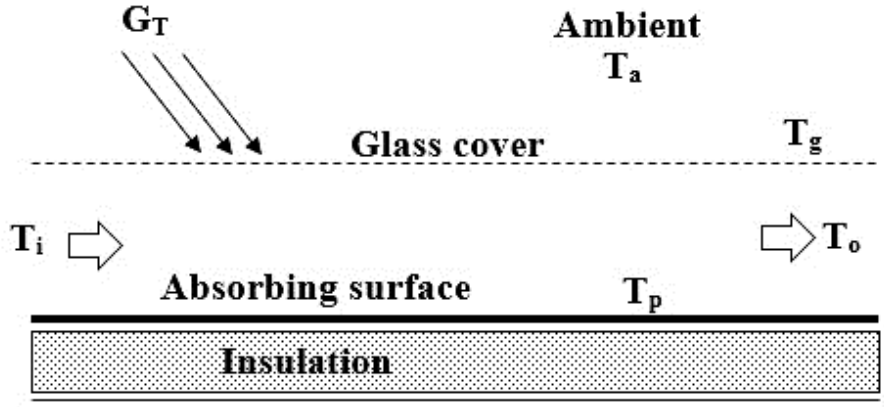

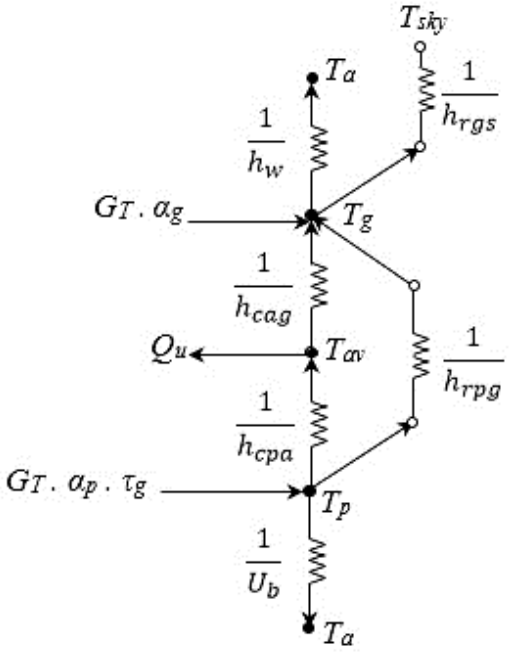

Fig. 3.2. Single-pass solar collector heat transfer network

The notations in Fig. 3.2 are as follows:

T_i, T_o, T_{sky}, T_a, T_g, T_{av}, and T_p: collector inlet, collector outlet, sky, ambient, glass transparent cover, average flow air and average absorbing surface temperatures (^oC) respectively,

h_w, h_{cag} and h_{cpa}: wind, ambient-glass transparent cover and absorbing surface-flow air convection heat transfer coefficients ($W/m^2 K$) respectively,

h_{rgs} and h_{rpg} : sky-glass transparent cover and absorbing surface-glass transparent cover radiative heat transfer coefficients ($W/m^2 K$) respectively,

G_T and Q_u: instantaneous global solar radiation intensity and useful heat gained from solar air collector respectively (W),

U_b and U_t: collector back and top heat loss coefficients ($W/m^2 K$) respectively,

α_g, α_p and τ_g: glass transparent cover absorptivity, absorbing surface absorptivity and glass transparent cover transmissivity respectively.

Steady state energy balance equations (3.12), (3.13) and (3.14) for transparent glass cover, absorbing surface and air flow channel of solar air collector can be written respectively as:

$$G_T.\alpha_g + h_{rpg}(T_p - T_g) + h_{cag}(T_{av} - T_g) = h_w(T_g - T_a) + h_{rgs}(T_g - T_s), \quad (3.12)$$

$$G_T.\alpha_p.\tau_g = h_{rpg}(T_p - T_g) + h_{cpa}(T_p - T_{av}) + U_b(T_p - T_a), \quad (3.13)$$

$$Q_u + h_{cag}(T_{av} - T_g) = h_{cpa}(T_p - T_{av}). \quad (3.14)$$

The value of radiative heat transfer coefficients h_{rgs} and h_{rpg} can be estimated from: (Karim et al. 2013) and (Fudholi, 2011):

$$h_{rpg} = \frac{\sigma\,(T_p + T_g)\,(T_p^2 + T_g^2)}{\frac{1}{\varepsilon_p} + \frac{1}{\varepsilon_g} - 1}, \quad (3.15)$$

$$h_{rgs} = \sigma.\varepsilon_g \frac{(T_g + T_s)(T_g^2 + T_s^2)(T_g - T_s)}{(T_g - T_a)}, \quad (3.16)$$

where:

σ: Stefan-Boltzman constant equal 5.67×10^{-8} J/s m^2 K^4 (Duffie and Beckman, 2013),
ε_g *and* ε_p *:* emissivity of the glass cover transparent and absorbing surface respectively.

Sky temperature T_s can be estimated from: (Fudholi, 2011):

$$T_s = 0.0552\, T_a^{1.5}. \quad (3.17)$$

Wind convection heat transfer coefficient with wind speed V_m can be estimated from (Ma et al., 2011):

$$h_w = 2.8 + 3\, V_w\,. \quad (3.18)$$

The back U_b heat loss coefficient has been calculated by the basic conduction heat transfer resistance. For insulation layer with thickness X_b and material thermal conductivity K_b: (Ong, 1995):

$$U_b = \frac{h_w\ K_b}{X_b\ h_w + K_b}\,. \quad (3.19)$$

The connective heat transfer coefficients h_{cag} and h_{cpa} can be estimated by assuming equal convection heating in a rectangular duct. The convection heat transfer coefficient is *h* represent the net coefficient for transferred heat from duct walls to the flowing air. The value of *h* can be calculated from Nusselt's number formula according to Reynold's number *Re* as:

$$Nu_D = \frac{h\ D_h}{K_a}, \quad (3.20)$$

$$Re = \frac{\dot{m}\ D_h}{A_{channel}\ \mu}\,. \quad (3.21)$$

The value of *Nu* depends mainly on the type of flow. Reynold's number *Re* is a dimensionless value which represents the natural of flow.

If *Re* less than 2300, then the flow is laminar. If 2300 < *Re* < 6000, then the flow in transition region. If *Re* more than 6000, then the flow is turbulent. Eq. (3.22) to (3.24) shows Nusselt's number empirical formulas for three flow streams forms respectively as:

$$Nu_D = 5.4 + \frac{0.0019\ \left[Re\ \mathrm{Pr}\left(\frac{D_h}{L}\right)\right]^{1.71}}{1+0.00563\ \left[Re\ \mathrm{Pr}\left(\frac{D_h}{L}\right)\right]^{1.17}}, \tag{3.22}$$

$$Nu_D = 0.116\ \left(Re^{\frac{2}{3}} - 125\right)\ Pr^{\frac{1}{3}} \left(1 + \left(\frac{D_h}{L}\right)^{\frac{2}{3}}\right) \left(\frac{\mu}{\mu_w}\right)^{0.14}, \tag{3.23}$$

$$Nu_D = 0.0158\ Re^{0.8}, \tag{3.24}$$

where:

$\dot{m}$: air mass flow rate through solar collector (kg/s),
$A_{channel}$: cross section area of solar collector air channel (m^2),
$P_{channel}$: the perimeter air channel (m),
K_a : air thermal conductivity (W/m K),
L : solar collector air channel length (m),
μ and μ_w : dynamic viscosity of air at bulk and channel wall temperatures respectively (kg/m s),
Pr : Prandtl number (dimensionless),
D_h : hydraulic diameter of rectangular air channel (m), can be calculated from:

$$D_h = \frac{4\ A_{channel}}{P_{channel}}. \tag{3.25}$$

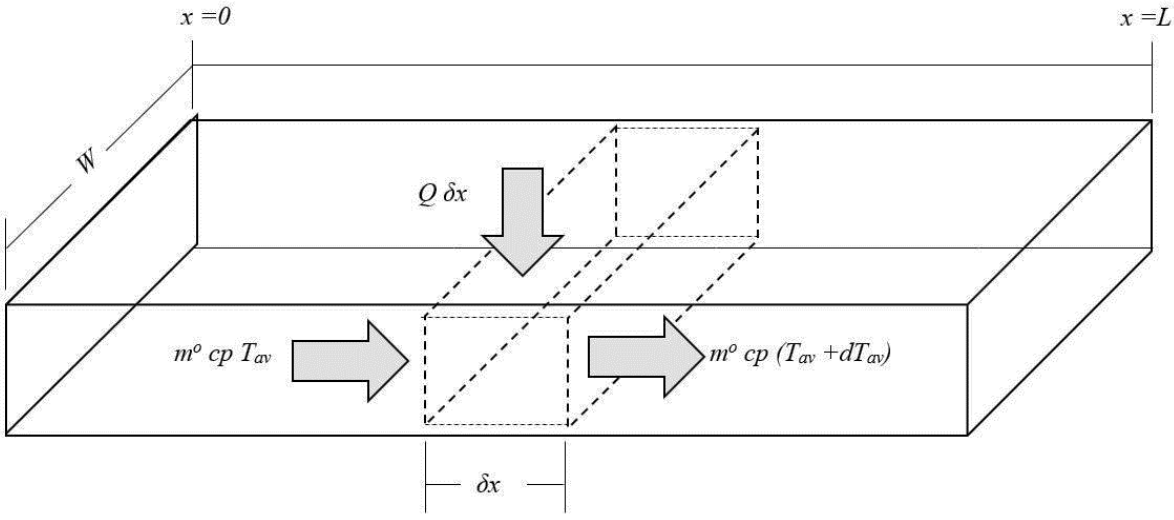

Fig. 3.3. Double-pass solar collector heat transfer scheme

The useful heat gained can be derived from temperature distribution analysis in the direction of air flow (see Fig. 3.3). If the gained useful heat is uniform along the collector channel length L, therefore the integrated equation of temperature differences can be as following:

$$\dot{m}\ Cp\ T_{av} + Q_u\ W\ x = \dot{m}\ cp\ \left(T_{av} + \left(\frac{dT_{av}}{dx}\right)\delta x\right). \tag{3.26}$$

If the average air temperature in solar collector channel is:

$$T_{av} = \frac{T_i + T_o}{2}. \tag{3.27}$$

By substitution Eq. (3.16) in Eq. (3.26), the value of useful heat gained can be as following:

$$Q_u = \frac{2\ \dot{m}\ Cp}{W\ L}\ (T_{av} - T_i), \tag{3.28}$$

where:

c_p: flow air specific heat at constant pressure (J/kg ^oC),
W: width of absorbing surface (m).

Finally, by substituting the formulas of radiative heat transfer coefficients, convective heat transfer coefficients and useful heat in Eq. (3.12) to (3.14), the values of temperatures can be calculated. The temperatures T_i, T_g, $T_{av,}$ and T_p can be obtained numerically by using any computer program.

3.2.2. Thermal analysis of double air pass solar collector

Fig. 3.4 shows the heat transfer coefficients network of double air pass solar collector.

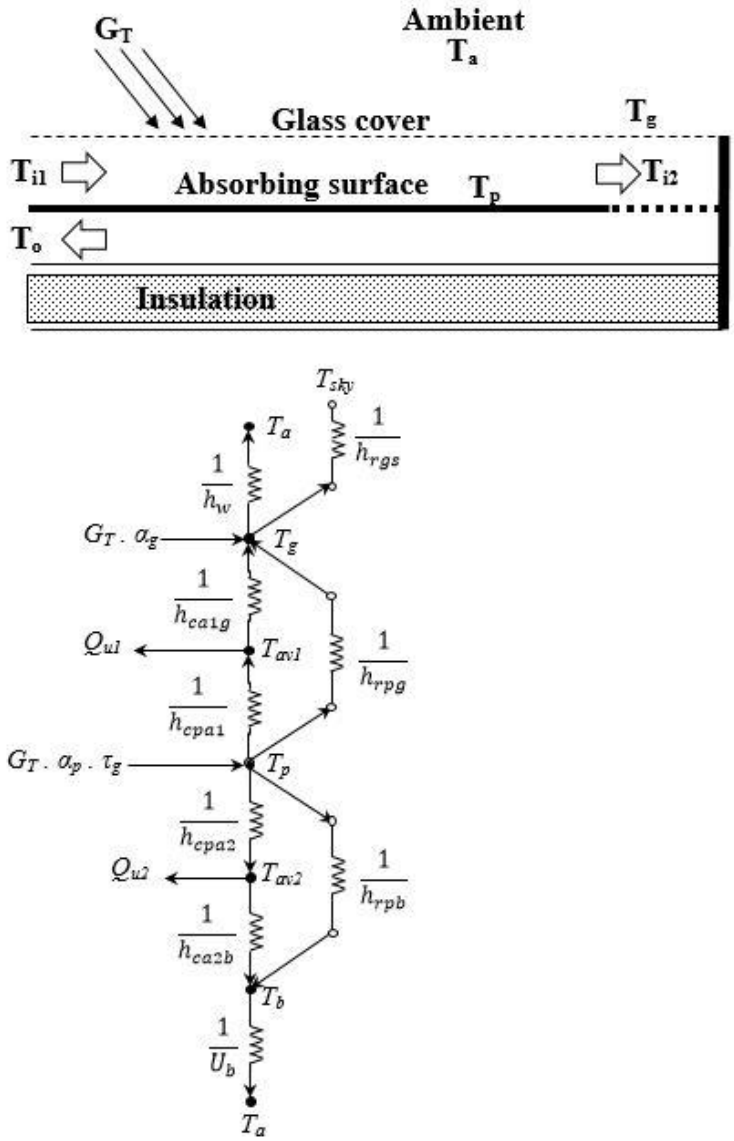

Fig. 3.4. Double-pass solar collector heat transfer network

The procedure to drive the energy formulas of double solar collector is the same steps which followed in single pass solar collector. So, the steady state energy balance equations for transparent glass cover, absorbing surface, upper and lower air flow channel of solar air collector can be written respectively as:

$$G_T\,\alpha_g + h_{rpg}(T_p - T_g) + h_{ca1g}(T_{av1} - T_g) = h_w(T_g - T_a) + h_{rgs}(T_g - T_s), \qquad (3.29)$$

$$G_T\,\alpha_p\tau_g = h_{rpg}(T_p - T_g) + h_{cpa1}(T_p - T_{av1}) + h_{rpb}(T_p - T_b) + h_{cpa2}(T_p - T_{av2}), \quad (3.30)$$

$$Q_{u1} + h_{ca1g}(T_{av1} - T_g) = h_{cpa1}(T_p - T_{av1}), \quad (3.31)$$

$$Q_{u2} + h_{ca2b}(T_{av2} - T_b) = h_{cpa2}(T_p - T_{av2}). \quad (3.32)$$

The radiative heat transfer coefficients can be calculated from Eq. (3.15) and (3.16). Convective heat transfer coefficients are estimated in the same way of Eq. (3.20) to (3.24). The value of useful heat gained from upper and lower collector's channels Q_{u1} and Q_{u2} are:

$$Q_{u1} = \frac{2\,\dot{m}\;c_p}{W\;L}\,(T_{av1} - T_{i1}), \quad (3.33)$$

$$Q_{u2} = \frac{2\,\dot{m}\;c_p}{W\;L}\,(T_{av2} - T_{i2}). \quad (3.34)$$

3.3. Thermal analysis of drying chamber

The total energy required for drying process for given quantity of any products items can be determined by using the basic energy balance equation for the evaporation of water, as shown in Fig. 3.5.

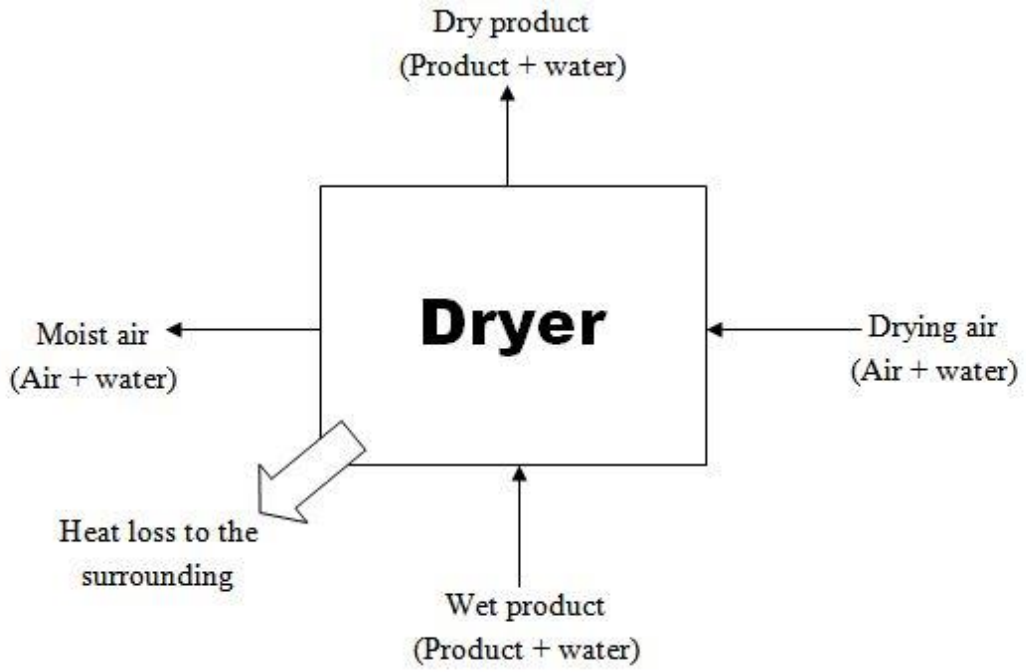

Fig. 3.5. Drying chamber energy balance diagram

According to the schematic diagram of dryer heat balance, the basic energy balance equation (mass and heat), can be written as follows:

$$Q_{air,inlet} + Q_{product,inlet} = Q_{air,outlet} + Q_{product,outlet} + \textit{energy losses}. \quad (3.35)$$

For perfect system insulated, the value of energy losses from the drying chamber will be very small; it can be neglected. Then, the latent energy of the evaporated water from the product with mass W_v and latent energy of vaporization equal L_v will equal the heat lost from the air which flowed through the dryer. Mathematically:

$$W_v\;L_v = \dot{m}\;c_p\;(T_{d,i} - T_{d,o}), \quad (3.36)$$

where:

$T_{d,i}$ and $T_{d,o}$: flow air inlet and outlet temperatures through the dryer (°C),
W_v: the mass of water evaporated from the product (kg), can be calculated from:

$$W_v = m_i \frac{w_i - w_f}{100 - w_f}, \quad (3.37)$$

where:

m_i: the initial mass of product items (kg),
w_i: the initial moisture content of dried product (%),
w_f: the final moisture content of dried product (%).

During the drying process, water at the surface layer of the product evaporates and water in the inner part transfer gradually to the surface to get evaporated. The ability of this water movement depends on the porosity of the product item material and the surface area available.

The basic theory of drying process was described by Lewis (1921) based on the partial similarity with Newton's law of cooling and is often used to mass transfer in thin-layer drying as following (Mahendra et al., 1987):

$$\frac{dw}{dt} = -k_d(w - w_e), \quad (3.38)$$

where:

k_d: drying process constant,
w_e: an equilibrium mass (kg).

By solving the above differential Eq. (3.38) for the conditions, at $t=0$, $w= w_o$ and at $t=\infty$, $w=w_e$, the solution will be as:

$$\frac{w_t - w_e}{w_o - w_e} = -e^{-kt}, \quad (3.39)$$

where w_t is the moisture content of dried product at time t. The term $-e^{-kt}$ in Eq. (3.39) called moisture ratio MR, then:

$$MR = \frac{w_t - w_e}{w_o - w_e}. \quad (3.40)$$

The product items material stills for a long time at a fixed temperature and relative humidity then they will reach eventually gradually an equilibrium moisture content with the moist air.

The equilibrium state does not mean that the product item and the air have the same moisture content. It simply means that an equilibrium condition exists such that there is no net exchange of moisture (latent heat energy) between the product material and the heated air. This equilibrium moisture content w_e is a function of the temperature, the relative humidity, and type of the dried product.

3.4. Solar collectors location and orientation

The location of the solar collectors is a critical aspect of efficient sun energy collection. The factor of shadowing should be considered (trees or surrounded buildings). As shown in Fig. 3.6, collector's location has been chosen according to the fact that the shadow effect will have no impact on the collector efficiency.

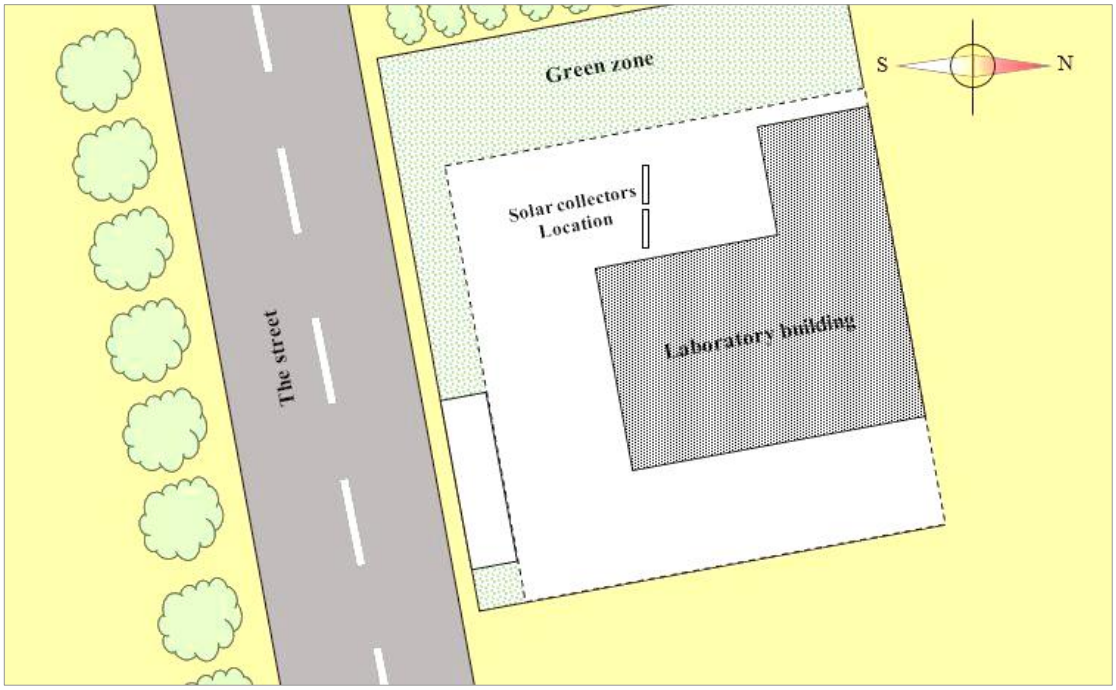

Fig. 3.6. Solar collector's system location

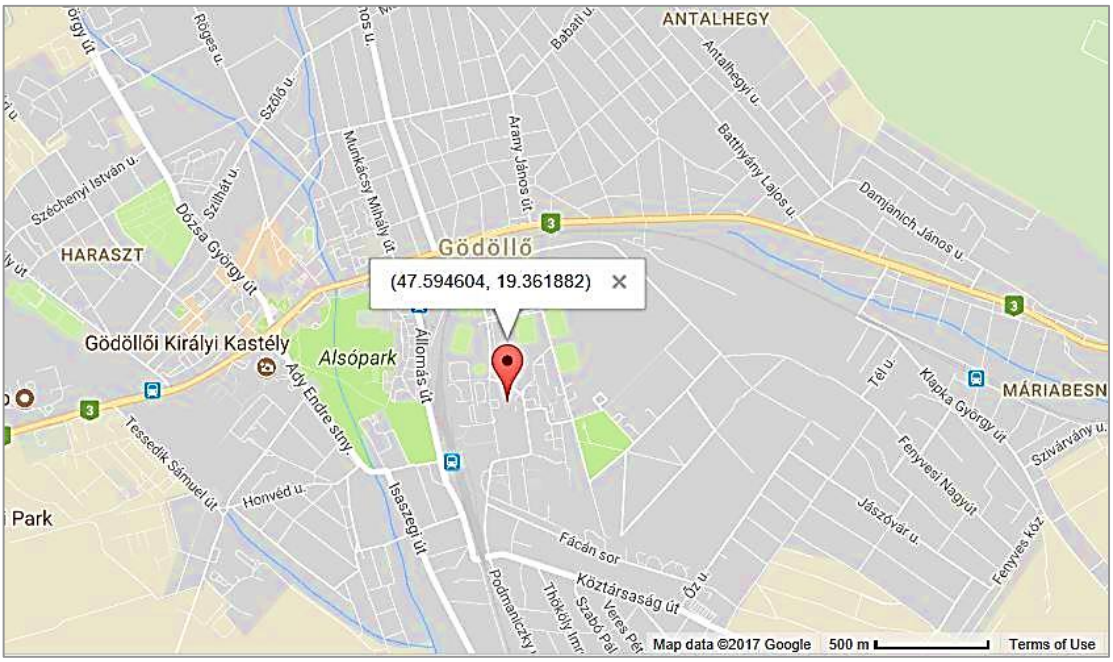

Fig. 3.7. Latitude and longitude of experiments location (Google map, 2018)

The orientation of the solar collector is described by its azimuth and tilt angles. The optimum tilt angle (β) and direction play an important factor in enhancing solar energy collection of solar collectors. Flat plate solar collector, it is always tilted in such a way that it receives maximum solar radiation during the day and to be perpendicular to solar radiation rays at noon.

The best stationary orientation is due south in the northern hemisphere and due north in the southern hemisphere (Duffie and Beckman, 2013) and (Waziri et al., 2014). Therefore, the solar air collectors in this work are oriented facing south line and tilted at 45^{o} to the horizontal according to the solar chart for the region as shown in Fig. 3.7 (47.59^{o} N, 19.36^{o} E).

3.5. Design and structure of solar collectors

The flat plate solar air heater has the same method of the heat exchanger, convert solar radiation energy into heat energy, which is passed on through convection from the absorber plate to the air. In the present work, three solar air collectors are designed and built in mechanical engineering department laboratory in Szent Istvan University. The first solar collector is single air pass while second and third are double air pass solar collectors. The main parts of each; absorbing surface, external box, transparent glass cover, and back insulation (see Fig. 3.8). These parts are explained in details in the next sections.

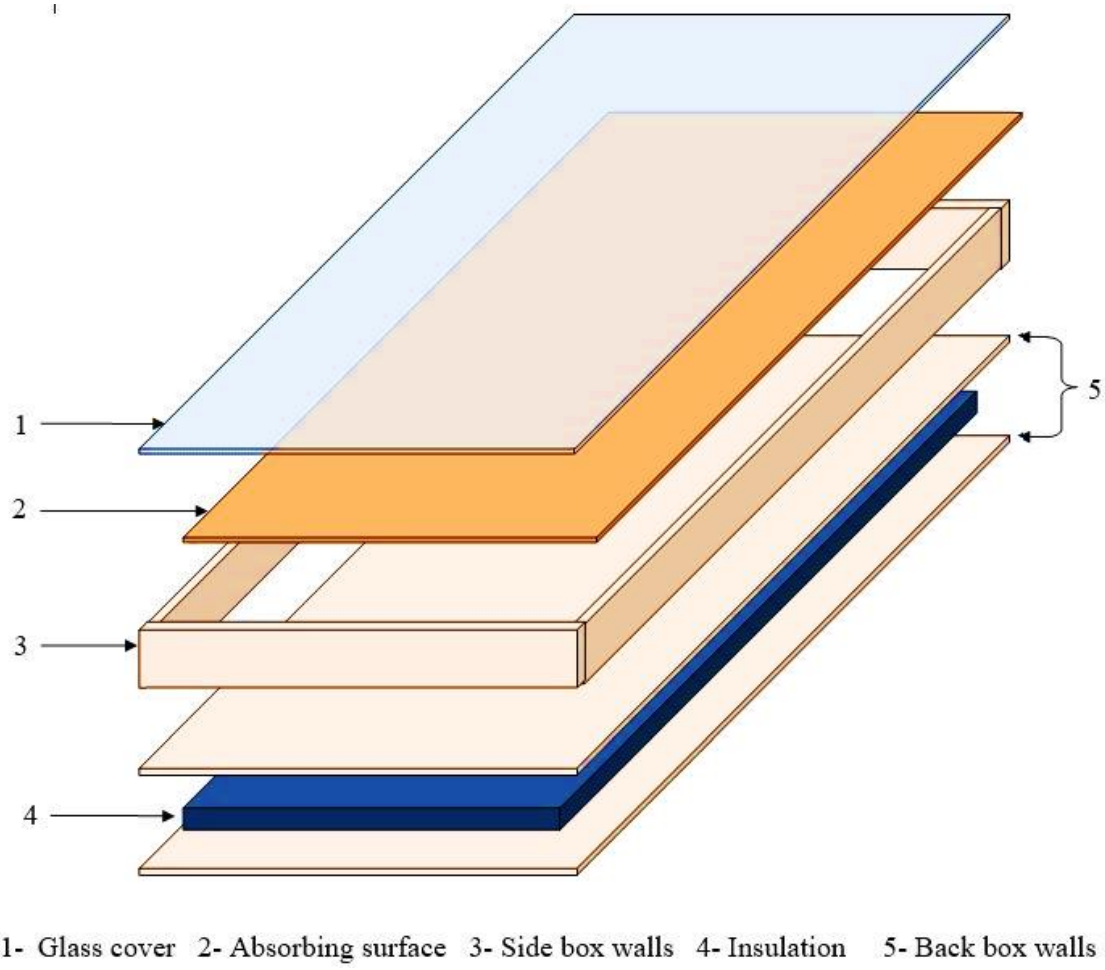

Fig. 3.8. Solar air collector main components

For study purpose, five absorbing surfaces are made from copper plate sheet with 1.2 mm thickness and thermal conductivity 385 W/m K as shown in Figs 3.9-13. To enhance these surfaces (selective surface) a black matt paint (black chrome) used to coat copper absorbing surfaces. Selective surfaces combine a high absorptance for radiation with a low emittance for the temperature range in which the surface emits radiation. Black paint also enables much of the absorbed energy to be lost by emittance (Madhukeshwara and Prakash, 2012).

The sizing of the collector components were designed according to the size of the drying chamber. The first is flat absorber (un-finned) with dimensions 46.2×121.8 cm length and width respectively. The second and third absorbing surfaces had made with the same dimensions of the the first surface with horizontal and vertical 18 fins to increase its area of surface. The forth is made with 45^{o} rectangular fins. An aluminium helical fins are attached to the copper surface of the

fifth absorbing surface. Fins function is expanding air stream length with the absorber surface to improve the useful heat transfer to the air. The space between every two lines of fins was 17 m. for double pass collector, 25 holes made on the absorber with the same area of the air inlet and exit to recirculate the air from the first to the second air channel.

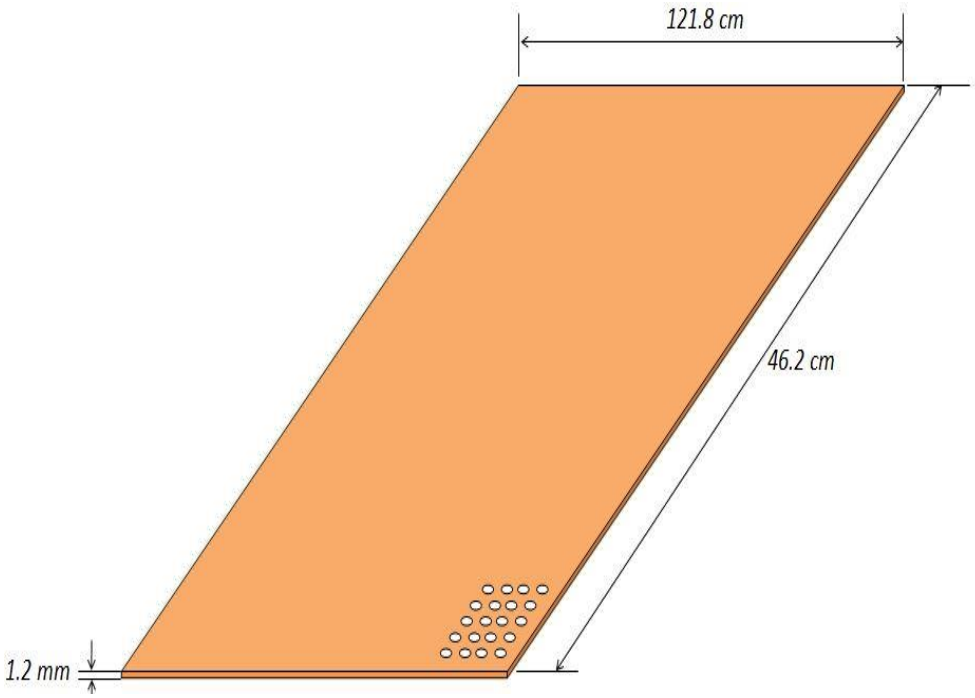

Fig. 3.9. Un-finned absorbing surfaces dimensions

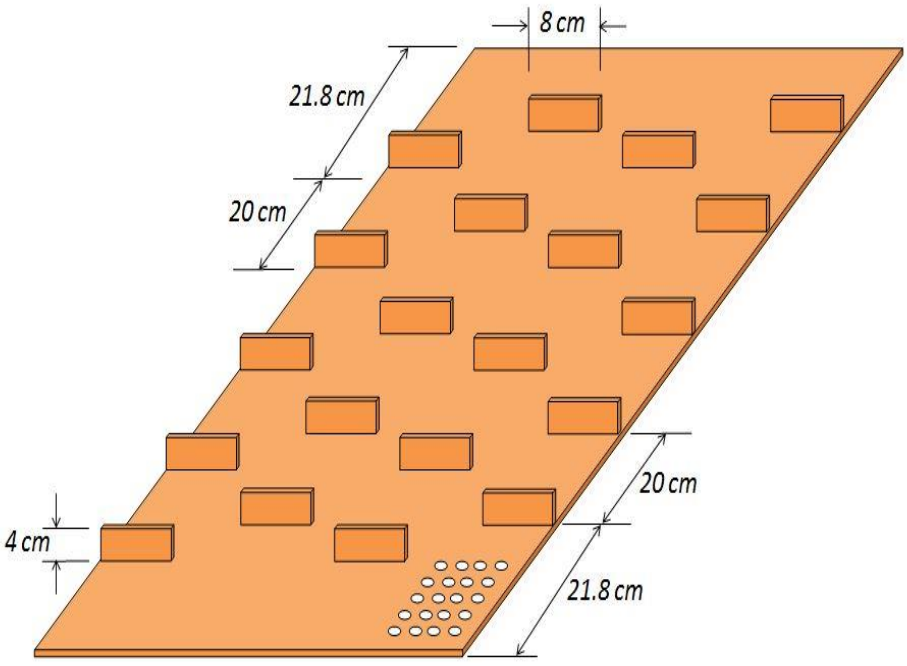

Fig. 3.10. Horizontally finned absorbing surfaces dimensions

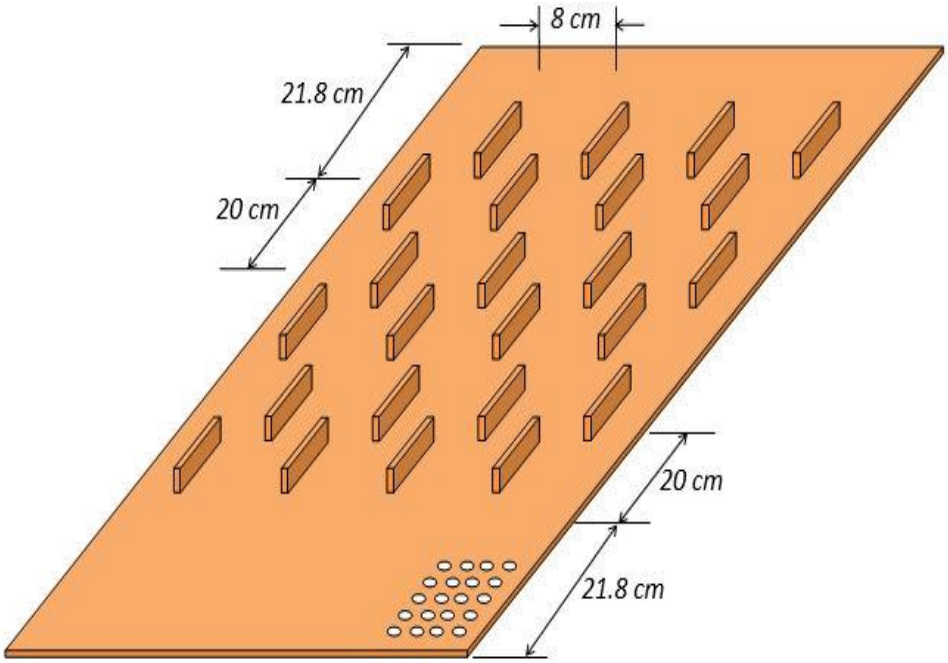

Fig. 3.11. Vertically finned absorbing surfaces dimensions

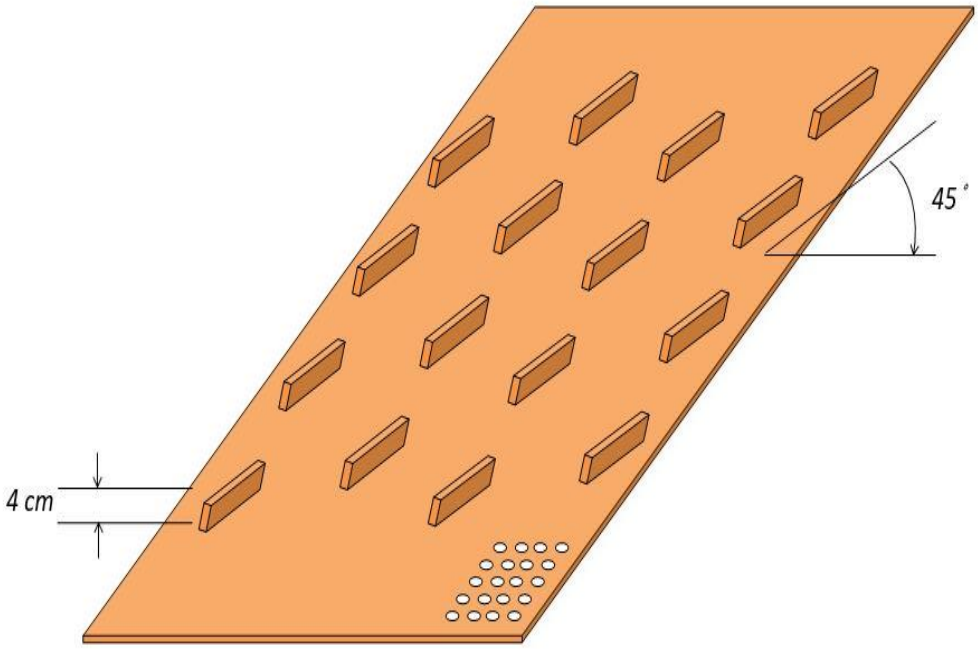

Fig. 3.12. 45^{o} inclined finned absorbing surfaces dimensions

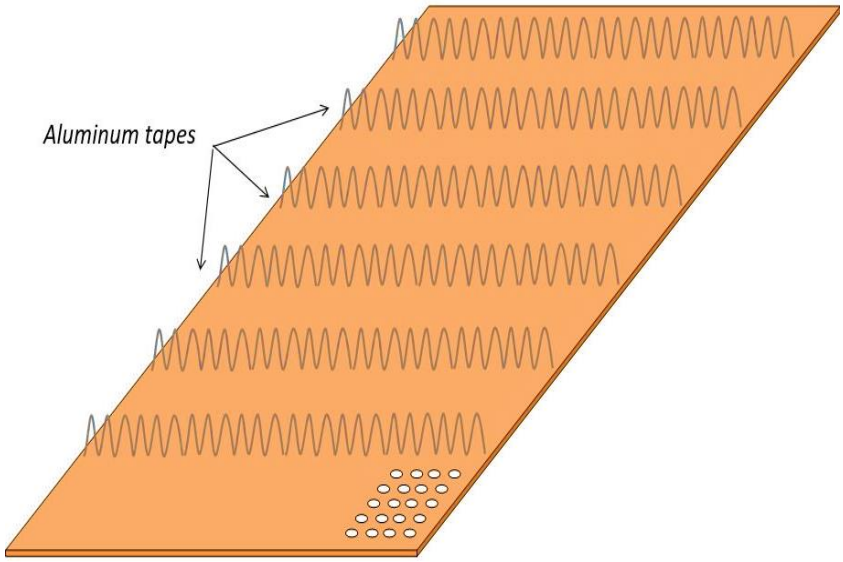

Fig. 3.13. Helically finned absorbing surface and fin dimensions

The dimensions of rectangular fin are 4 cm and 10 cm length and width respectively. The helical fins had been made from aluminium sheets with thickness 0.5 mm and fixed on the absorbing surface as shown in Fig. 3.13. The dimensions of fin are 66.2 cm and 4 cm length and width respectively. Nine fins are attached on absorbing and painted by black matt paint. The areas of five absorbing surfaces are shown in Table 3.2.

Table 3.2. The total exposed area to solar radiation for absorbing surfaces

Surface	Flat area	Holes area	Fins area	Total area
Un-finned surface (single-pass)	46.2×121.8 ≈ 0.5627 m^2	0	0	0.5627 m^2
Un-finned surface (double-pass)	0.5627 m^2	25×(π/4)×(1)^2 ≈ - 0.002 m^2	0	0.5607 m^2
Horizontally finned (double-pass)	0.5627 m^2	- 0.002 m^2	18×2×4×10 ≈ 0.144 m^2	0.7047 m^2
Vertically finned (double-pass)	0.5627 m^2	- 0.002 m^2	0.144 m^2	0.7047 m^2
45^o finned (double-pass)	0.5627 m^2	- 0.002 m^2	0.144 m^2	0.7047 m^2
Helically finned (double-pass)	0.5627 m^2	- 0.002 m^2	9×2×66.2×4 ≈ 0.476 m^2	1.036 m^2

The external dimensions of solar heater are 120×50×15 cm length, width and thickness respectively. The external box of solar collectors is made from wood sheets and bars with different thicknesses with dimensions. Wood had been chosen for many important reasons that were taken into account which are lighter in weight rather than using metal, the low cost, easy to form and

can be considered as insolation specially at very low temperatures. The second air channel of double pass solar collector was designed with many attached buffers which fixed on back surface of solar collector. Buffers function is to increase air stream length with the absorber surface to enhance the useful heat transfer to the air. The space between every two buffers is 17 m. Wooden-made zigzag baffles are attached in the lower channel in order to give homogenous air distribution under absorber surface. The areas of inlet, exit and second channel entrance of solar air collector are the same, to avoid pressure reduction through solar air collector.

The sides of the body were well insulated to prevent heat loss by using self-adhesive rubber foam tape with thickness of 3 mm. Fig. 3.14 and Fig. 3.15 show the first and second channels of solar air collector with details.

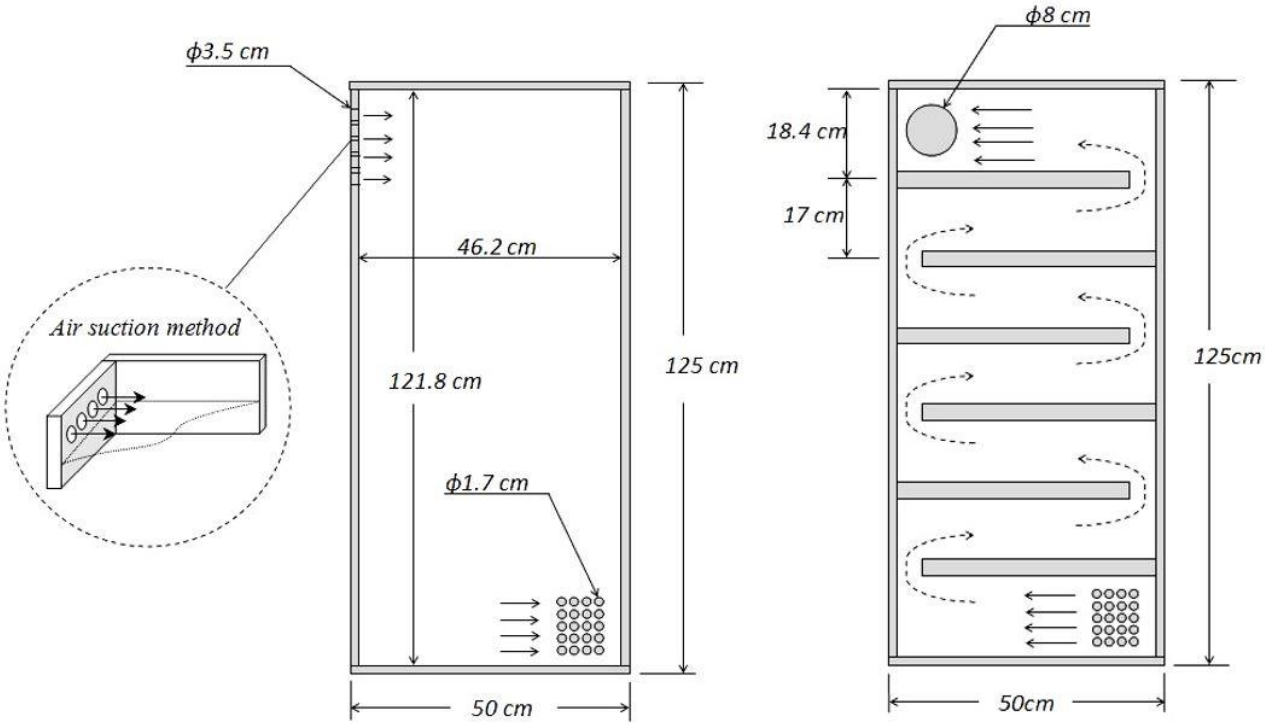

Fig. 3.14. First and second air pass of solar air heaters design

At the back side of the collector, sheets of expanded polystyrene insulation (EPS) with smooth edges fixed at the bottom base side of the wooden box. The heat transfer coefficient of back insulation is 0.036 W/mK. Back insulation thickness is 2 cm and dimensions are 120×50 cm length and width respectively. The sides of the body were well insulated to prevent heat loss by using self-adhesive rubber foam tape with thickness of 3 mm.

A transparent glass cover fixed on the top edges of the heater wood case and thermal insulation at the bottom base side of the wooden case. The transparent cover made from high quality hard thermal plastic glass with 4 mm and 0.16 W/mK thickness and heat transfer coefficient, respectively. Cover dimensions are 120 cm×50 cm length and width respectively. The remaining space between the absorber plate and glass cover represents the upper air flow channel with 57.5 mm height. It is important in the solar air collector components arrangements, tight any air leakage because the leakage of air will effect on the performance of the solar collector (especially air temperature) and decrease its thermal efficiency.

Fig. 3.15. First and second air pass of solar air heaters manufactured

All the mentioned parts are arranged together to produce the final structure of single and double solar air collectors with different absorbers geometries as shown in Fig. 3.16. The solar units ordinated to the south on a simple iron frame to be ready to connect them with other parts of solar drying system.

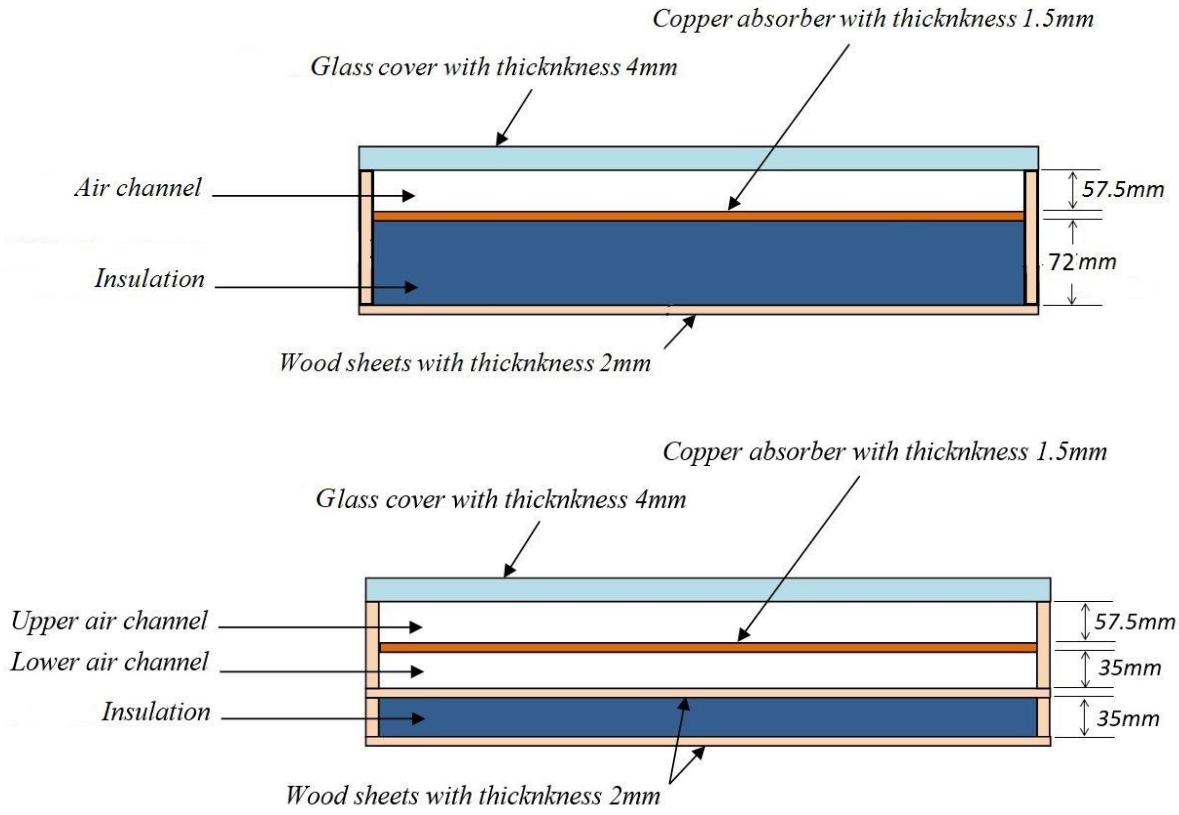

Fig. 3.16. Cross section view of single and double pass solar collectors

3.6. Design and structure of drying chambers

The second essential part of drying system is drying chamber (drying cabin). In this study, polystyrene blocks with 5 cm thickness and thermal conductivity 73 W/m K had been used to build drying chamber. This material was used due to many important reasons; which are low thermal conductivity (insulated), cheap, easy to preform it and light.

The drying chamber (the dryer) with five trays for the different products items is made from. The drying cabin dimensions are 50 cm×50 cm×100 cm length, width, and height, respectively as shown in Fig. 3.17. The dimensions of the chamber and the tray numbers were set-up according to the practical drying requirements. Dryer walls have been made from polystyrene, except the front wall of the chamber made from 4 mm plastic glass sheet for observing. The five trays made from plastic nets and fixed with 10 cm distance between them as shown in Fig. 3.18. The dimensions of every tray are 38 cm × 40 cm length and width respectively. The chamber is integrated with the solar collector by a small duct (indirect drying), then the exit heated air from the collector enters the chamber with high temperature and low humidity. The moist and hot air rises and escapes from the upper vent of drying chamber. Inlet and outlet of drying chamber have a diameter 10 cm with a small slop angle for the upper side of the chamber to keep the smooth movement of the air.

Also, all air leakages from drying space closed totally as possible. The product sample which used through this study is apple. Apple selected as a sample (see Table 3.3) because of its high initial moisture content and its high maximum allowable temperature. The initial moisture content and maximum allowable temperature for apple during drying process are 80% (wet base) and 70 ^{o}C respectively as it was reported by Sharma et al., (2009).

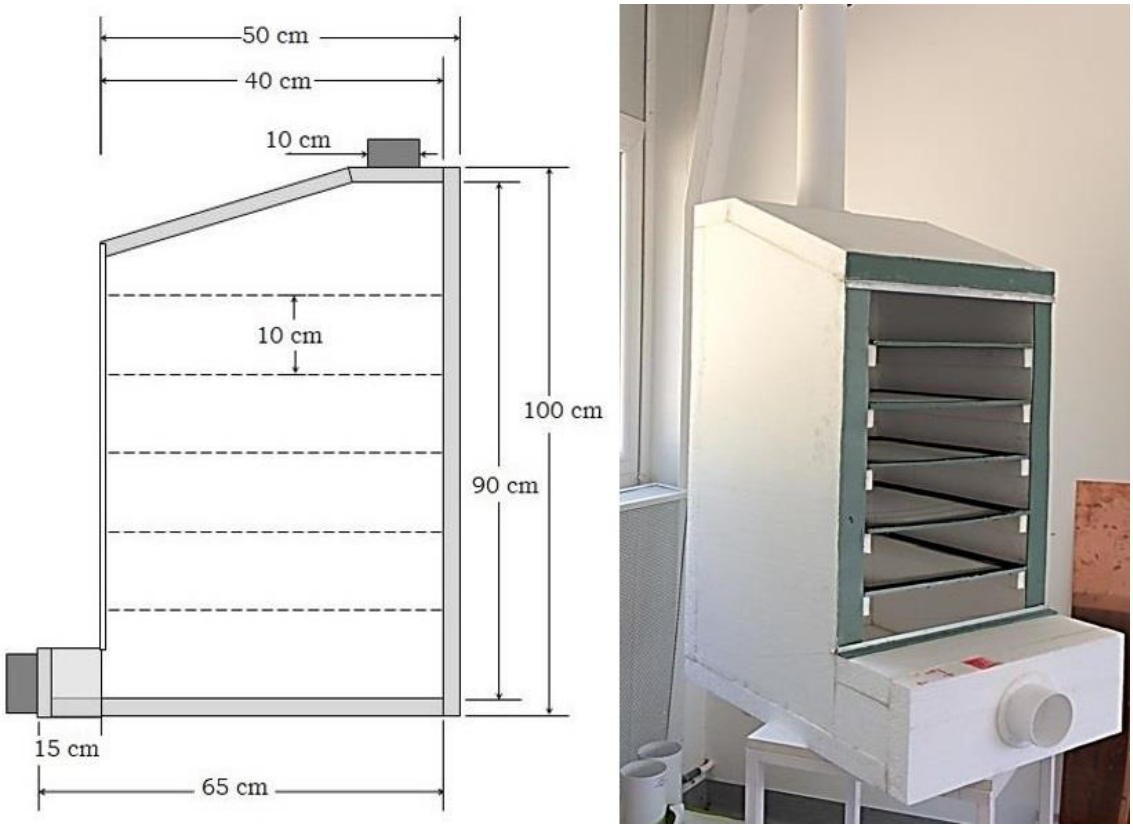

Fig. 3.17. Drying chamber dimensions and illustration

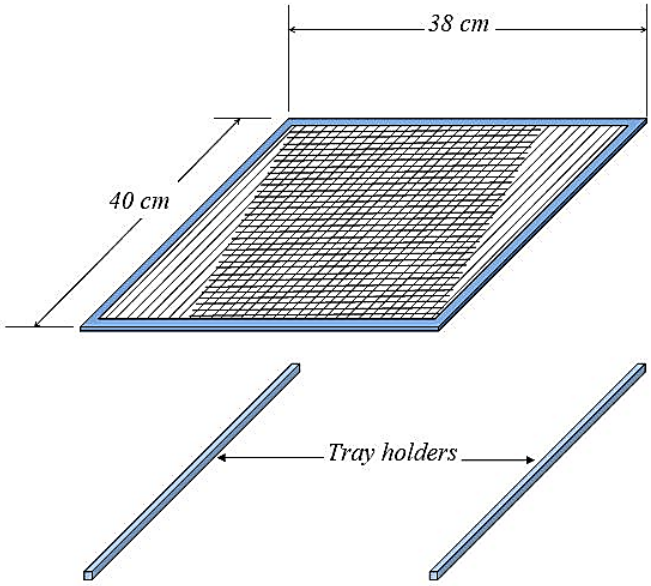

Fig. 3.18. Tray dimensions and installation

Table 3.3. Dried product specifications (apple slices)

Parameter	Value
Initial moisture content	80% (wet base)
Desired final moisture content	24%
Maximum allowable temperature	70 ^{o}C
Average thickness of slices	4 mm
Average diameter of slices	65mm
Initial total weight	2000 g
Type of air flow	turbulent

3.7. Chimney design and structure

The chimney increases the amount of air flow, through the solar dryer by speeding up the flow of the exhaust air. Hence the effects of natural convection will be improved by adding a chimney in which exiting air is heated even more and enhance the buoyant flow of air. The chimney should be designed so that the rate of heat losses within the chimney should be considered in determining the optimum height of the chimney so as not to exceed the height at which the chimney air cools to same temperature as ambient. The design will maintain mean chimney temperatures above ambient temperature. In ideal gases when the temperature increases, the density decrease, thus a movement between the cold and warm zones appears. This movement is knowledge as Stack effect. The pressure ΔP_{stack} difference of the stack effect is shown in the following equation:

$$\Delta P_{stack} = g\ H\ \Delta\rho, \tag{3.41}$$

where:

g: acceleration due to gravity (m/s^2),
H: height of the chimney (m).

In the flowing condition, the mean temperature inside the chimney is relatively higher than the ambient air temperature. In this case, there exists a pressure head which creates an upward air flow. Therefore the relation among the buoyancy force that is the pressure drop that creates the air flow, the height, density difference of the ambient air and chimney is related as follows:

$$\Delta P_b = \rho\, g\, H\, (T_{ch} - T_a\,). \tag{3.42}$$

Over the temperature range 25-90 °C, the density of dry air is related to the temperature by the following empirical expression:

$$\rho = 1.11363 - 0.00308\, T. \tag{3.43}$$

By substituting Eq. (3.43) into Eq. (3.42):

$$\Delta P_b = 0.00308\, g\, H\, (T_{ch} - T_a\,). \tag{3.44}$$

Within the chimney, pressure drops are due mainly to wall friction. Assuming turbulent flow, the pressure drop due to friction loss can be given as:

$$\Delta P_b = f \frac{\acute{\rho}\, v^2 H}{2D}, \tag{3.45}$$

where

$\acute{\rho}$: is the average density of fluid through the cylindrical duct. Combining Eq. (3.44) and Eq. (3.45):

$$f \frac{\acute{\rho}\, v^2 H}{2D} = 0.00308\, g\, H\, (T_{ch} - T_a\,). \tag{3.46}$$

By assuming turbulent air flow with a friction coefficient *f* of 0.035, thus:

$$v = 0.453 \left[\frac{D\, g\, \Delta T_{ch}}{\acute{\rho}}\right]^{½}. \tag{3.47}$$

The velocity is a function of temperature change across the chimney. It should be noted that the above expression is derived without taking into account the additional buoyancy arising from the increased humidity of the air stream.

Experimentally, the chimney had been built from plastic material with flexible length from 0.5 m to 1.5 m. It has a circular cross section with 10 cm diameter. The chimney is tested with three different lengths 50 cm, 100 cm and 150 cm.

3.8. Solar drying system accessories

Many accessories and minor devices are arranged with the solar drying system to achieve the purpose of this experimental work such as air blower, photovoltaic module, electrical power supply regulator, and insulated air ducts.

3.8.1. Inline air blower

To circulate the air through the solar drying system, air inline blower in air duct between solar heater and drying chamber has been used. The suction and discharge of blower is bigger than ducts with 10.5 cm diameter. The blower works with 12 V and 270 CFM. A circulation duct of 10 cm diameter is used to circulate air through the solar drying system. These ducts were insulated by using a 1 cm thickness of special type of polystyrene to decrease heat loss to the surroundings. The scheme of the drying chamber and blower dimensions is shown in Fig. 3.19.

3.8.2. Photovoltaic modules

A two photovoltaic modules were installed in the same direction and tilt angle of solar air collectors to supply the electrical power to the blowers as shown in Fig. 3.20. The modules are connected to power supply regulator to supply constant voltage. The modules system voltage is 12 V.

3.8.3. Power supply controller

A laboratory power supply controller type Voltcraft PS 1440 was using to supply and control the electrical power to the solar air collector blower and to regulate the outlet voltage therefore the velocity can be changed indeed as shown in Fig 3.20. The working ranges for this device are 0-36 V/DC, 0.01-40 A voltage and current respectively.

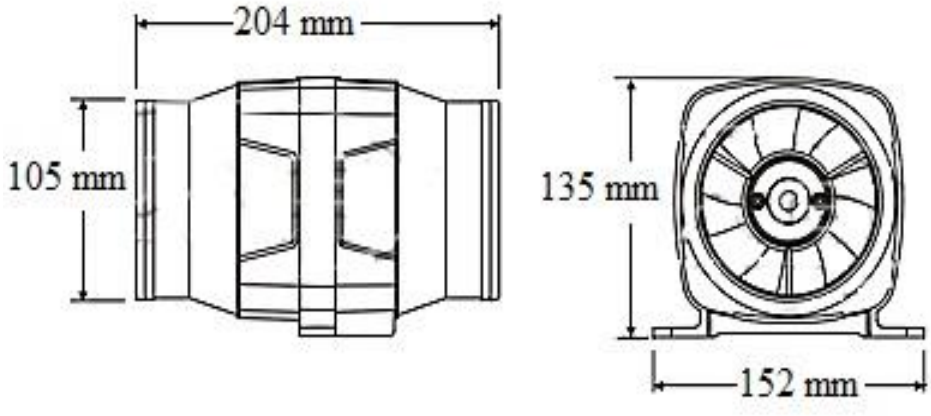

Fig. 3.19. Drying chamber and blower dimensions and illustration

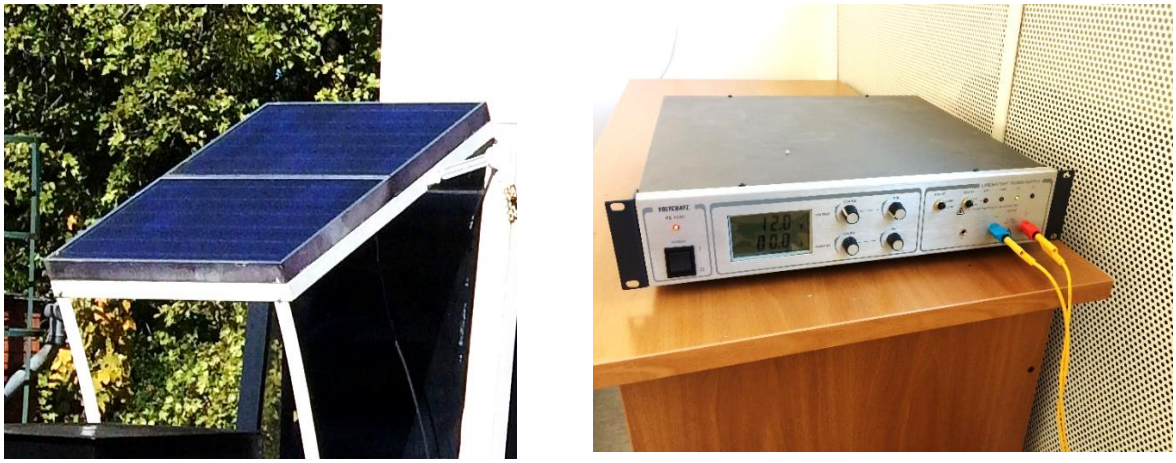

Fig. 3.20. The applied photovoltaic modules and the power supply regulator

3.8.4. Air ducts

An insulated air ducts have been connected the essential components of solar drying system. The ducts are insulated with a 10 mm special type of polystyrene to decrease heat loss to the surroundings and fixed carefully. The diameter of air ducts is 10 cm with different lengths which depend on the positions of solar units.

3.9. Installation and measurements

The constructed solar air collectors and drying chamber were fixed at the laboratory and mounted to the south on an iron simple frame as shown in Fig. 3.21. The schematic diagram of the entire solar drying system is illustrated in Fig. 3.22. The system designed, manufactured and installed in the open laboratory area of department of physics and process control, Szent István University. Insulated air ducts have connected the main components. Temperature, humidity, solar radiation, and airspeed were measured.

Many sensors have been fixed in many points of the system to measure system variables, then logged them on the computer to analysis them for system performance investigation. The blowers are connected to the power supply which connected to the photovoltaic modules. The drying chamber exit is integrated with a simple short chimney with length 100 cm.

Fig. 3.21. Solar drying system illustration in laboratory

The following characteristics were measured to get the experimental results then analysing them to calculate the efficiency and the performance parameters of solar drying system as:

- The temperature measurements.
- Air speed measurements.
- Global solar radiation intensity measurement.
- Air relative humidity measurements.
- Initial and final weight of dried product items.

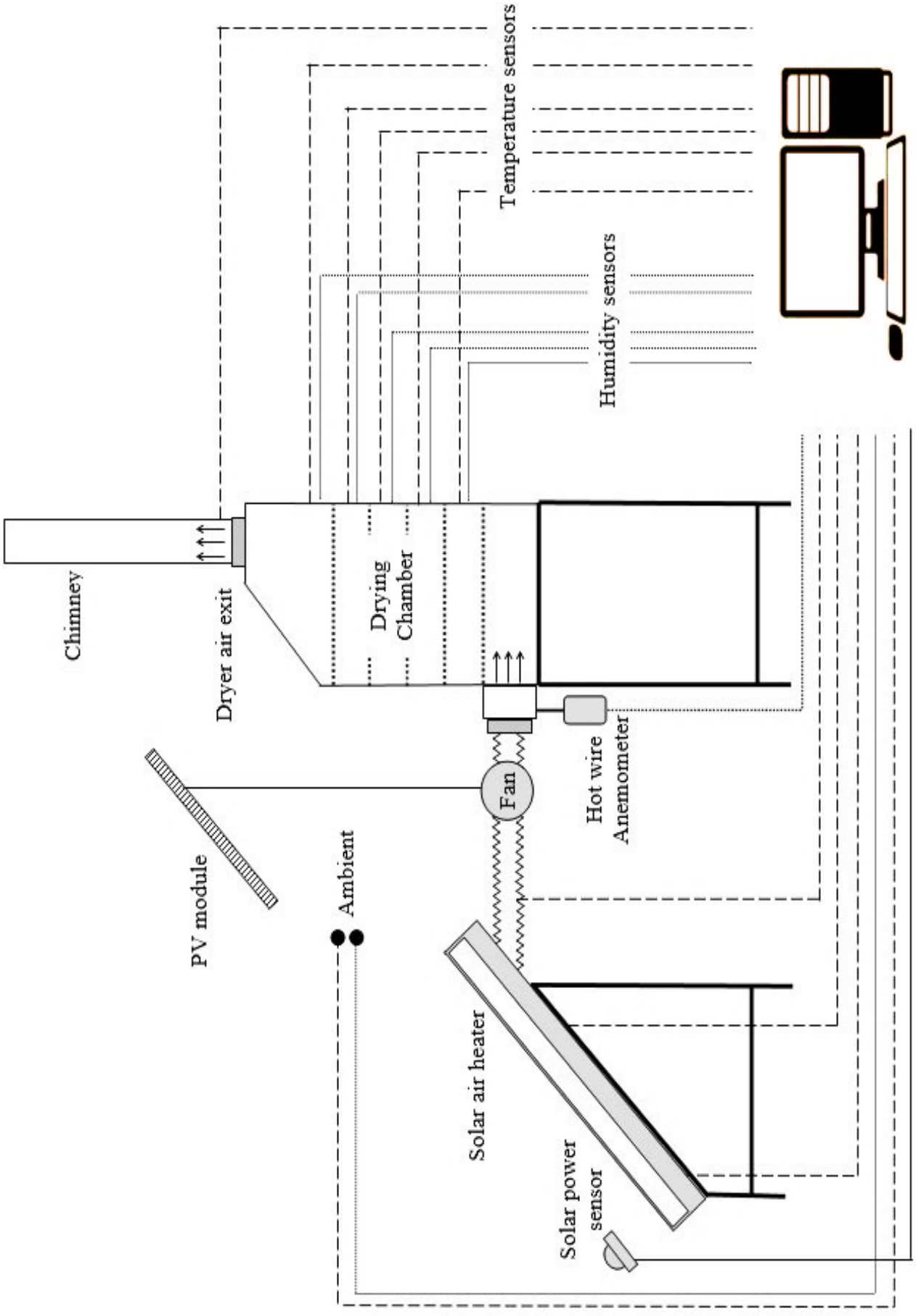

Fig. 3.22. Schematic diagram of solar drying system

3.9.1. Thermocouples and thermometers

The temperatures in different points of solar air heater needs to be measured to achieve the temperature distribution. For this purpose, the K-type twisted thermocouples wire were used as shown in Fig. 3.23. Thermocouples are the most widely easiest temperature sensors to be used. All the thermocouples have been soldered, calibrated and tested before installing.

Table 3.4. Thermometers instruments specifications

Parameter	Details
Temperature range	-200~1372°C
Accuracy	>100 °C: ±1 °C <100 °C: ±2 °C
K-type thermocouple resolution	<1000 °C: 0.1 °C/ °F/K
Power supply	9V Battery
Size	20×8.5×4 cm

The thermocouples are connected with digital thermometer which specifications are shown in Table 3.4. Eleven temperature points had been measured in solar drying system; Two on absorbing surface, one for solar collector inlet, one for solar collector outlet, one for second pass double solar collector inlet, one for ambient and five for drying chamber trays. The thermocouples are calibrated with a simple mercury thermometer for water temperature from 0 ^{o}C to 100 ^{o}C. The K-type thermocouples are connected to calibrated digital thermometer to records temperature values. The thermometer can be used to measure at most 4 channels temperature simultaneously.

3.9.2. Solar power meter

The global solar radiation is measured by a digital solar power meter with its sensor. It is placed on the same tilt angle of the collector at the same direction. The spectral response of solar meter from 400 to 1100 nm and measurement range varies from 1 W/m^2 to 1300 W/m^2. The specifications of the instrument are shown in Table 3.5.

Table 3.5. Solar power meter instruments specifications

Parameter	Details
Solar irrigation measuring range	1 W/m^2 to 1300 W/m^2
Frequency of measurement	2/s
Accuracy	5%
Operating temperature	-10°C to +50°C
Power supply	3 LR3-AAA batteries
Size	20× 8.5×4 cm

3.9.3. Anemometer

One of the main properties that affects the performance of the collector is the air velocity. A MS6252A digital anemometer instrument was used to measure the air velocity then the air mass

flow can be calculated by multiplying with the cross-section area and the air outlet density as shown in Fig. 3.23. The measuring range is 0.4-30 m/s. The anemometer woks with power supply 9 V. It has dimensions 16 mm×85 mm×38 mm and 200 g weight. The accuracy is ±2% with mentioned working range. The air flow rate had been measured in the inlet and outlet of solar system with a constant voltage power supply to air blower.

Fig. 3.23. Experimental measurements instruments

3.9.4. Relative humidity meters

Air relative humidity is measured in many points of solar drying system. Five points on the trays of drying chamber and one point for ambient. A digital humidity meters with their sensors are used as shown in Fig. 3.24. The measuring range for these meters varies from 10% RH to 99% RH with humidity accuracy ±4%. Humidity meter display resolution is 1% RH and measuring temperature range from -50 °C to +70 °C. It has dimensions 4.8×2.8×1.5cm and working with 2×1.5 V batteries. Sensor cable length is 1.5 m with probe length 6 cm.

3.9.5. Weight scale

To measure the weight of dried product before and after drying process, a simple digital kilograms scale had been used as shown in Fig. 3.24. Measuring range of this scale varies from 10 g to 5000 g. It is working with 3 V battery.

Fig. 3.24. Air relative humidity meter and weight scale

4. RESULTS

The experimental collected detailed results are showed and discussed in this chapter. The solar drying system which mentioned in the previous section was tested in different conditions and different working cases in the lab of Szent István University. The result achieved served as a basis of the new scientific results.

4.1. Parameters and calculations

The terms of solar air collectors inlet, outlet and absorbing surface temperatures with the time of experiments are obtained. The temperature and humidity stratification of drying chamber trays are shown for the time of examinations with using different solar collectors. The effect of air mass flow rate on the daily efficiency of solar collector is shown. Also, the manufactured chimney investigated experimentally. The final weight analysis of dried product has been measured and discussed in details for several types of solar air collectors. The experimental results are compared and validated with many kinds of previous studies to explain the agreement of collected results and improvements percents.

In this section, the thermal performance formulas which used are explained. The useful heat energy Q_u of solar air collectors had been obtained by using Eq. (4.1) with collector inlet temperature T_i and collector outlet temperature T_o.

$$Q_u = \dot{m}\ c_p\ (T_o - T_i). \tag{4.1}$$

The instantaneous thermal efficiency η of the solar air collectors represents the ratio of the amount of instantaneous useful heat collected which obtained from Eq. (4.1) to the instantaneous total amount of radiation striking the collector surface A_c during any period as following in Eq. (4.2):

$$\eta = \frac{Q_u}{G\ A_c}. \tag{4.2}$$

Air mass flow rate m^o calculated by multiplying air density ρ, the area of air flow duct A_{duct} and airspeed v which measured by digital anemometer as shown in Eq. (4.3):

$$\dot{m} = \rho\ v\ A_{duct}. \tag{4.3}$$

Numerically, trapezoidal integration method has been used to calculate the amount of daily solar radiation and hourly gained useful heat energy that flat plate solar air collectors can afford. Trapezoidal rule is a method of numerical integration and can be defined as following in Eq. (4.4):

$$\int_{x_o}^{x_n} f(x)dx = \frac{h}{2}\ (y_o + 2y_1 + 2y_2 + \cdots\cdots\cdots\cdots + y_n), \tag{4.4}$$

where, h is the time increments, y is useful heat energy at time t and y_o and y_n are initial and final useful heat energy experiment. As a sample of calculations, the reordered measurements of double-pass solar air collector:

$T_{c1,i}$ = 22 ºC	T_a = 21.3 ºC
$T_{c2,i}$ = 30.9 ºC	$T_{c,o}$ = 37.3 ºC
v = 2.3 m/s	G = 946 W/m^2
c_p = 1000 J/kg.K	ρ = 1.2 kg/m^3
A_c = 0.5607 m^2	d_{duct} = 9 cm = 0.09 m

The area of air duct calculated as:

$$A_{duct} = \frac{\pi}{4} \ (d_{duct})^2 = \frac{\pi}{4} \ (0.09)^2 = 0.00635 \ m^2.$$

The mass flow rate of air is (according to Eq. (4.3)):

$$\dot{m} \ = \ \rho \ v \ A_{duct} \ = \ 1.2 \times 2.3 \ \times 0.00635 \ = 0.01753 \text{ kg/s.}$$

The instantaneous useful heat of upper channel can be calculated as:

$$Q_{u1} = \ \dot{m} \ c_p \left(T_{c2,i} - T_{c1,i}\right)$$

$$Q_{u1} = \ 0.01753 \ \times 1000 \times (30.9 - 22) = 156 \ W.$$

The instantaneous useful heat of lower channel can be calculated as:

$$Q_{u2} = \ \dot{m} \ c_p \left(T_{c,o} - T_{c2,i}\right)$$

$$Q_{u2} = \ 0.01753 \ \times 1000 \times (37.3 - 30.9) = 112.18 \ W.$$

The total instantaneous useful heat of solar air collector is:

$$Q_u = \ Q_{u1} + \ Q_{u2,}$$

$$Q_u = \ 156 + \ 112.18 = 268.17 \ W.$$

The thermal instantaneous thermal efficiency η of the solar air collectors (Eq. (4.2)) is:

$$\eta = \frac{268.17}{946 \ \times 0.5607} \times 100\% = 50.56 \ \%.$$

4.2. Effect of air passes number

4.2.1. Single air pass solar collector experimental analysis

The experimental data of single-pass solar collector have been recorded with 10min constant time step from 10:00 to 15:00 of 2nd of October 2017. The collector arranged to drying chamber with dried items (apple slices) by inline air blower with 2.3 m/s air velocity as shown in Fig. 4.1.

The instantaneous variation of the measured inlet and outlet air temperatures for single-pass solar air collector are shown in Fig. 4.2. It is clear that the outlet air temperature increases with the time of test till it reaches the maximum value at maximum ambient temperature, then it decreases gradually when the values of ambient temperature and solar irradiance decreases. The highest value of the outlet air temperature for solar collector was between 13:00 and 14:00 with more than 31°C. The behaviour of solar collector outlet temperature agreed with what mentioned in the previous studied (Sencan and Özdemir, 2007; Yang et al., 2012). Temperature difference ΔT through solar air collector decreased significantly between 12:40 and 13:40 due to radiation decreasing. The experimental data shows that the maximum temperature difference between inlet and outlet of solar air collector were reached at maximum radiation intensity values of about 6 - 6.7 °C between 11:10 to 11:40. It is observed that the suctioned air and outdoor temperature are approximately the same with very small deviations because of inlet temperature sensor position affected by suctioned fresh air. Inlet and outlet temperature curves fluctuate rapidly in some points due to ambient air temperature instability.

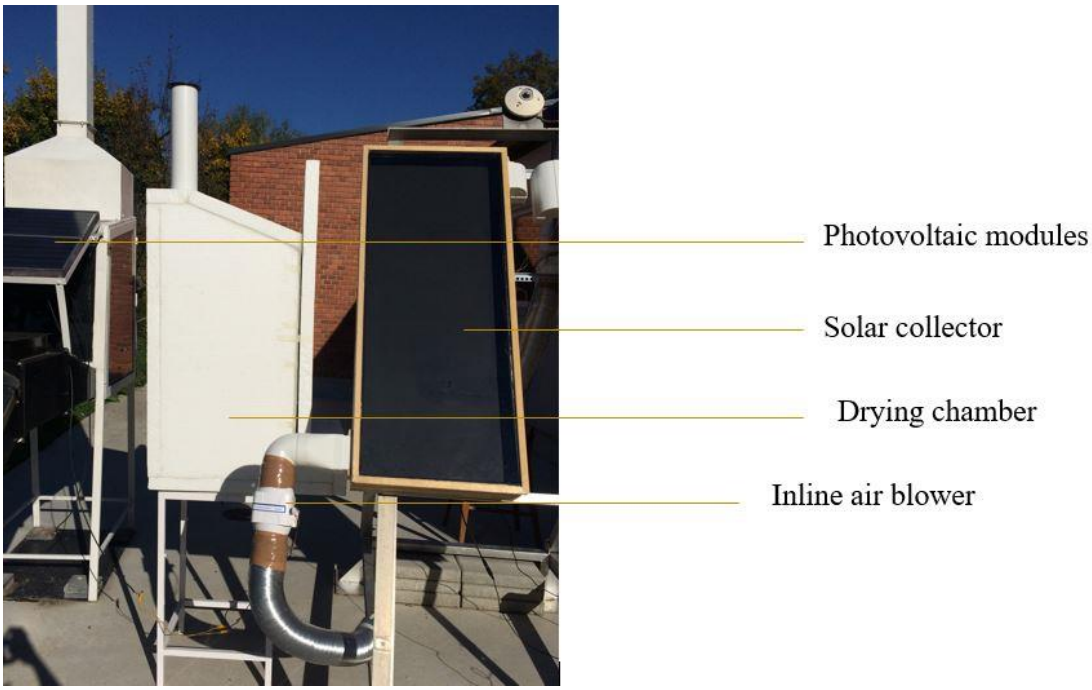

Fig. 4.1. Single-pass solar collector integrated with drying chamber

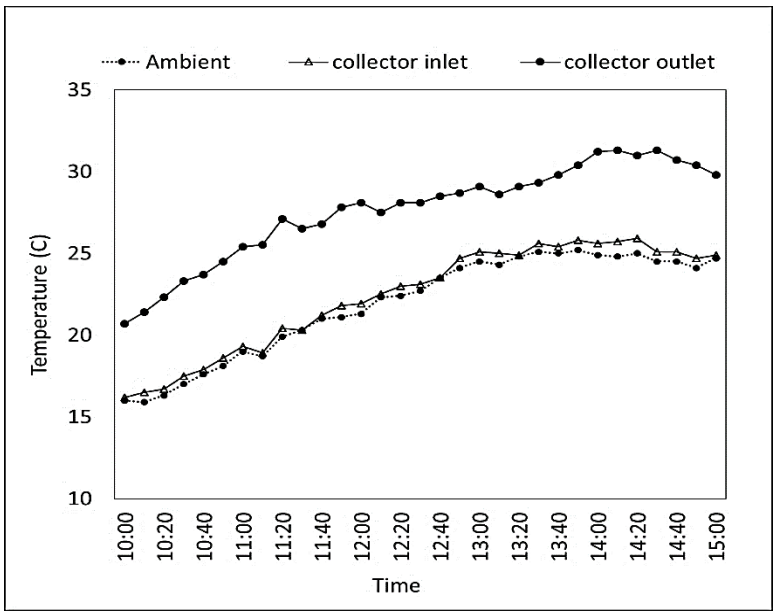

Fig. 4.2. Single-pass collector's inlet, outlet and ambient temperature vs time

Fig. 4.3 shows the variation of the average absorbing surface temperature for single-pass solar air collector and ambient temperature with the time of experiment duration at 2.3 m/s air flowed speed. The experimental temperature dates of the absorbing surface measured by two fixed sensors on it. It seems that the behaviour of the absorbing surface temperature with time look like the behaviour of solar irradiance intensity curve with time as is shown in Fig 4.3. The maximum value of the average absorbing surface temperature was 60.6 ^{o}C at solar radiation intensity 927 W/m^2 and ambient air temperature 22.7 ^{o}C. There are two effects of absorbing surface temperature variation or increasing. The increasing of plate temperature leads to gain more of useful heat. In parallel with the same time, it will cause more heat losses.

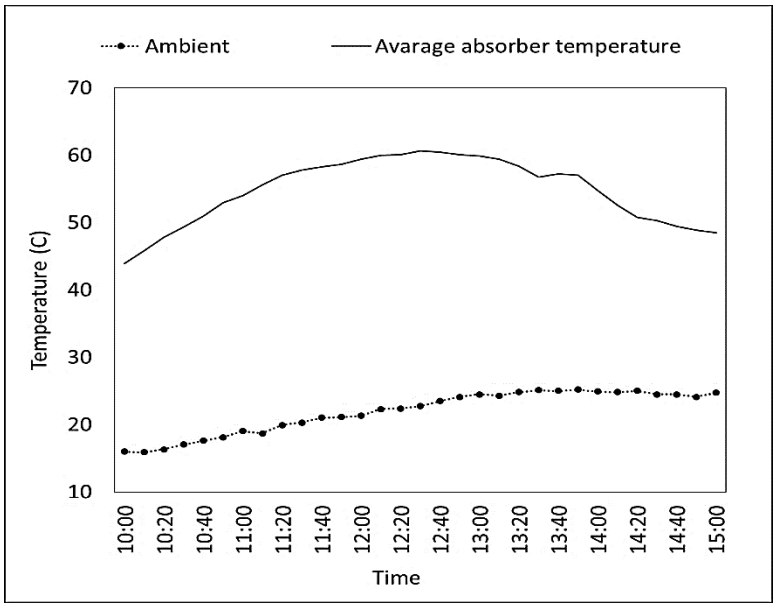

Fig. 4.3. Average absorbing plate and ambient temperatures vs time

Fig. 4.4 showed the solar radiation intensity variation and calculated useful heat during 5 hours of experiments days. The maximum radiation intensity was 948 W/m^2 at noon. The solar radiation blocked by some sporadic clouds between 12:40 and 13:40. The useful heat obtained from the solar air collector was proportional directly to the values of temperature change through the collector in Fig. 4.2. The useful heat increases to reach the maximum value 230 W/m^2 at the same time of maximum temperature differences at 11:30. The experimental daily useful heat energy calculated by using the trapezoidal rule in Eq. (4.4). The daily total useful heat for flat plate single-pass solar air collector is 3261 kJ.

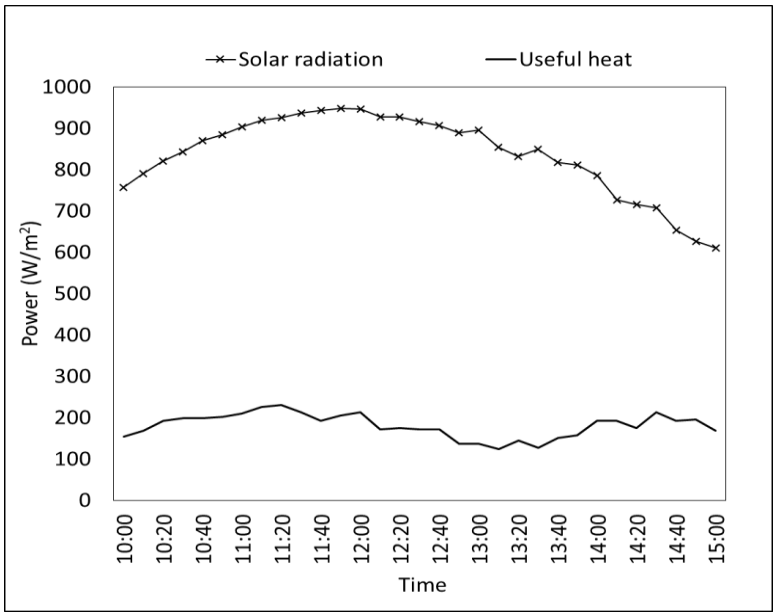

Fig. 4.4. Useful gained heat and solar radiation intensity vs time

Fig. 4.5 shows the instantaneous efficiency of flat plate single-pass solar collector for 5 hours of the experiment. The thermal efficiency depends mainly on gained useful heat from absorbing surface according to Eq. (4.2), as a result, depends on collector temperature rise. The instantaneous efficiency of solar air collector has salient variation during variation of climate aspects such as

wind speed, ambient temperature, and solar radiation intensity. Efficiency curve fluctuated and formed the same shape of useful heat curve fluctuation, which proves the dependence of thermal efficiency on the useful heat. The lowest value of efficiency occurred at the lowest value of useful heat was 25.6% while highest value 55.4%. The instantaneous efficiency is not giving a clear idea about the performance of solar collector, that is the reason for daily efficiency calculating.

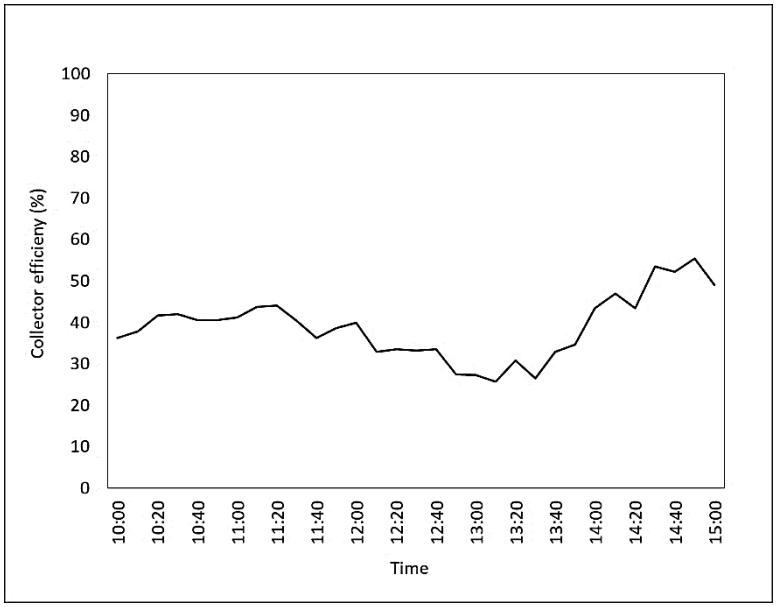

Fig. 4.5. Instantaneous efficiency of single-pass solar air collector efficiency vs time

Fig. 4.6 and Fig. 4.7 shows the stratification of temperatures (T_1 to T_5) and relative humidity(RH_1 to RH_5) for the five trays inside drying chamber using single-pass solar collector as a heat source. The drying periods are sufficiently affected by temperature and relative humidity of the air. The increasing of drying temperature at a constant RH results decreasing drying times, while increasing RH at constant temperature results increased drying times. Drying rates are higher at elevated drying temperature with constant RH, and lower at higher RH (at constant temperature) (Sigge et al., 2007). As mentioned before in Chapter 3, the dried product is 2 kg of green apple. The product has been cut into different sizes of circular slices with an average thickness 4 mm to decrease shell thermal resistance for the drying process.

The stratification of temperature in drying chamber is very obvious (see Fig. 4.6). Atmospheric air is a mixture of many gases (dry air) plus water vapor and many pollutants. Any amount of air carries two types of heat energy; sensible and latent. The heated air delivers solar collector with high temperature (sensible high heat). In drying chamber, the temperature of dry air decreases while relative humidity increases. The shapes of all curves are hardly affected by the curve of solar radiation in Fig. 4.4. The temperature difference in the first two trays (1 and 2) is higher than the difference in the last two trays (4 and 5) because the capacity of air to catch more heat was decreased. The values of relative humidity decrease with time in spite of the significant increase of solar collector outlet temperature increasing. After 12:00, the temperature differences between the five trays fluctuate with the approximately constant rate.

In Fig. 4.7, at the beginning of the process the moisture content of the product is high which leads to very high moisture loss rate, so the ability to catch more moisture by heated air higher at the beginning of experiments. It is clear that the product loses its moisture faster from the beginning of the process to the noon, afternoon much time is needed for the moisture content to be lost.

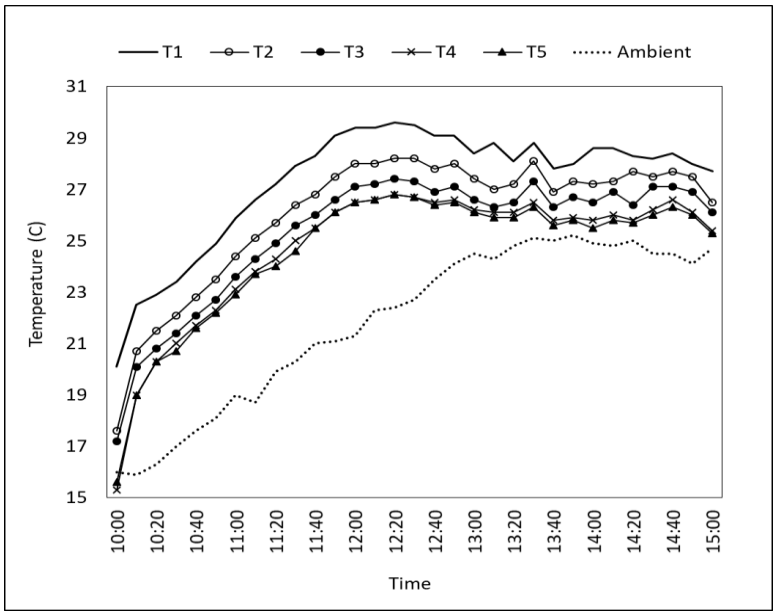

Fig. 4.6. Temperature stratification of drying chamber by using flat plate single-pass solar air collector vs time

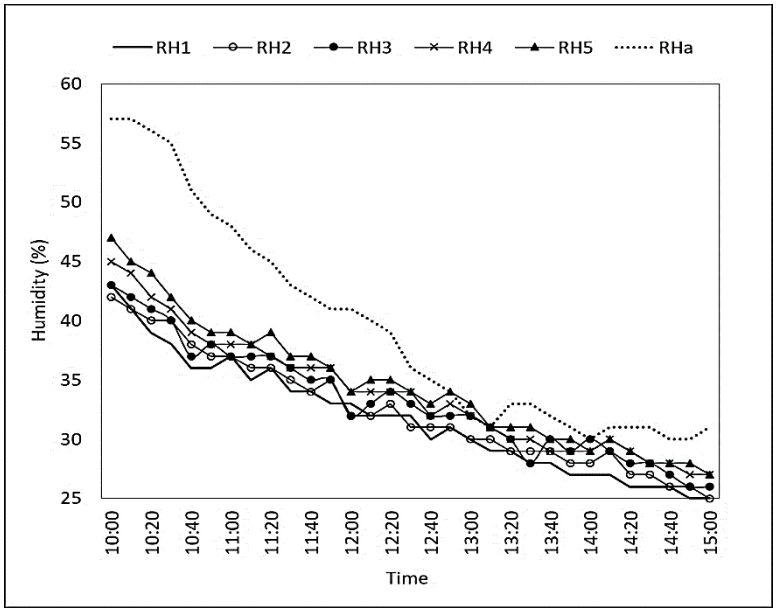

Fig. 4.7. Relative humidity stratification of drying chamber by using flat plate single-pass solar air collector vs time

The performance of single-pass solar air collector can be represented in the form of relation between thermal efficiency of solar air collector and (($T_{s,av}$ - T_a)/ I) according to the slandered test of solar collectors (Duffie and Beckman, 2013). The closest obtained curve in Fig. 4.8. shows a linear relationship between the horizontal and vertical axis, where *x* represents the term of (($T_{s,av}$- T_a)/ I), while *y* represents the thermal efficiency of solar collector (η, %). So, the linear model formula can be written as following:

$$\eta = a \frac{T_{av,s} - T_a}{I} + b. \quad (4.5)$$

The parameters of linear equation *a* and *b* can be obtained mathematically for the range of experimental cases for single-pass solar collectors group:

$$a = -3308.3 \ and \ b = 168.8.$$

During the approximation the correlation coefficient was 0.42 along with the standard deviation of 7.76%. The model represents the closest expression of the relationship between temperature difference, solar radiation intensity and thermal instantaneous efficiency. The developed theoretical model can be applied in the range of 0.036 and 0.0415 of (($T_{s,av}$ - T_a)/ I).

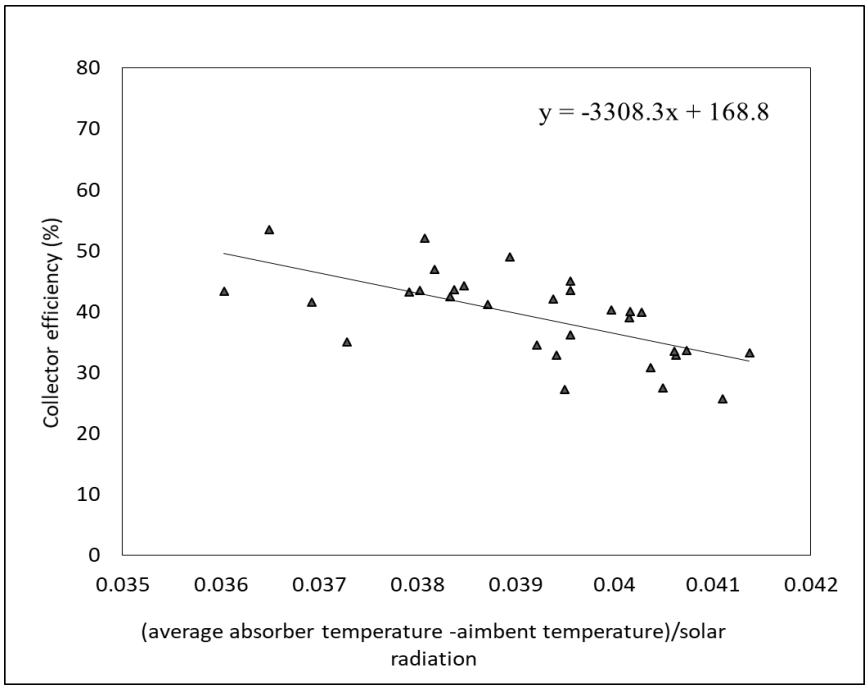

Fig. 4.8. Performance diagram of single-pass solar air collector

4.2.2. Double air pass solar collector experimental analysis

The experimental results have been recorded under same working conditions of single air pass solar collector with 10min constant time step from 10:00 to 15:00 of 2nd of October 2017. The double solar collector with a flat absorbing surface had been arranged to drying chamber which contains the apple slices (dried items) by a small inline air blower with 2.3 m/s air velocity as shown in Fig. 4.9.

Fig. 4.10 shows the variation of inlet and outlet air temperatures for flat plate double-pass solar air collector. It is clear that the outlet air temperature altered indirectly with ambient temperature during the time of the test. It decreases and increased gradually when the values of ambient temperature and solar irradiance increase and decreases. At the beginning of the experiment, the values of temperature differences are significant. The curves of the inlet, second pass, and outlet temperatures are increased steadily with some fluctuated points to reach the maximum values between 12:00 and 13:00 with 25.7, 34.8 and 39.5 ^{o}C respectively. Afternoon, the ambient and inlet air temperature values approximately constant with some fluctuating up and down. 12:40 while the curve of solar collector outlet temperature decline gradually due to solar radiation decreases. It is obvious that the temperature difference ΔT through solar air collector indirectly reduced during the time of day due to radiation decreasing. The experimental data shows that the maximum upper channel and lower channel temperature differences were 9.5 ^{o}C and 6.4 ^{o}C at 12:20 and 12:00. The curves behaviour are agreed with the results of many studies as (El-Sebaii et al., 2011; Prasartkaew and Kumar, 2014).

Fig. 4.9. Double-pass solar collector integrated with drying chamber and the un-finned absorbing surfaces

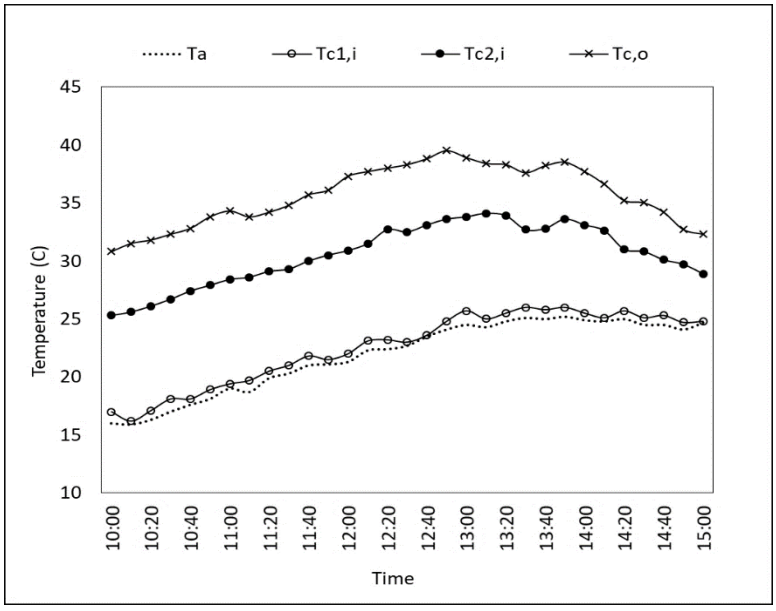

Fig. 4.10. Flat plate double-pass collector's inlet, second pass inlet, outlet and ambient temperature vs time

Fig. 4.11 explains the variation of the average absorbing surface temperature for double-pass solar air collector and ambient temperature with the time of experiment duration at 2.3 m/s air flowed speed (air mass flow rate equals 0.021 kg/s). It seems that the shape of absorbing surface temperature curve performed the same behaviour of solar irradiance intensity curve with time as is shown in Fig 4.12. The maximum value of the average absorbing surface temperature was 47.1 ^{o}C at solar radiation intensity 907 W/m^2 and ambient air temperature 23.5 ^{o}C at 12:40. The curve has some fluctuated points due to solar radiation instability. It is very clear that the values of absorber temperature of double-pass solar collector are lower than the single-pass solar collector absorber temperature, because of the effect of second pass heat transfer. In single-pass collector,

the useful heat gained from one side of absorbing surface while gained heat from the two sides of double-pass solar collector absorbing surface.

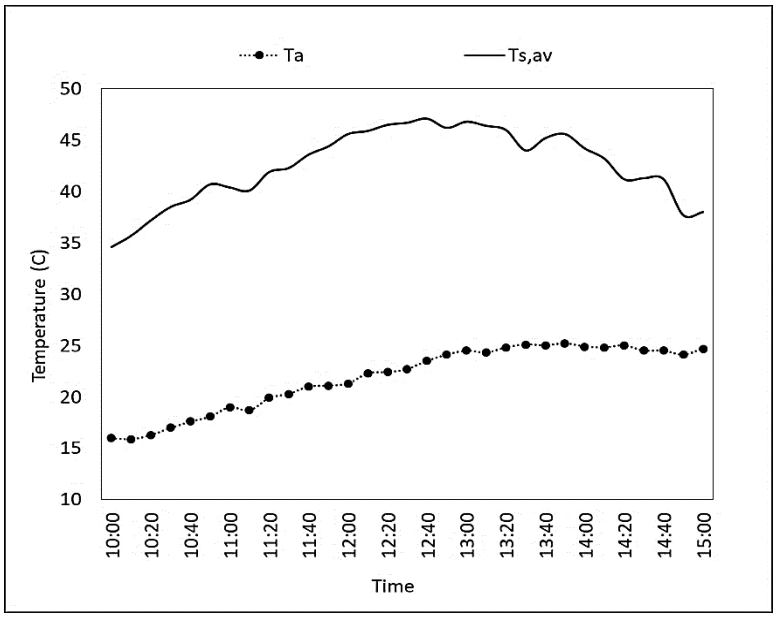

Fig. 4.11. Average absorbing plate and ambient temperatures vs time

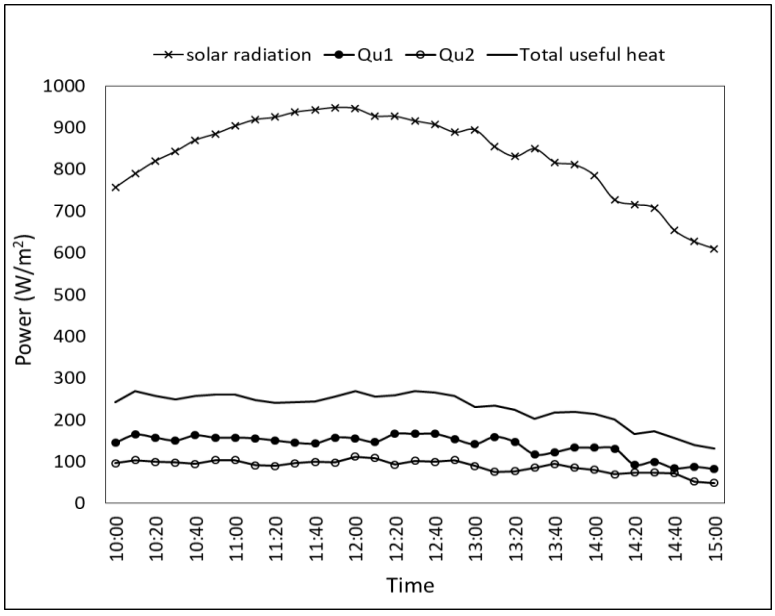

Fig. 4.12. Useful gained heat and solar radiation intensity vs time

The measured solar radiation intensity irradiance curve and calculated total useful heat during 5 hours of experiments days are shown in Fig. 4.12. The maximum radiation intensity was 948 W/m^2 at noon. The solar radiation blocked by some sporadic clouds between 12:40 and 13:40. The useful heat consists of two components; first is upper channel useful gained heat and the second is the lower channel useful gained heat. The figure obtained that the useful heat gained curves were proportional directly to the solar radiation intensity and air temperature difference through the collector. The two channels useful heat increases to reach the maximum values 166.5 and 112.2 W/m^2 at the same time of maximum temperature differences. The experimental daily useful heat energy calculated by using the trapezoidal rule in Eq. (4.4). The total useful heat of solar collector is the summation of two channels useful heat. The values of upper pass useful heat are higher than

lower channel due to the high-temperature difference in the upper channel and direct sun heated. The behaviour of absorbing surface temperature curve has been shaped the same configuration of the published curve which drawn by (Bhushan and Singh, 2014).

Fig. 4.13 shows the instantaneous thermal efficiency of flat plate double-pass solar air collector for 5 hours of the experiment. The instantaneous efficiency of solar air collector has very fluctuated variation due to useful heat and temperature variations. The general view of the curve obtained a decreased percentages of efficiency. The maximum value of thermal efficiency is 60.5% at the beginning of test while the minimum percentage is 37.2%. The instantaneous efficiency is not giving a clear idea about the performance of solar collector. The percentages of efficiency are higher than single-pass collector values because of the higher useful heat.

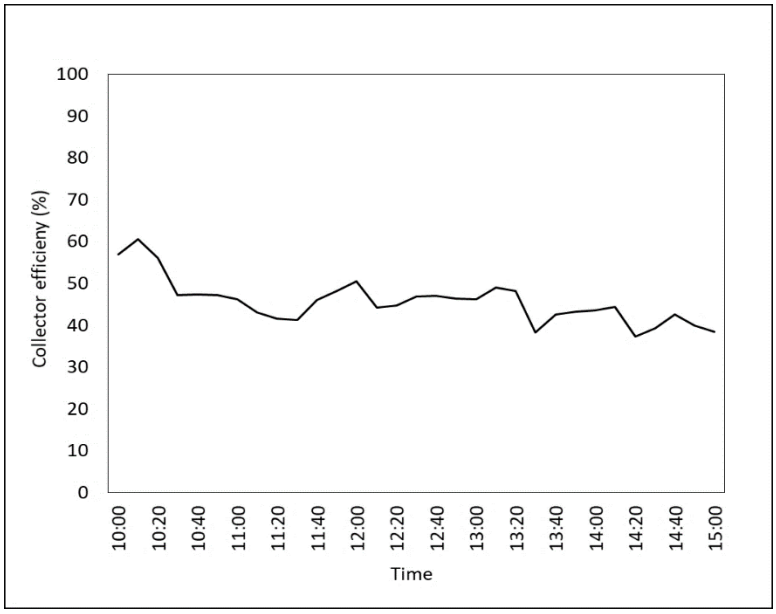

Fig. 4.13. Instantaneous efficiency of flat plate double-pass solar air collector efficiency vs time

The stratifications of temperatures in drying chamber are shown in Fig. 4.14. The temperature differences in double-pass solar air collector are more sufficient than the single-pass solar collector. The shapes of temperature curves are hardly affected by the curve of solar radiation in Fig. 4.12. The temperature difference between the first two trays T_1 and T_2 is higher than the difference between the last two trays T_4 and T_5 due to the thermal capacity of heated air decrease. It is obvious the agreement between the behaviour of drying chamber temperatures and absorbing surface, collector's inlet and outlet temperatures. In the first 10 minutes of the experiment, the temperature fluctuated down because of the small decrease in ambient temperature. After that, the values of temperature in five trays increased with the time to reach the maximum peak values 29.4, 28.4, 27.8, 26.8, 25.5 ^{o}C respectively at 13:20.

At the end of the experiment, the values of temperature are more close to the values of ambient temperature. After 13:20, the temperature differences between the five trays fluctuate with the approximately constant rate except for the temperature in the first tray. Generally, the curves show that the air at dryer entrance has more capacity to catch the moisture from the dried product than exit region.

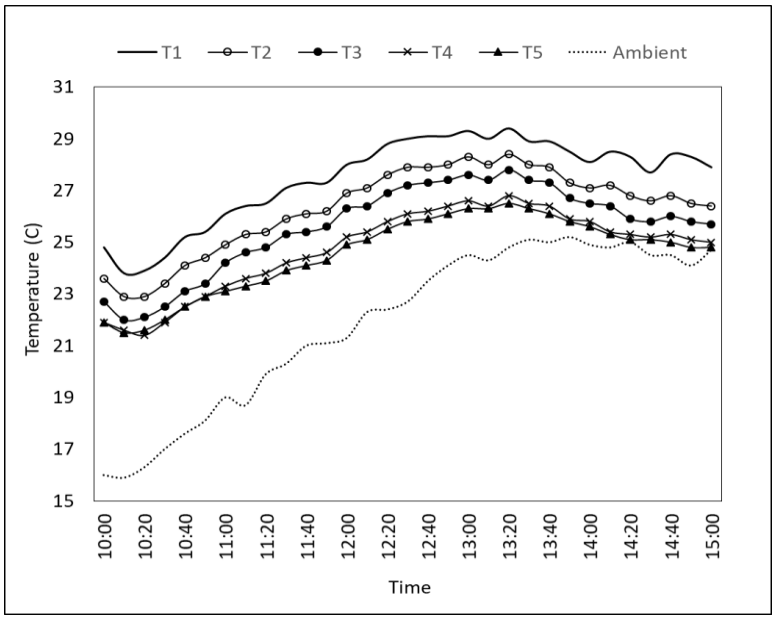

Fig. 4.14. Temperature stratification of drying chamber by using flat plate double-pass solar air collector vs time

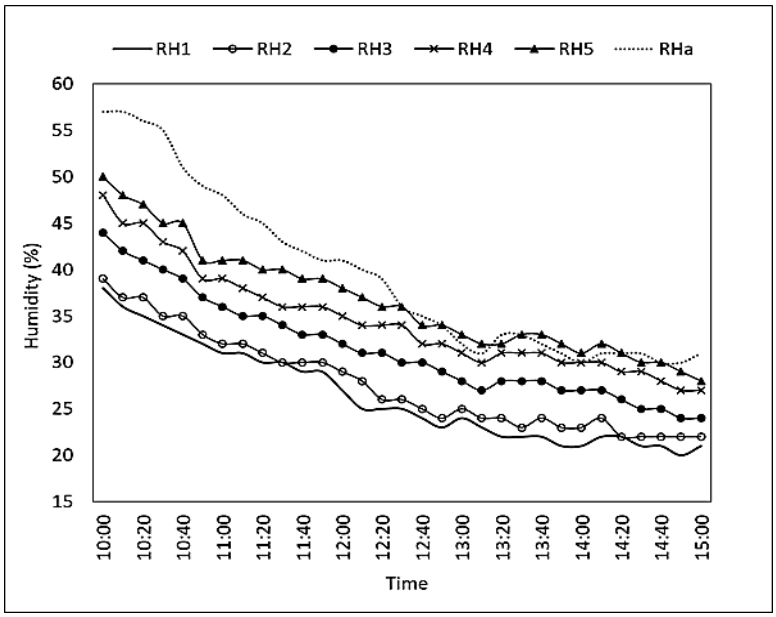

Fig. 4.15. Relative humidity stratification of drying chamber by using flat plate double-pass solar air collector vs time

The relative humidity stratification in drying chamber trays are shown in Fig. 4.15. At the beginning of the drying process the moisture content of the product is high which leads to very high moisture loss rate, so the ability to catch more moisture by heated air higher at the beginning of experiments. It is clear that the product loses its moisture faster from the beginning of the process to the noon, afternoon much time is needed for the moisture content to be lost. The differences between five curves are more sufficient than the curves which gained by using single-pass solar air collector. The maximum differences of relative humidities are not at the same time as temperature curves in Fig. 4.14. The maximum value of relative humidity in every tray were 38, 39, 44, 48 and 50% from the first to the fifth tray respectively at the first record at 10:00 due to the high ambient temperature and low solar radiation intensity. The minimum values were 12,

22, 24, 27 and 28% from the first to the fifth tray respectively at the end of the experiment. After 12:20, the values of relative humidity in the fifth tray are lower than ambient relative humidity in some time intervals because of the high-temperature values at these times.

By the same way of single-pass solar collector, the performance of double-pass solar air collector has been investigated according to the standard test of solar air collectors as shown in Fig. 4.16. The obtained relationship can be represented by a linear model in Eq. (4.5). The parameters of *a* and *b* can be obtained mathematically for the range of experimental cases for double-pass solar collectors group:

$$a = -1881.8 \ \ and \ \ b = 63.09.$$

During the approximation the correlation coefficient was 0.335 along with the standard deviation of 3.62%. The theoretical model can be applied in range of 0.0078 and 0.0123 of $((T_{s,av} - T_a)/ I)$.

The values of constants are much less than the obtained with using single-pass solar collector, because the values of *x* axis of double-pass are less than single-pass values. The slope of performance line by single-pass solar collector higher than double-pass solar collector.

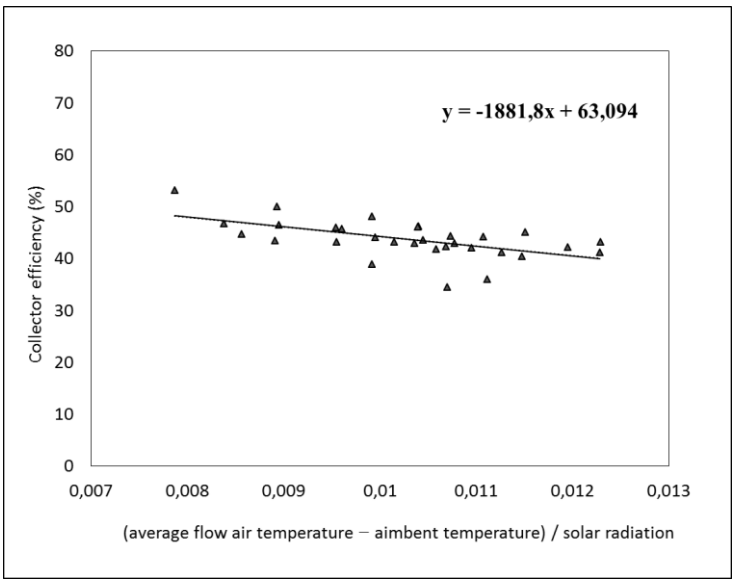

Fig. 4.16. Performance diagram of double-pass solar air collector

4.3. Effect of direction and shape of extended surfaces

4.3.1. Horizontally finned plate solar air collector experimental analysis

The experimental data of horizontally finned plate double-pass solar air collector have been collected with 10min constant time step from 10:00 to 15:00 of 12 of October 2017. The configuration difference between flat (un-finned) and horizontally finned absorbing surface is shown in Fig. 4.17.

Fig. 4.18 shows the variation of the inlet, second pass inlet and outlet air temperatures for horizontally finned plate double-pass solar collector. The general behaviour of temperature curves has the same behaviour which mentioned in Fig. 4.10 for flat plate solar collector. In this set, the solar radiation and ambient temperature much fluctuate during the time of day. As shown in the graph, the ambient and inlet temperature are increased significantly from the beginning of the

experiment to the noon. Afternoon, ambient temperature has continued slow rise to the maximum value 27.6 ^{o}C at the end of the test. The graph shows some differences between inlet solar collector and ambient temperature curves with a maximum deviation ±2 ^{o}C. The second pass inlet and outlet temperature increased to reach the highest value 46.2 and 40.8 ^{o}C at 12:10. Afternoon, the curves decreased gradually with much-fluctuated performance due to solar radiation fluctuation. The lowest value of outlet temperature is 36.5 ^{o}C at the beginning. The maximum temperature differences of upper and lower channels are 17 and 7.34 ^{o}C at 12:30 and 13:40.

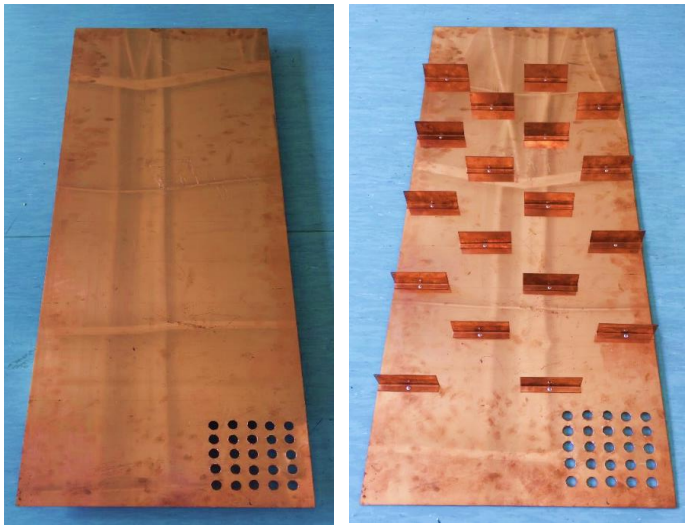

Fig. 4.17. Configuration difference between flat and horizontally finned absorbing plate

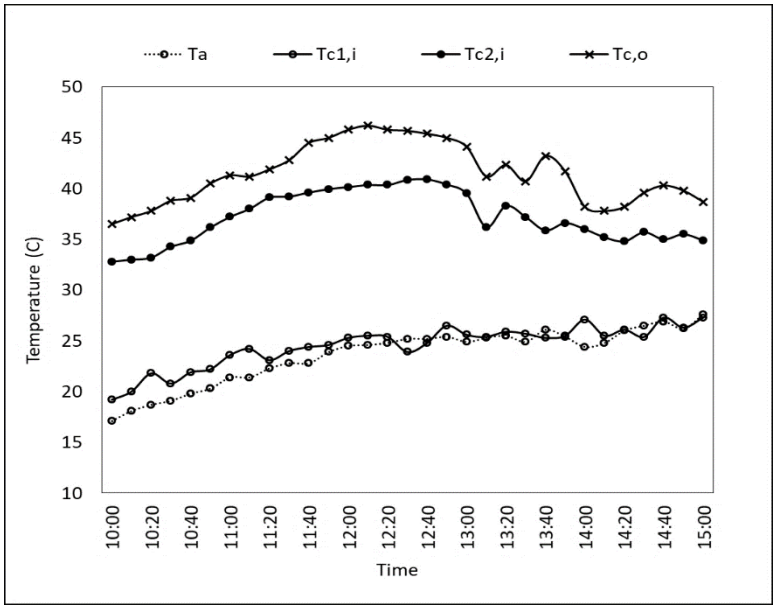

Fig. 4.18. Horizontally finned plate double-pass collector's inlet, second pass inlet, outlet and ambient temperature vs time

Generally the values of outlet temperatures of finned plate collector are higher that outlet temperatures of flat plate solar collector. In the previous literature, the outlet temperature plate-fin solar thermal collector investigated in higher ambient temperatures conditions. The study showed a little bit high outlet temperatures values about 10 ^{o}C difference with the same curve configuration (Ajiwiguna et al., 2016). The temperature differences of upper solar collector channel are much higher than the lower channel which leads to higher amounts of useful gained heat at the upper

channel. The fins are decelerating the movement of air in the collector which increase collector outlet temperature.

Fig. 4.19 explains the relation between ambient and absorbing surface temperature with the time of the experiment. Absorbing surface temperature curve performed unstably due to the unstable solar radiation curve. As mentioned, the temperature values are average of two measured points. The values of temperatures are increased from the morning to reach highest levels around noon. The maximum absorbing surface temperature is 50.22 ^{o}C with the highest amount of solar radiation 1018 W/m^2 at 12:30. After 13:00, the temperature curve has very fluctuated decease to reach 42.5 ^{o}C at the end of the day. The difference between ambient and absorbing surface temperature varies indirectly with the time. The temperature difference was high at the beginning of the process and decreased gradually with time direction. The turbulence and friction forces between flowed air and surface increase the temperature of the surface. The main objective to paint the surface is to increase its roughness and decrease its reflectivity.

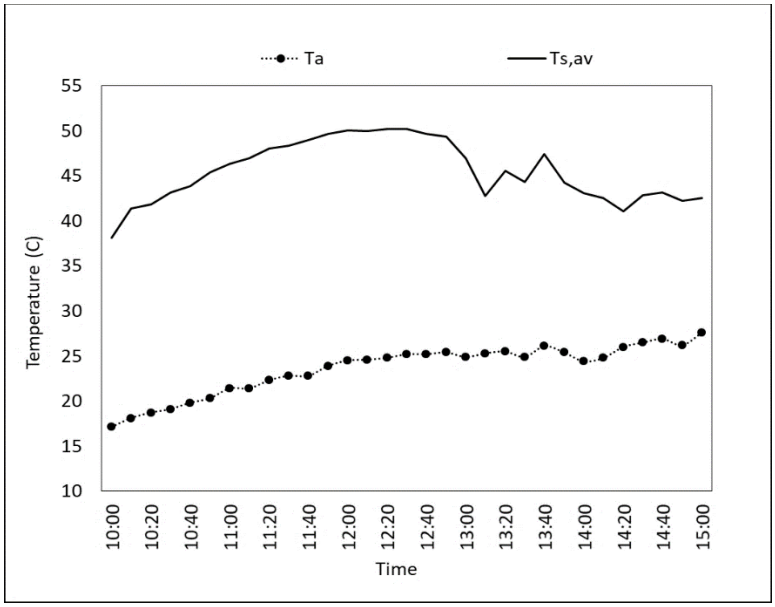

Fig. 4.19. Average absorbing plate and ambient temperatures vs time

The instantaneous useful heat for two channels of horizontally finned plate double pass solar air collector and solar radiation intensity is plotted with the time in Fig. 4.20. As shown, the curve of solar radiation intensity has some fluctuated points due to some clouds. The values of gained heat are higher than the rates which recorded with using flat plate solar collector in the previous section. The highest levels of useful heat gained around noon time because of the high solar radiation intensity and solar collector temperature difference. The maximum value of total useful heat was 408.1 W/m^2 at 12:30.

The instantaneous Efficiency of horizontally finned plate double-pass solar collector is shown in Fig. 4.21. The curve is fluctuating sharply with time due to unstable solar radiation variation. From the beginning to 12:40, the curve is not altered significantly compared with the performance after 12:40 to the end. The maximum value of thermal efficiency is 70.4% at 13:00 while the minimum percentage is 39.17% at 14:00. The instantaneous efficiency is not giving a bright idea about the performance of solar collector. It is clear that the percentages of thermal efficiency of finned plate collector are higher than flat plate collector values (see Fig. 4.13) because of the increase of heat transfer area by integrated horizontal fins.

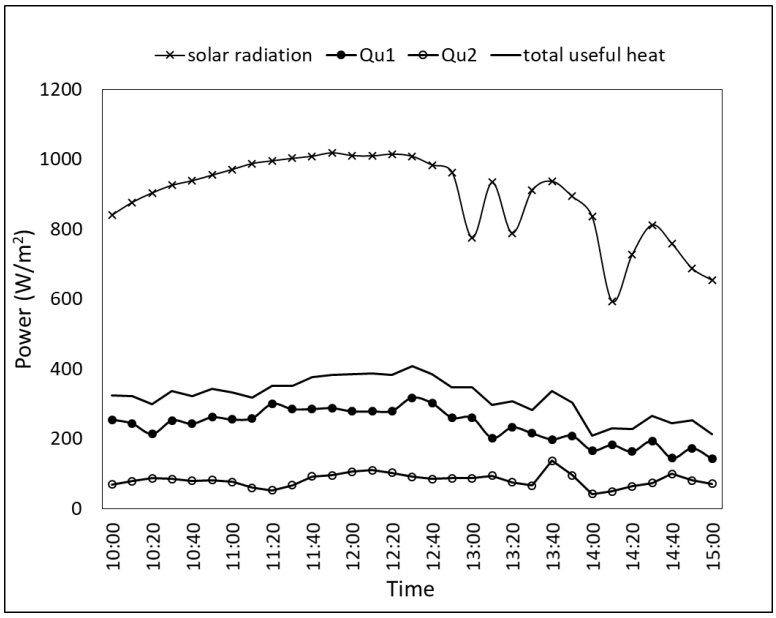

Fig. 4.20. Useful gained heat and solar radiation intensity vs time

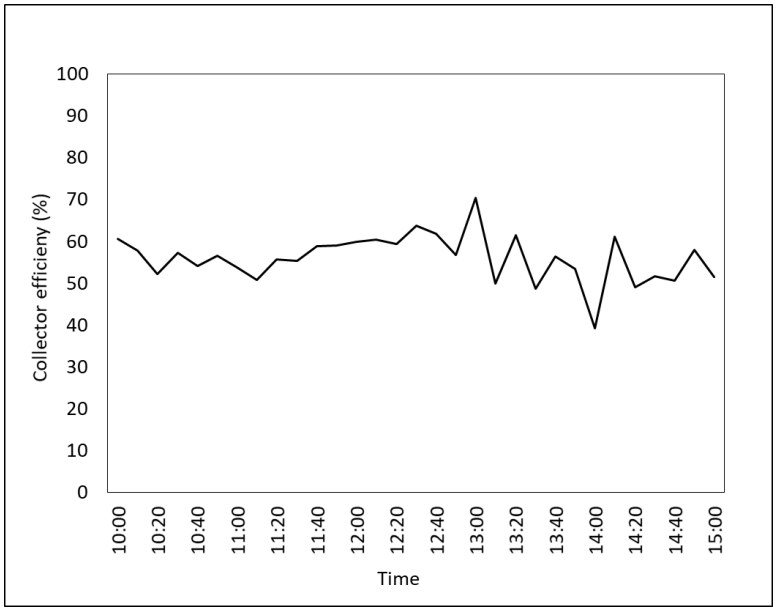

Fig. 4.21. Instantaneous efficiency of horizontally finned plate solar collector efficiency vs time

The stratifications of trays temperatures in drying chamber with the time of drying process are shown in Fig. 4.22. The temperature differences by using horizontally finned double-pass solar air collector have more steady behaviour than the flat plate double-pass solar collector. The temperature difference between the first two curves T_1 and T_2 is higher than the difference between the last two curves T_4 and T_5 due to the thermal capacity of heated air decrease. Curves have some fluctuation around 14:10 because of ambient temperature variation and some clouds which affected the solar radiation. It is obvious the agreement between the behaviour of drying chamber temperatures and absorbing surface, collector's inlet, second pass inlet and outlet temperatures. The curves of temperature in five trays increased with the time to reach the maximum peak values 39.4, 37.8, 36.9, 35.6, 34.6 ^{o}C respectively at 12:20. The temperatures of trays using this collector are higher than the temperatures which recorded with using flat plate collector; this is because of higher the ambient temperature, and solar radiation intensity.

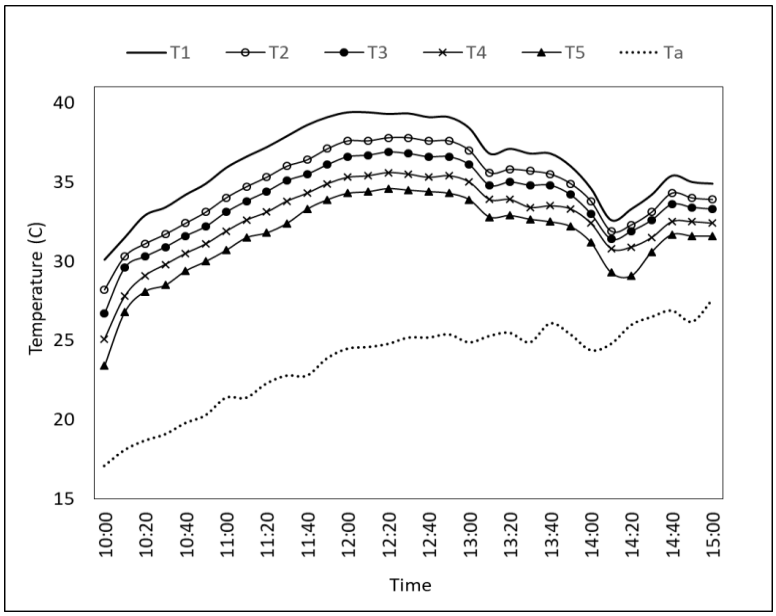

Fig. 4.22. Temperature stratification of drying chamber by using horizontally finned plate double-pass solar air collector vs time

The distributions of relative humidity in drying chamber trays by using horizontally finned plate solar air collector are shown in Fig. 4.23. At the beginning of the drying process, the relative humidity values are high with the high moisture content product items. The maximum value of relative humidity in every tray were 49, 49, 53, 56 and 58% from the first to the fifth tray respectively at the first record at 10:00 due to the high ambient relative humidity and low absorbing surface temperature. As shown, the relative humidity differences are very close to each other at the beginning. The minimum values were 20, 23, 26, 29 and 30% from the first to the fifth tray respectively at the end of the experiment. The general trend of relative humidity curves shows a fast decrease from the morning (10:00) to the noon, while the performance is an approximately constant afternoon with some fluctuation due to weather aspects variation.

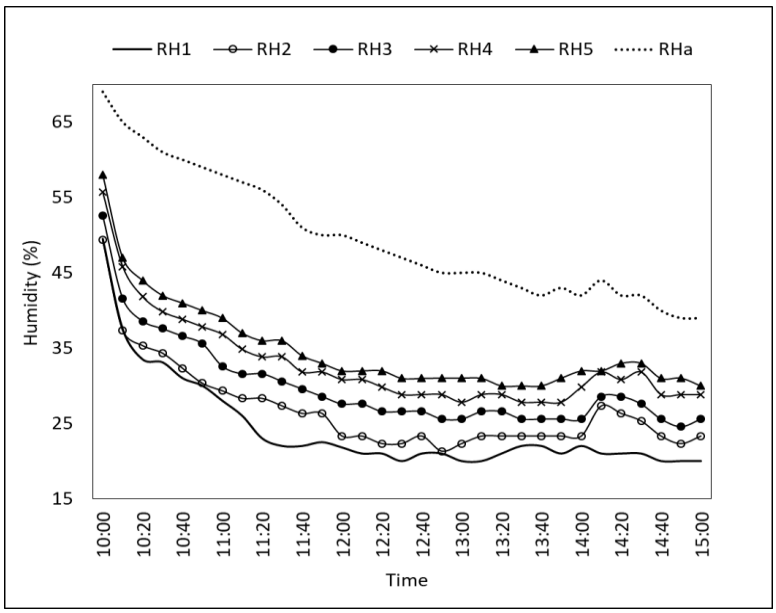

Fig. 4.23. Relative humidity stratification of drying chamber by using horizontally finned plate double-pass solar air collector vs time

4.3.2. Inclined by 45^o finned plate solar air collector experimental analysis

In this set, the fins are inclined 45^o to show the effect of fins direction on the thermal performance of solar air collector and drying chamber as shown in Fig. 4.24. The experimental data of 45^o finned plate double-pass solar air collector have been collected with 10min constant time step from 10:00 to 15:00 of 9 of October 2017. Air speed through the drying system was 2.3 m/s by an inline air blower.

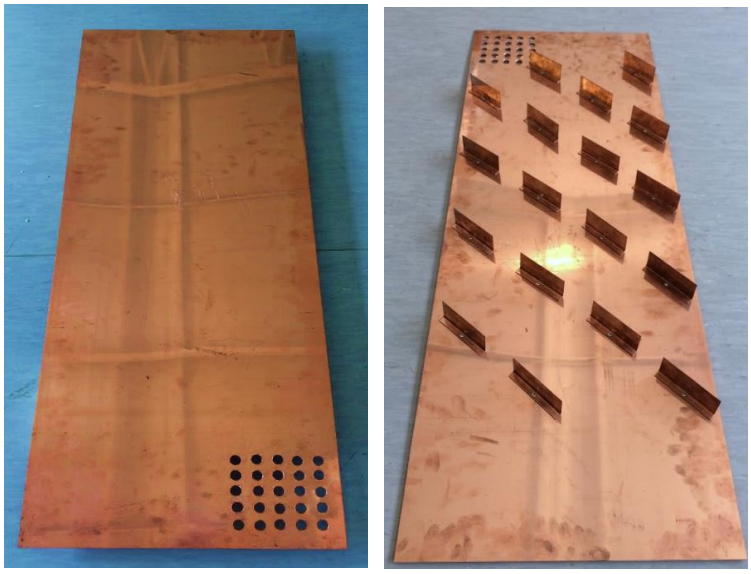

Fig. 4.24. Configuration difference between flat and 45^o inclined finned absorbing plate

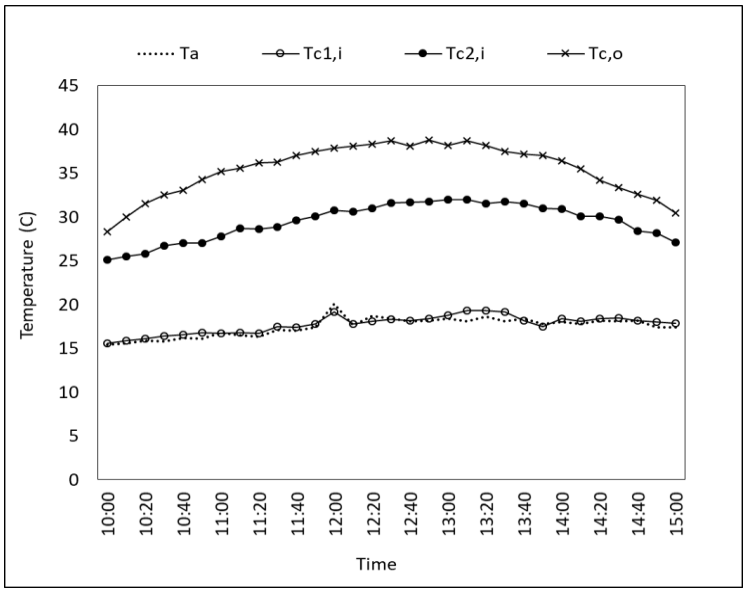

Fig. 4.25. 45^o inclined finned plate double-pass collector's inlet, second pass inlet, outlet and ambient temperature vs time

Fig. 4.25 shows the variation of solar collector inlet, second pass inlet, and outlet air temperatures. The curves are showing more stable behaviour than flat and horizontally finned solar collectors. The dates of this solar collector have been recorded through very clear day with stable values of solar radiation intensity and ambient temperature. Collector's outlet temperature increased from the beginning of experiment indirect with ambient temperature to reach the maximum value 38.8 ^{o}C at 12:40. The maximum temperature differences for upper and lower collector channel are 13.5

^{o}C and 7.5 ^{o}C at 12:40 and 12:10 respectively. After 12:40, temperature curves deceased smoothly indirect with solar radiation intensity.

Fig. 4.26 explains the average absorbing surface temperature variation by using 45^{o} finned double-pass solar air collector with the time. Absorbing surface temperatures are increased from the morning to reach highest levels around noon. The maximum absorbing surface temperature is 58.1 ^{o}C with the solar radiation intensity 1033 W/m^2 at 12:30. After 13:00, the temperature curve has smooth decease to reach 42.9 ^{o}C at the end of the day. The difference between ambient and absorbing surface temperature varies indirectly with the time. The maximum difference between absorbing surface and ambient temperature was 39.7 ^{o}C at 12:20.

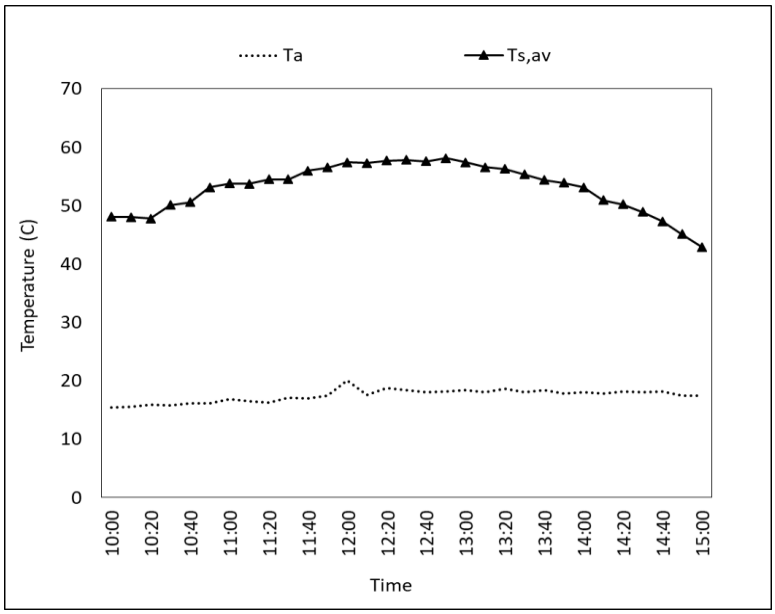

Fig. 4.26. Average absorbing plate and ambient temperatures vs time

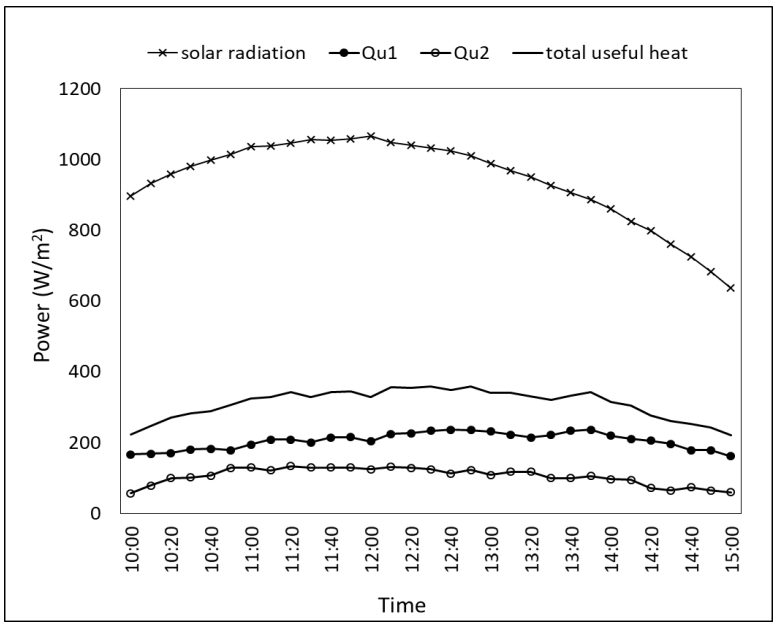

Fig. 4.27. Useful gained heat and solar radiation intensity vs time

Fig. 4.27 shows the plotted instantaneous useful heat for the two channels of 45^{o} finned plate double-pass solar collector and solar radiation intensity with the time. As shown, the curve of solar

radiation intensity has very stable rates during the day. The maximum recorded solar radiation is 1066 W/m^2 at 12:00. The values of gained heat are lower than the rates which recorded by using horizontally finned plate solar collector in the previous section. The highest useful heat is 355.5 W/m^2 at 12:30 because of the highest levels of solar radiation intensity and solar collector temperature difference. The extended surfaces (Fins) attachment are not increasing heat transfer area only; it is increasing the turbulence of flowed air through solar collector which increase surface temperature.

The instantaneous thermal efficiencies of 45^o finned plate solar collector are plotted as shown in Fig. 4.28. The curve shows a very slowly rise from the morning to the noon. Also, it does not much change afternoon. The highest reached efficiency during the day was 61.6% at 13:50, while the minimum value was 39.7% at the beginning of test day. The general view of the curve shows a lower percentage of thermal efficiency than horizontally finned plate solar collector values because of the changing of fins angle. The results showed that the horizontal fins have more advantage on the instantaneous efficiency of double pass solar air collector than the inclined fins.

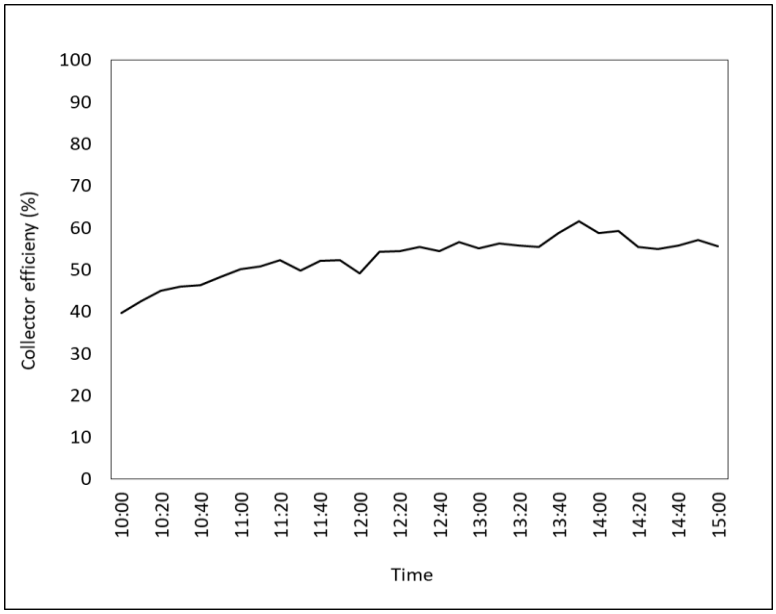

Fig. 4.28. Instantaneous efficiency of 45^o inclined finned plate double-pass solar air collector efficiency vs time

Temperatures stratifications of trays in drying chamber by using 45^o finned plate double-pass solar collector with the time of drying process are shown in Fig. 4.29. The stratification is very clear in this graph. The temperature difference between the first and second tray is higher than the difference between the fourth and fifth tray due to the thermal capacity of heated air decrease. The beginning and end of curves are fluctuated due to the instability of working conditions in these periods. It is obvious the agreement between the behaviour of drying chamber temperatures and absorbing surface, collector's inlet, second pass inlet and outlet temperatures. The curves of temperature in five trays increased with the time to reach the maximum peak values 29.4, 28.4, 27.8, 26.8 and 26.5 ^{o}C respectively at 13:20.

The distributions of relative humidity in drying chamber trays by using 45^o finned plate solar air collector are shown in Fig. 4.30. At the beginning of the drying process, the relative humidity values are high with the high moisture content product items.The maximum value of relative

humidity in every tray were 38, 39, 43, 48 and 50% from the first to the fifth tray respectively at the first record at 10:00 due to the high ambient relative humidity and low absorbing surface temperature. The general trend of relative humidity curves shows a fast decrease from 10:00 to 13:20 afternoon, while the performance is an approximately constant afternoon with some fluctuation due to weather aspects variation. The main difference between these curves and curves which collected by using flat and horizontally finned plate solar collector is the humidity difference between drying chamber and ambient. In 45^{o} finned plate collector, the difference between trays and ambient increases with the time, while it decreased with using flat and horizontally finned plate solar collectors.

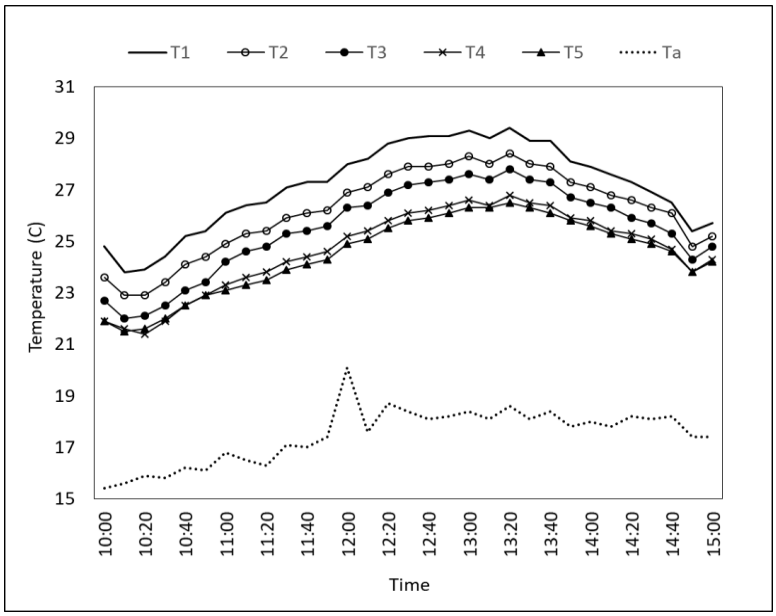

Fig. 4.29. Temperature stratification of drying chamber by using 45^{o} inclined finned plate double-pass solar air collector vs time

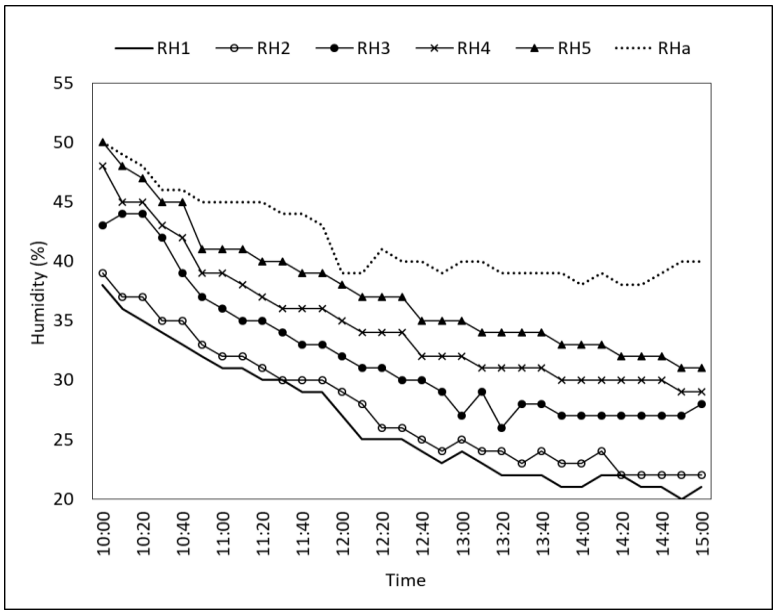

Fig. 4.30. Relative humidity stratification of drying chamber by using 45^{o} inclined finned plate double-pass solar air collector vs time

4.3.3. Vertically finned plate solar air collector experimental analysis

In this set of experimental results, the rectangular vertical fins (parallel to air stream flow) are integrated with absorbing surface in order to investigate the thermal performance of double-pass solar air collector and drying chamber as shown in Fig. 4.31. The experimental data of vertically finned plate double-pass solar air collector have been graphed and reported with 10min constant time step for five hours from 10:00 to 15:00 of 12 of October 2017. The conditions of climate were approximately clear with some part clouds with some up and down fluctuations of ambient relative humidity and temperature afternoon (between 12:40 and 15:00). The wind was approximately quit low speed during test's hours.

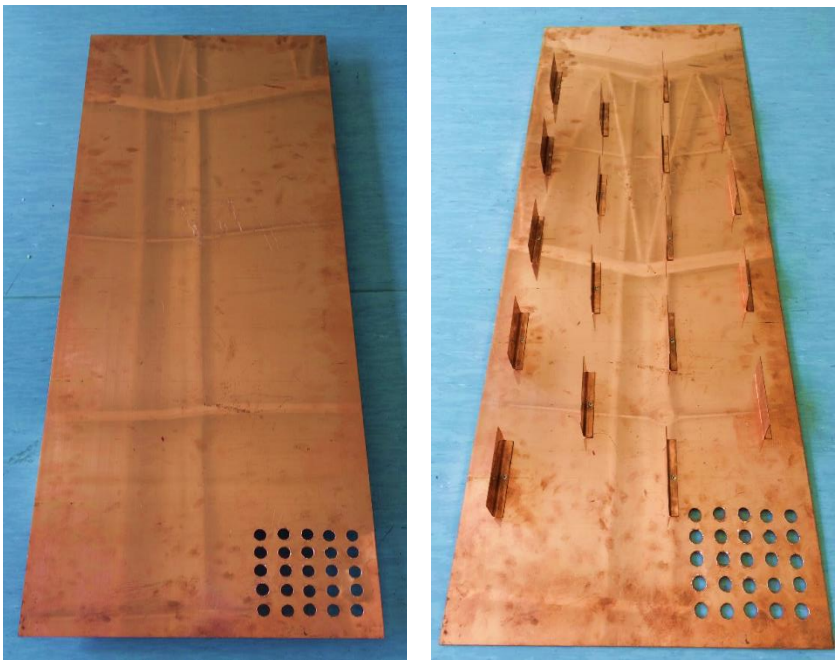

Fig. 4.31. Configuration difference between flat and vertically finned absorbing plate

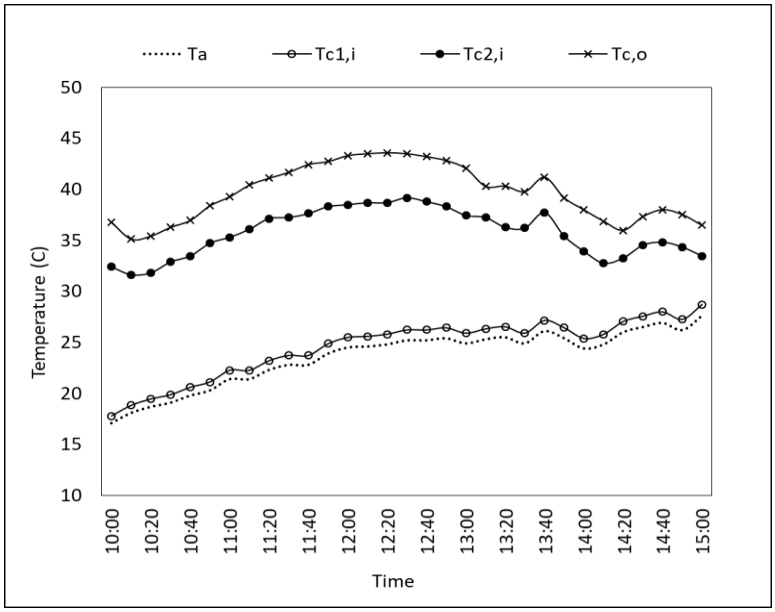

Fig. 4.32. Vertically finned plate double-pass collector's inlet, second pass inlet, outlet and ambient temperature vs time

Fig. 4.32 shows the variation of solar collector inlet, second pass inlet, and outlet air temperatures of vertically finned solar air collector. Collector's second pass inlet and outlet temperatures increased from the beginning of experiment indirect with ambient temperature to the maximum values 43.6 ºC and 39.2 ºC respectively at 12:20. The maximum temperature differences for upper and lower collector channel are 14 ºC and 4.5 ºC at 11:40 and 12:20 respectively. After 12:30, temperature curves deceased indirect with solar radiation intensity.

The average absorbing surface temperature variation by using vertically finned double-pass solar air collector with the time are explained in Fig 4.33. Absorbing surface temperatures increased from the morning to reach highest levels around noon. The maximum absorbing surface temperature is 49.7 ºC with the solar radiation intensity 1014 W/m^2 at 12:20. After 13:00, the temperature curve has fluctuated decline to reach 39.8 ºC at the end of the test. The maximum difference between absorbing surface and ambient temperature was 25.2 ºC at 11:50.

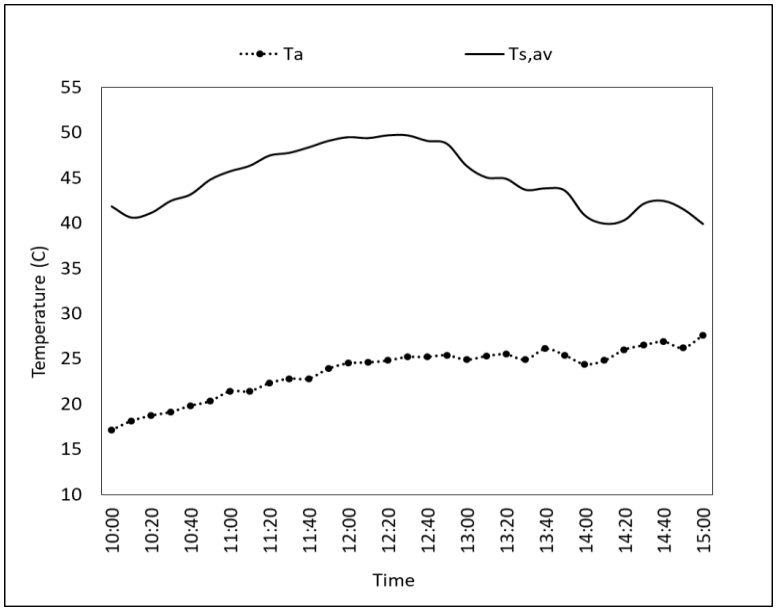

Fig. 4.33. Average absorbing plate and ambient temperatures vs time

Fig. 4.34 shows the instantaneous useful heat variation for the upper and lower channels of vertically finned plate double-pass solar collector and solar radiation intensity with the time. As shown, the curve of solar radiation intensity has very fluctuated rates after 12:40. The maximum recorded solar radiation is 1017 W/m^2 at 12:00. The values of gained useful heat are lower than the values which recorded by using horizontally and 45^o finned plate solar collector in the previous sections. The highest useful heat is 328 W/m^2 at 11:50 because of the highest levels of solar radiation and solar collector temperature differences. The direction of extended surfaces (vertical Fins) does not produce high air turbulence as noticed with horizontal fins or 45^o fins which leads to highest air temperatures. The instantaneous thermal efficiencies of vertically finned plate solar collector are plotted as shown in Fig. 4.35. The curve shows a prolonged decrease from the morning to the end of test with some fluctuations are noticed due to solar radiation instability. The highest reached efficiency during the day was 62.2% at the beginning, while the minimum value was 32.7% at the end of test day. The general view of the curve shows a lower percentage of thermal efficiency than horizontally and 45^o inclined finned plate solar collector values because of the changing of fins angle. The results showed that the horizontal fins have more advantage on the instantaneous efficiency of double pass solar air collector than the inclined fins and vertical fins.

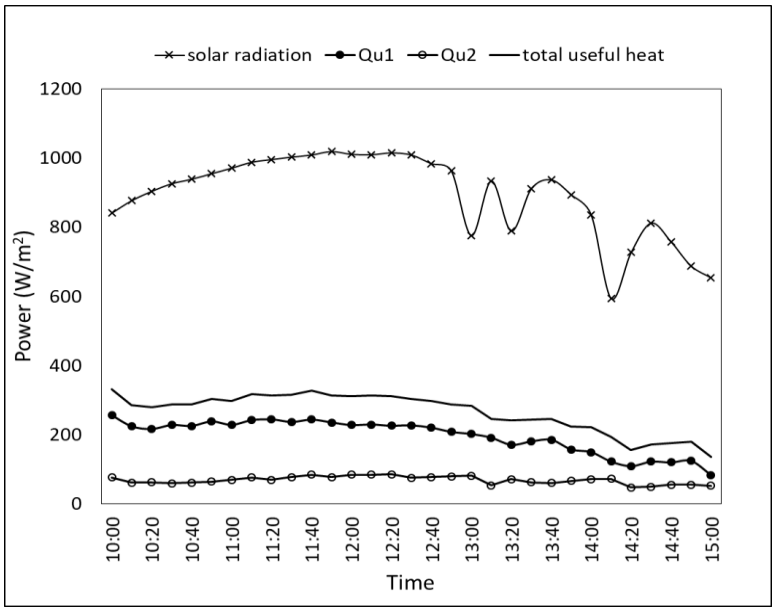

Fig. 4.34. Useful gained heat and solar radiation intensity vs time

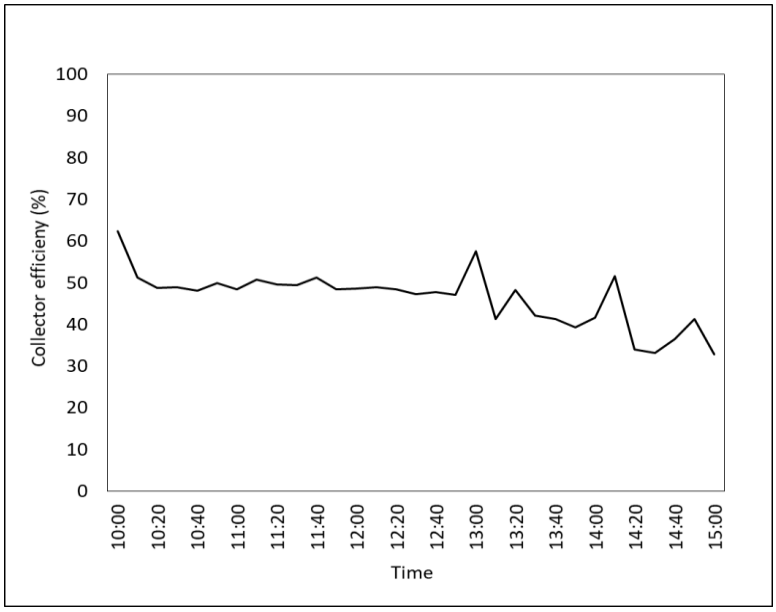

Fig. 4.35. Instantaneous efficiency of vertically finned plate double-pass solar air collector efficiency vs time

Temperatures stratifications of trays in drying chamber by using a vertically finned plate double-pass solar collector with the time of drying process are shown in Fig. 4.36. The temperature difference between the first and second tray is higher than the difference between the third and fourth tray due to the thermal capacity of heated air decrease. The values of temperatures in the last two tray are approximately the same with a very neglected difference. After 12:40, the curves are fluctuated due to the instability of solar radiation intensity in this period. It is obvious the agreement between the behaviour of drying chamber temperatures curves and absorbing surface, collector's inlet, second pass inlet, outlet temperatures and solar radiation curve. The curves of temperatures in five trays increased indirectly with the time to reach the maximum peak values 38.7, 37, 36.2, 34.9 and 34.7 ^{o}C respectively at 12:20. The difference between ambient and trays temperatures are decreasing with time to reach minimum values at the end of the test.

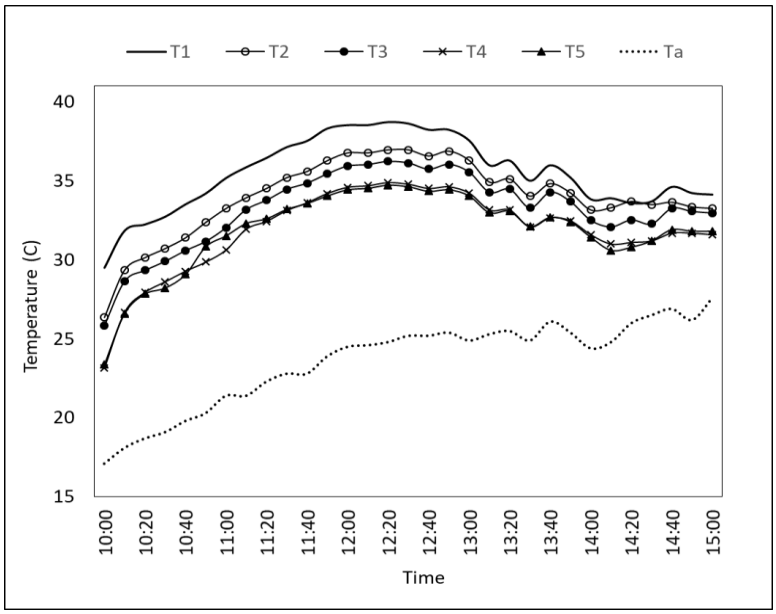

Fig. 4.36. Temperature stratification of drying chamber by using vertically finned plate double-pass solar air collector vs time

The distributions of relative humidity in drying chamber trays by using vertically finned plate solar air collector are shown in Fig. 4.37. The maximum relative humidities of air in the five trays are 47, 53, 56, 61 and 64% from the first to the fifth tray respectively at the first record at 10:00 due to the high ambient relative humidity and low absorbing surface temperature. The general trend of relative humidity curves shows a fast decrease from 10:00 to 13:20 afternoon, while the performance is fluctuated afternoon with some due to weather aspects variation

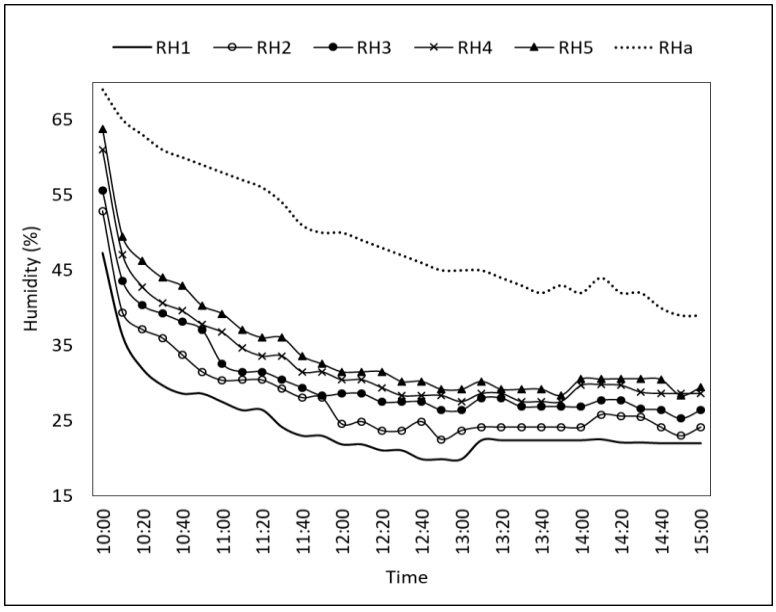

Fig. 4.37. Relative humidity stratification of drying chamber by using vertically finned plate double-pass solar air collector vs time

4.3.4. Helically finned plate solar air collector experimental analysis

The aluminium helical fins are integrated with absorbing surface in order to investigate the thermal performance of double-pass solar air collector and drying chamber as shown in Fig. 4.38. The experimental data of helically-finned plate double-pass solar air collector have been collected with 10min constant time step for five hours from 10:00 to 15:00 of 26 April 2018. The conditions of climate were very clear with some part small clouds. The wind was approximately quit low speed during test's hours.

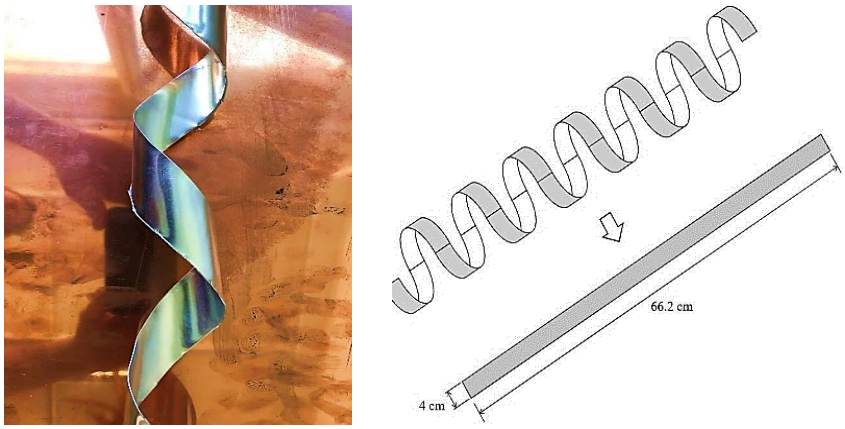

Fig. 4.38. Configuration and dimensions of helical fins

Fig. 4.39 explains the variation of solar air collector inlet, second pass inlet, and outlet air temperatures of helically-finned solar air collector. Collector's second pass inlet and outlet temperatures vary indirectly with the solar radiation intensity variation. The maximum second pass and collector's outlet temperatures were 59.5 ^{o}C and 65.9 ^{o}C at 12:20 respectively. The maximum temperature differences for upper and lower collector channel are 33 ^{o}C and 8 ^{o}C at 11:50 and 12:00 respectively. After 12:20, air temperature values are deceased indirectly with the decreasing of solar radiation intensity. As shown, values of outlet temperatures are much higher than the outlet temperatures of discussed five collectors due to high ambient temperatures and radiation intensity.

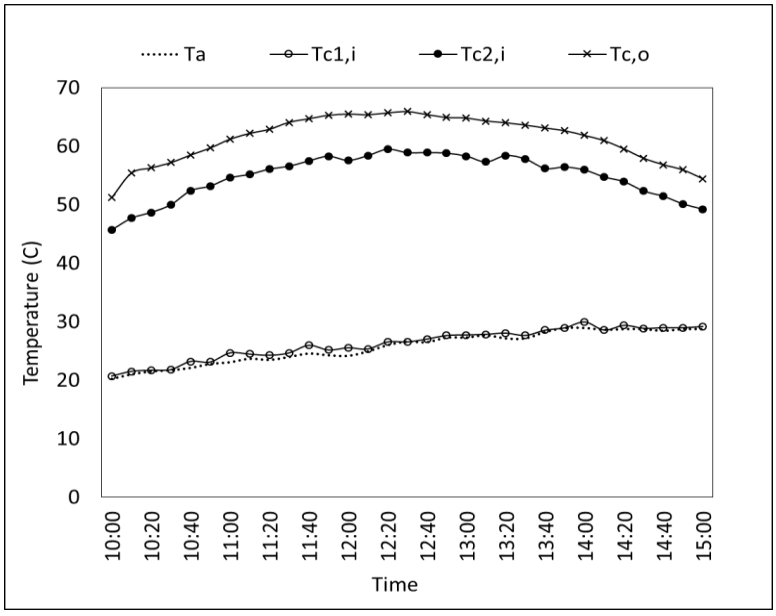

Fig. 4.39. Helically finned plate double-pass collector's inlet, second pass inlet, outlet and ambient temperature vs time

The average absorbing surface temperature variation by using helically-finned double-pass solar air collector with the time are explained in Fig 4.40. Absorbing surface temperatures formed the same shape of collector's outlet temperature curve to reach highest levels around noon. The maximum absorbing surface temperature is 81.3 ^{o}C with 998 W/m^2 solar radiation intensity and 26.7 ^{o}C at 12:30. After 13:00, the temperature curve declined smoothly to reach 63.7 ^{o}C at the end of the test. The maximum difference between average absorbing surface and ambient temperature was 56.7 ^{o}C at 12:00. The graphed curves of the helically-finned solar collector are less fluctuated than the last curves of another solar collector due to the stability of ambient conditions.

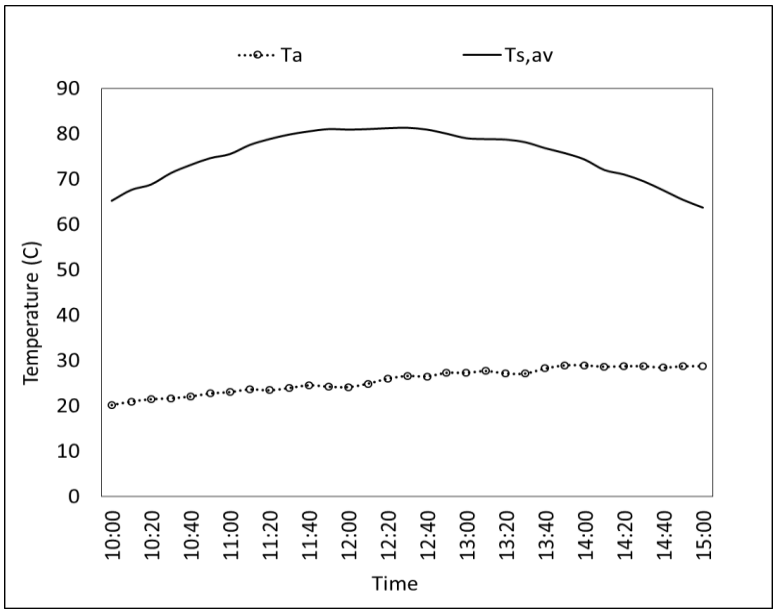

Fig. 4.40. Average absorbing plate and ambient temperatures vs time

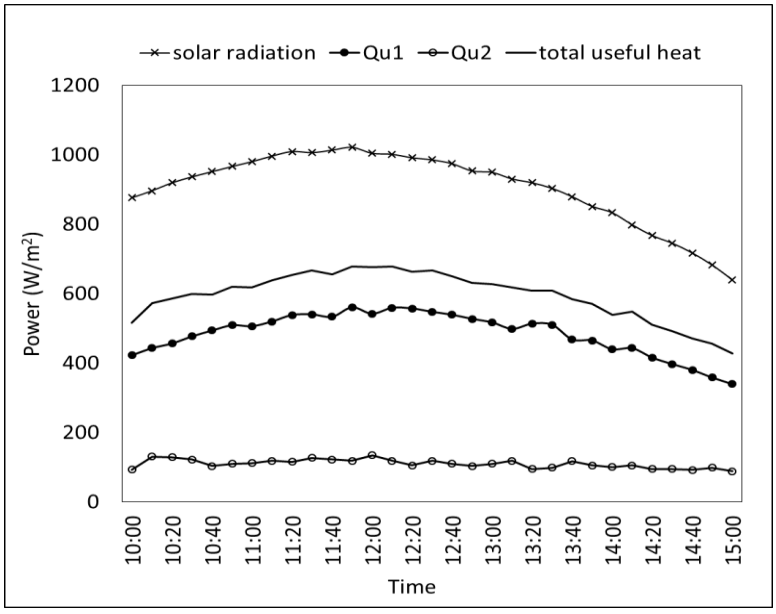

Fig. 4.41. Useful gained heat and solar radiation intensity vs time

Fig. 4.41 explains the plotted instantaneous useful heat gained for the two channels of helically-finned plate double-pass solar collector and solar radiation intensity with the time. The maximum recorded solar radiation is 1021 W/m^2 at 12:00. The values of useful gained heat are higher than the rates which recorded by using un-finned, horizontally finned, vertically finned and 45^{o} finned

plate solar air collectors in the previous section. The highest useful gained heat is 678.6 W/m^2 at 12:00 because of the highest levels of solar radiation intensities and solar collector temperature differences.

Fig. 4.42 shows the instantaneous variation of thermal efficiencies of helically-finned plate solar collector. The curve indicates approximately constant efficiency curve during test time. The highest reached efficiency during the day was 65.3% at 12:20, while the minimum value was 56.8% at the beginning of test day. The general view of the curve shows a higher percentage of thermal efficiency than un-finned and another finned plate double-pass solar collector's values because of the changing of fins shape and area. The results showed that the helical fins have more advantage on the instantaneous efficiency of than the other tested double-pass solar air collectors. The previous studies and last sections results showed that the increasing area of absorbing surface plays an important factor to increase the efficiency of solar air collector. According to this study, the increasing of absorbing surface area not enough to get the optimum efficiency, the shape and direction of the extended surfaces should be taken into account. The helical surfaces (Fins) attachment are not increasing heat transfer area only; it is increasing the turbulence of flowed air through solar collector which increase surface temperature.

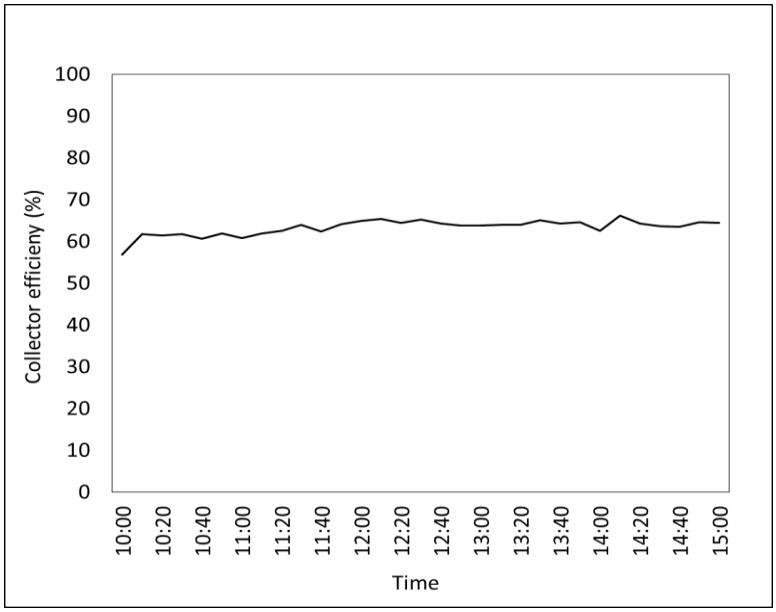

Fig. 4.42. Instantons helically-finned plate double-pass solar air collector efficiency vs time

Fig. 4.43 explains the distribution of temperatures in drying chamber trays for five hours. The stratifications of temperature differences are very sufficient. The shapes of temperature curves are hardly affected by solar radiation values. The temperature difference between the first two trays T_1 and T_2 is higher than the difference between the last two trays T_4 and T_5 due to the thermal capacity of heated air decrease. The values of temperature in five trays increased with the time to reach the maximum peak values 41.2, 39.2, 37.9, 37 and 36.1 ^oC respectively at 12:10.

The relative humidity stratification distribution in drying chamber trays are shown in Fig. 4.44. At the beginning of the drying process, the moisture content of the product is high which leads to very high moisture loss rate. The differences between five curves are more sufficient than the curves which gained by using previous tested solar air collectors. The maximum relative humidity in every tray were 36, 38, 41, 46 and 47% from the first to the fifth tray respectively at 10:00 due to

the high ambient temperature and low solar radiation intensity. The minimum values were 18, 20, 24, 27 and 28% from the first to the fifth tray respectively at the end of the experiment.

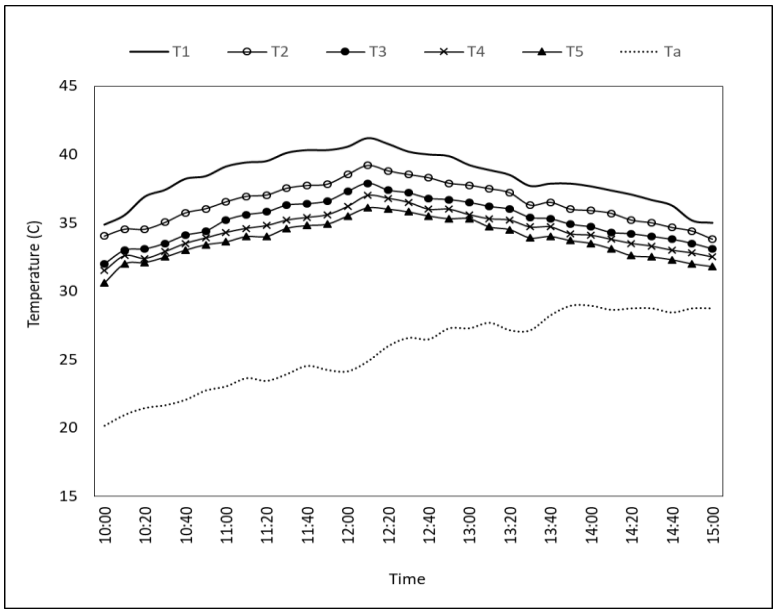

Fig. 4.43. Temperature stratification of drying chamber by using helically-finned plate double-pass solar air collector vs time

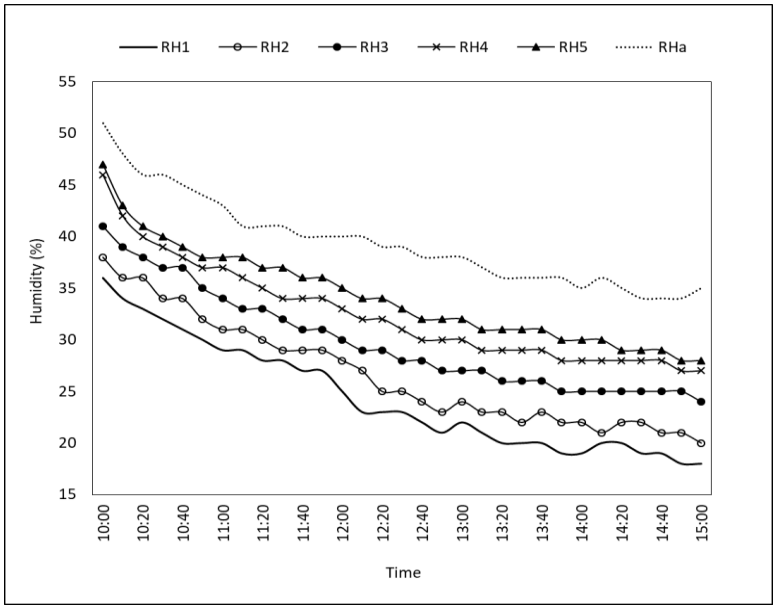

Fig. 4.44. Relative humidity stratification of drying chamber by using helically-finned plate double-pass solar air collector vs time

Finally, the effect of fins direction with the thermal efficiency of double-pass solar air collector is obtained in Fig. 4.45. The horizontal (0^o) showed the highest efficiency compared with the other angles. The experimental curve shows an inverse relation between fins angle and thermal efficiency. Theoretically, a second order polynomial model gives the closest shape for relation, where x axis represents the angle of rectangular fins ψ, while y axis represents the thermal efficiency of solar collector (η) as following:

$$\eta = a\,\psi^2 + b\,\psi + c. \tag{4.6}$$

The parameters *a*, *b* and *c* of polynomial model are calculated analytically for the case of rectangular finned double-pass solar air collectors groups, as follows:

$$a = -0.0006,\ b = -0.0536\ and\ \ c = 55.975.$$

During the approximation the correlation coefficient was 0.99 along with the standard deviation of 3.9%. The first term can be neglected if the angle is very small due to low value of *a* parameter. The efficiency is a function of the geometry of surface.

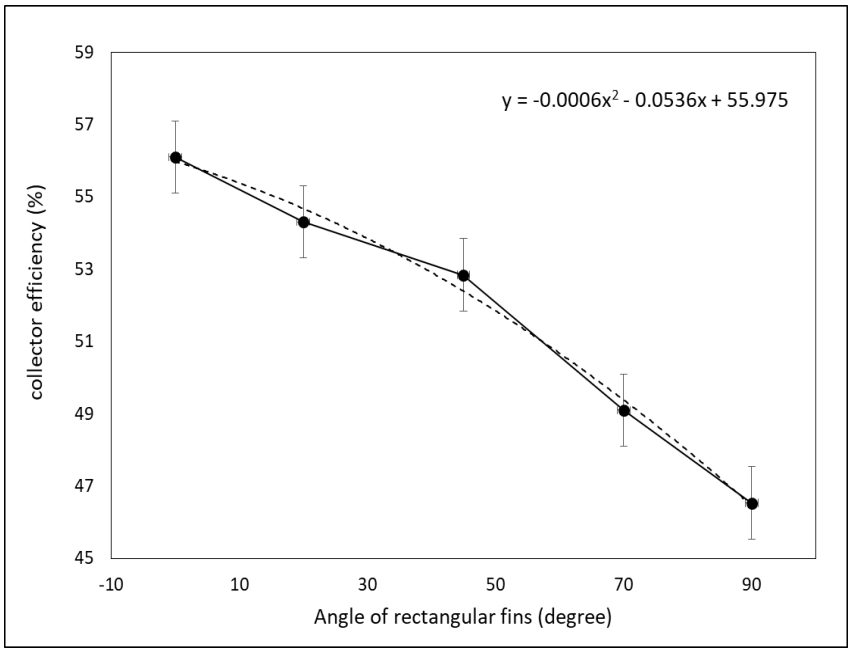

Fig. 4.45. Relationship between rectangular fins direction and collector thermal efficiency

4.4. Daily efficiency analysis

The final performance of examined solar air collectors were compared in the form of daily thermal efficiency (for five hours). The instantaneous thermal efficiency is not giving a clear idea about solar collector performance due to its variation with test parameters variation and because the collectors are tested in different days and climate conditions. To estimate the total daily thermal efficiency, trapezoidal integration method has been used with time interval 10min for instantaneous efficiencies values (Eq. 4.4).

Fig. 4.46 shows the improvement of flat plate solar air collector's efficiency by increasing number of air passes. The calculated daily efficiency of the single-pass solar collector is 38.25%, while it is 45.56% for double-pass solar air collector. Actually, the main reason for that increase is the increasing of heat transfer area between the absorbing surface and flowed air.

Single-pass and double-pass solar collector has been studied in the previous studies with different collector's dimensions and working conditions, the higher thermal efficiency and heat transfer rate was obtained during the double pass. The heat loss is significantly reduced in the double pass and assisted in heat retention. They explained that multi-pass solar collector could also be made for further improvement in performance efficiency of solar collector (Kareem et al., 2013; Velmurugan and Kalaivanan, 2013). In this study, the value of efficiency improvement by duplicating air pass was very agreed with the past works with the acceptable difference due to the different location and weather conditions of the experiments.

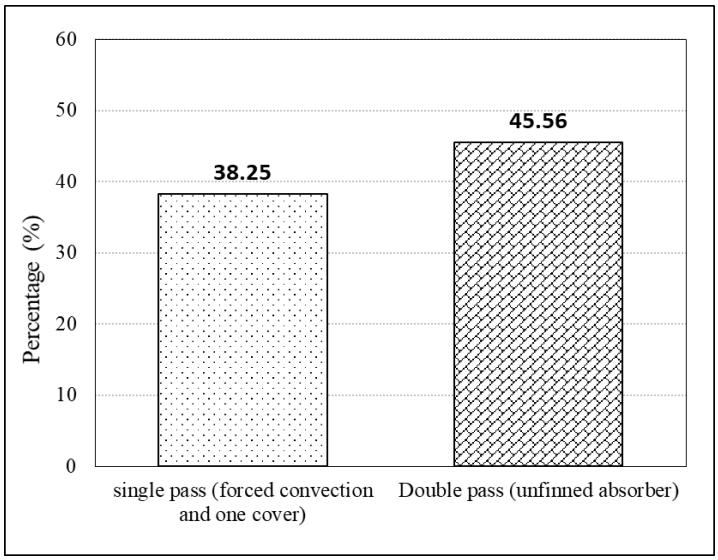

Fig. 4.46. Daily efficiency of single and double-pass solar air collectors

Fig. 4.47 shows the improvement of double-pass solar air collector's efficiency by change absorbing surface's area and shape. The daily efficiency is calculated for five types of absorbing surfaces solar collectors; flat plate, horizontally finned plate, 45^{o} finned plate, vertically finned plate and helically-finned plate solar collectors. As shown, the thermal efficiency of double-pass solar air collector hadn't significant improvement with about 1% by integrating vertical rectangular extended surfaces (fins). This is because two main reasons, first is the direction of fins parallel to the direction of air flow and the second is the extended surfaces are not exposed in an optimum way to the solar radiation.

The efficiency improvement is much obvious by turning the fins by 45^{o}. The thermal efficiency increased about 7% with integrating 45^{o} finned absorbing surface. The turbulence of flowed air through solar collector increased, and the exposed area to sun arrays is increased. The bar diagram shows the best direction of rectangular fins is the horizontal direction. The calculated daily efficiency of horizontally finned solar air collector is 56.01%, while 45.56% for flat plate solar collector. The enhancement of thermal efficiency was very obvious with about 11%. According to the mentioned, not only the increase of the absorbing surface area plays the main factor to increase solar collector performance, however, the direction of and position of extended surfaces.

The last tested solar air collector which showed the most efficient performance is the helically-finned plat solar air collector. In spite of the fins are made from aluminium, but the daily efficiency was higher than other finned tested solar collectors. The daily efficiency of this solar collector was about 63.3%. The enhancement of thermal efficiency compared with flat plate solar collector (reference collector) were obvious with about 18%. The helical shape of fins had a very effective rule to increase the turbulence of air in solar collector channel. The turbulence of flowed air leads to more friction forces between air and an absorbing surface which results in a wanted rise in air temperature.

In the previous studies, the effects of extended surfaces are studied with different shapes. The highest collector efficiency were achieved by the finned plate solar collector, whereas the lowest efficiencies were obtained from the collector without fins. It obtained that the efficiency of the solar air collectors depends significantly on the area and geometry of absorbing surface (Chabane et al., 2013; Rai et al., 2016).

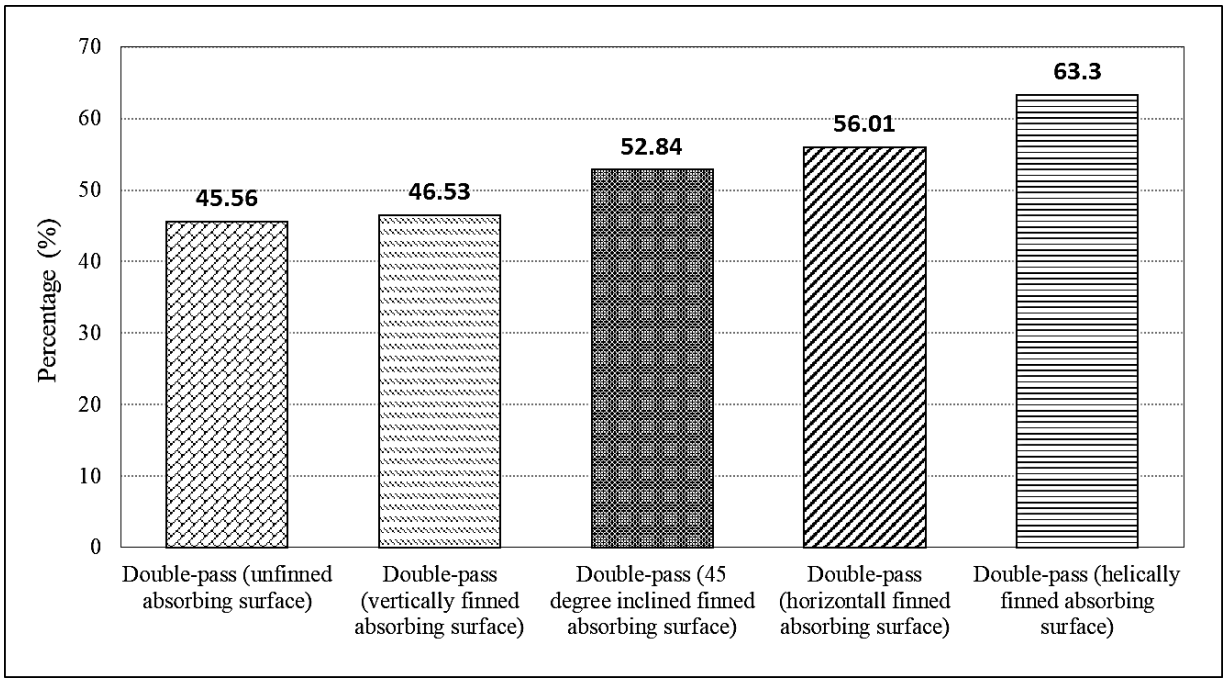

Fig. 4.47. The daily efficiency of finned and un-finned double-pass solar air collectors

4.5. Effect of air mass flow rate

4.5.1. Forced air movement

In order to estimate the effect of air flow rate, the flat plate double-pass solar air collector examined experimentally with different values of air mass flow rates. As shown in Fig. 4.48, the flow rate of air has a sufficient effect on the thermal efficiency of solar air collector. As shown, the thermal efficiency of solar air collector varies indirectly with air mass flow rate variation. The solar air collector investigated with four values of air mass flow rate 0.0175, 0.0198, 0.0228 and 0.025 kg/s. The highest value of thermal efficiency was about 59% at 0.0251 kg/s air mass flow rate, while the lowest was approximately 45.5% at 0.0175 kg/s.

The effect of air mass flow rate has been studied in the previous studies, and our results showed a good agreement with the published results. The experimental published results showed that the collector efficiency increases with increasing the solar radiation intensity and mass flow rate (Aldabbagha et al., 2010; Ibrahim et al., 2013; Chabane et al., 2013; Umayorupagam et al., 2017; Sharma and Saha, 2017). The increasing of airspeed through the solar air collector increases the turbulence which leads to higher friction forces between flowed air and absorbing surface. The higher air velocity results decreasing of absorbing surface temperatures which minimize the thermal losses of the solar collector to the ambient.

In this study, the solar air collectors in the previous sections are tested under the lowest value of air mass flow rate (airspeed 2.3 m/s) to obtain the real thermal performance of solar collectors under most depressed working conditions. The flow rate can be affected by some flow losses due to some uncontrolled leakages in an air duct or solar collector, but the value of flow rate has been measured in inlet and outlet of the solar collector to keep it constant.

In another hand, the air mass flow rate is affecting solar air collector's outlet temperature sufficiently (Vyas and Punjabi, 2014; Bayrak and Oztop, 2015). The increasing of airspeed through

solar air collector increases the amount of transferred heat energy to the air which leads to rising outlet temperature value.

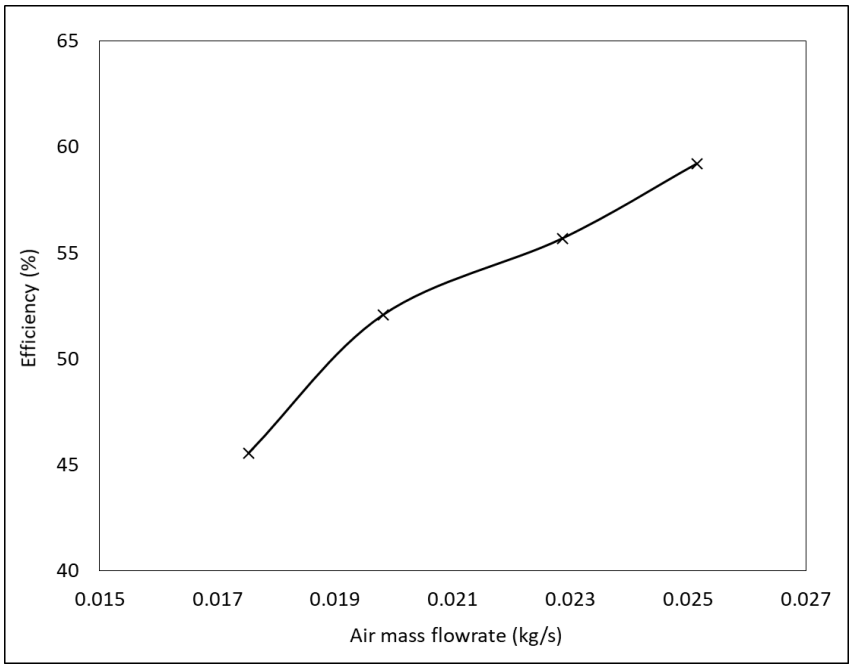

Fig. 4.48. The relation between air mass flow rate variations with the daily efficiency of flat plate double-pass solar air collector

4.5.2. Natural air movement by chimney effect

The solar drying system has been tested under free air movement with and without chimney by using single-pass solar air collector. The integrated chimney has a circular cross-section and 1.5 m length. The experimental results are collected in 9 of October 2017 with free air velocity as shown in Fig. 4.49.

Fig. 4.49. Solar drying system with and without chimney integration

Fig. 4.50 shows the variation air speed in the chimney with the time of the experiment (five hours). The speed of air stream increased with the time due to solar radiation and temperature increase. The maximum speed of air was 0.91 m/s at 12:00.

Fig. 4.50. The chimney air speed of drying system with chimney integration

Fig. 4.51 explains the variation of air speed with solar radiation intensity variation for two radiation ranges. The figure shows the indirect relation between speed and solar radiation. The speeds increased sharply at the beginning of experiment due to temperature increase. In fact, the curve grew up to reach the maximum value at the maximum solar radiation. Theoretically, a second order polynomial model is the closest expression which represent the behaviour, where *x* represents the intensity of solar radiation *I*, while *y* represents the speed of air through chimney V_{ch} as following:

$$V_{ch} = a\, I^2 + b\, I + c. \tag{4.7}$$

To find the final model morning and afternoon, the numerical constants *a*, *b* and *c* of polynomial model are calculated analytically for solar radiation range from 600 W/m^2 to 1100 W/m^2. The parameters *a*, *b* and *c* of polynomial model are estimated analytically as the following values:

$$a = 10^{-6},\ b = -0.002\ and\ \ c = 1.3806.$$

During the approximation the correlation coefficient was 0.96 along with the standard deviation of 0.075 m/s. The decline of airspeed afternoon was slower than the increasing before noon. This is because the stored heat in absorbing surface needs a long time to be lost. The behaviour of curve in Fig. 4.51 agreed with the behaviour in Fig. 4.50. The fluctuation of curves due to the pressure and flow losses through solar drying system.

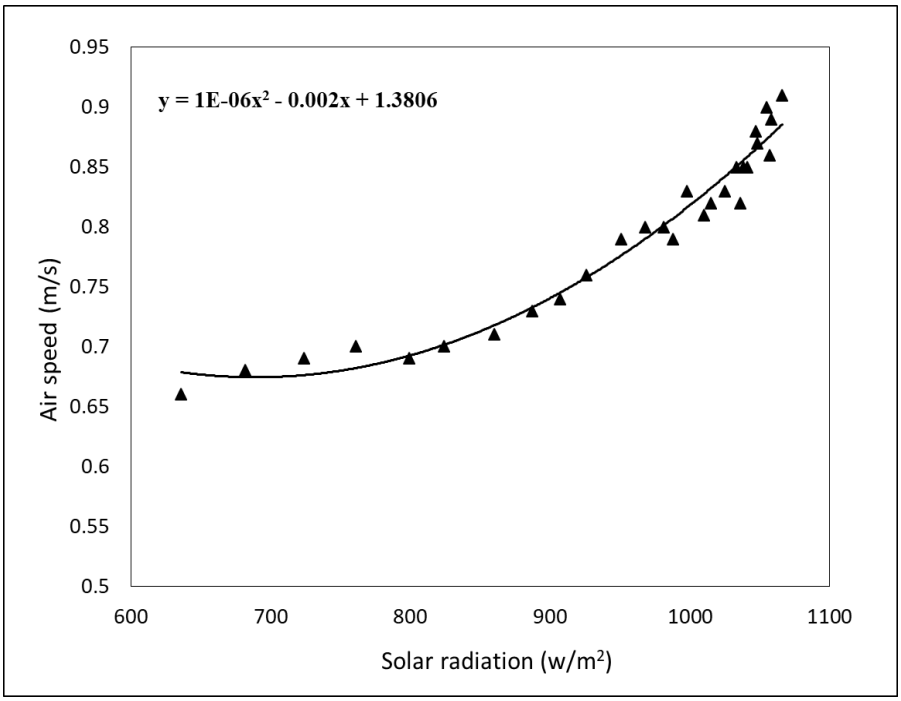

Fig. 4.51. The chimney air speed of drying system with solar radiation intensity variation

Fig. 4.52 shows the variation of chimney air speed with the absorber plate temperature. The increasing of absorber temperature leads to the more useful heat gained to the air. The temperature rise of air decrease the density of air which results a bouncy force. The density difference or bouncy force produce the needed flow in the solar chimney. The design of solar chimney plays important rule to increase the speed of air due to the angle of entrance and length. The little slope which done in the top of drying chamber leads to smooth movement of air flow.

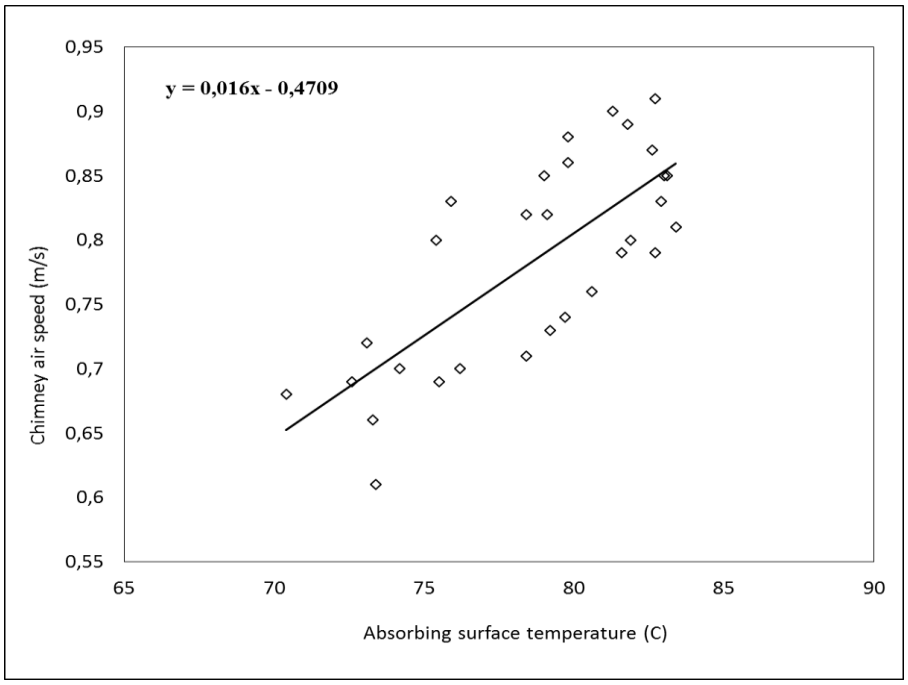

Fig. 4.52. The chimney air speed of drying system with absorbing surface temperature variation

The height function of a solar chimney is to increase friction forces of flow and to decrease the area of flow to get higher speed. The indirect relation between temperature and speed showed the

maximum airspeed was 0.91 m/s at the maximum absorbing surface 83 ^{o}C. A linear model has been obtained to state the relation between air speed in chimney and average absorbing temperature as following:

$$V_{ch} = a\,T_{s,av} + b. \tag{4.8}$$

As mentioned before, the numerical constants are estimated analytically for absorber temperature range between 70 and 83 ^{o}C with the following values:

$$a = 0.016 \quad and \quad b = -0.4709.$$

During the approximation the correlation coefficient was 0.57 along with the standard deviation of 0.082 m/s. The recorded results are in good agreement with the previous studies, the speed of air proportional directly to the temperature and solar radiation (Tan and Wong, 2013; Budijono et al. 2016). Also, the thermal efficiency of solar drying system enhanced by the integrated chimney (Russon et al., 2009). To estimate the type of flow through drying chamber by calculating Reynold's number is very important in case of uniform structure, but in our case the structure of duct is not uniform. The flow of air through drying chamber is turbulent. The turbulence of air have been produced by the trays of chamber and friction forces.

4.6. Final weight analysis of dried product

The weights of dried product (apple slices) in every tray of drying chamber after and before drying process by using a single-pass flat plate solar air collector are shown in Fig. 4.53. The total initial weight of product items is 2000 g; it has been divided into five parts (400 g for each).

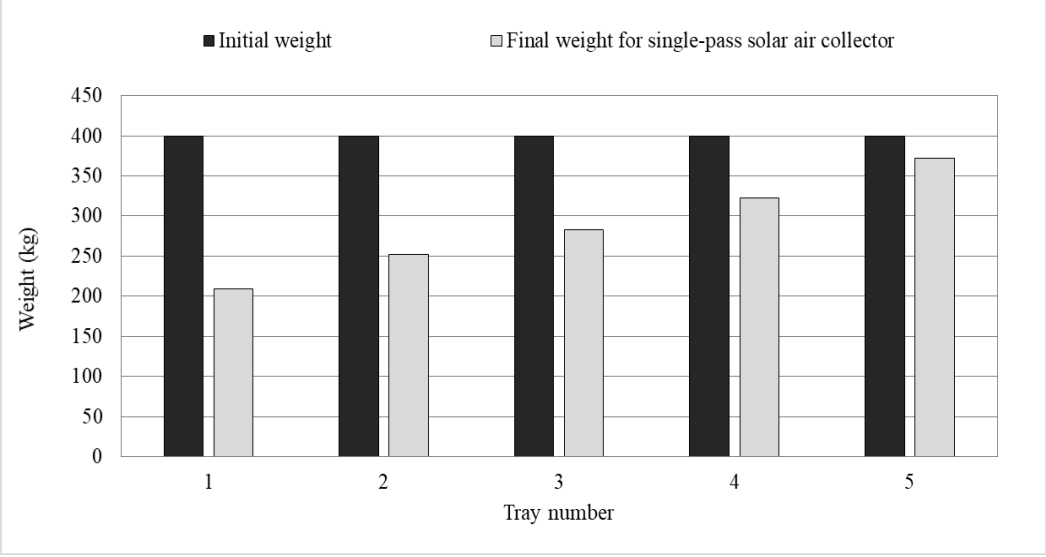

Fig. 4.53. The final weights of dried product in drying chamber trays by using single-pass solar air collector

After five hours of the drying process, the final weights of apple slices are 209, 252, 283, 323 and 372 g from the first to the fifth tray respectively. The lost weight represents the amount of water content which transferred from the product to the heated air. The increasing of product's water content temperature by the heated air leads to evaporate the water to the air. As shown, the lost weight of apple slices after drying graded from the higher value at the first tray to the lowest at the fifth tray. This is due to the decreasing of sensible heat of the air in the direction of flow and the increasing of air moisture content.

Fig. 4.54 shows the initial and final weights of dried product (apple slices) in every tray of drying chamber after and before drying process by using a flat plate double-pass solar air collector. The total initial weight of apple slices is 2000 g which has been divided into 400 g for every tray. After five hours of the drying process, the final weights of items are 173, 210, 258, 289 and 307 g from the first to the fifth tray respectively. The final weights are less than the recorded weights by using single-pass solar air collector.

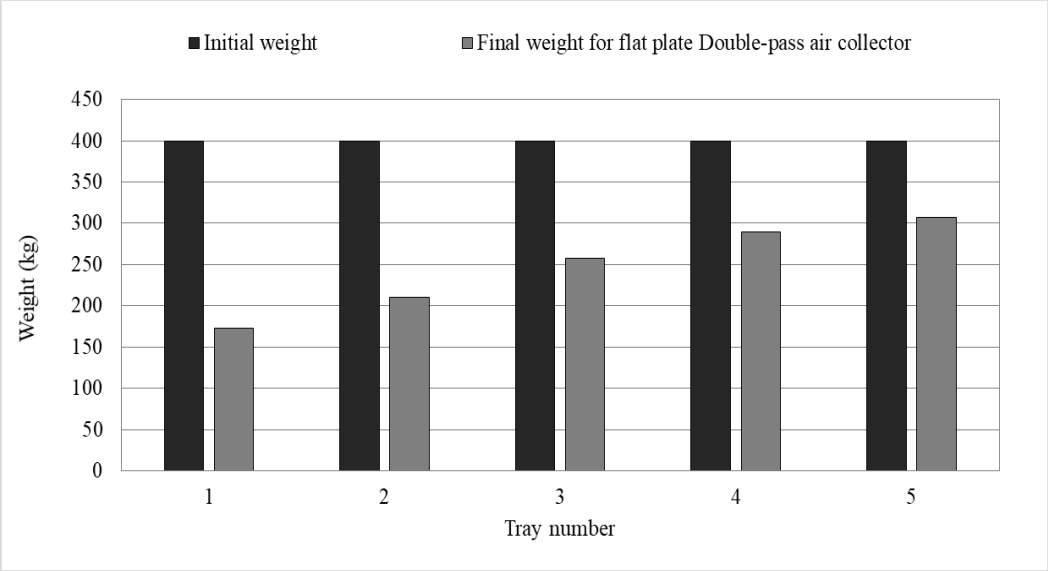

Fig. 4.54. The final weight of dried product in drying chamber trays by using flat plate double-pass solar air collector

The final recorded weights of product items by using horizontally finned plate double-pass solar air collector are shown in Fig. 4.55. The horizontal attached fins increased the amount of evaporated water from the slices. The final weight less than the recorded by using flat plat double-pass solar collector. After five hours of the drying process, the final weights of items are 179, 211, 231, 258 and 282 g from the first to the fifth tray respectively.

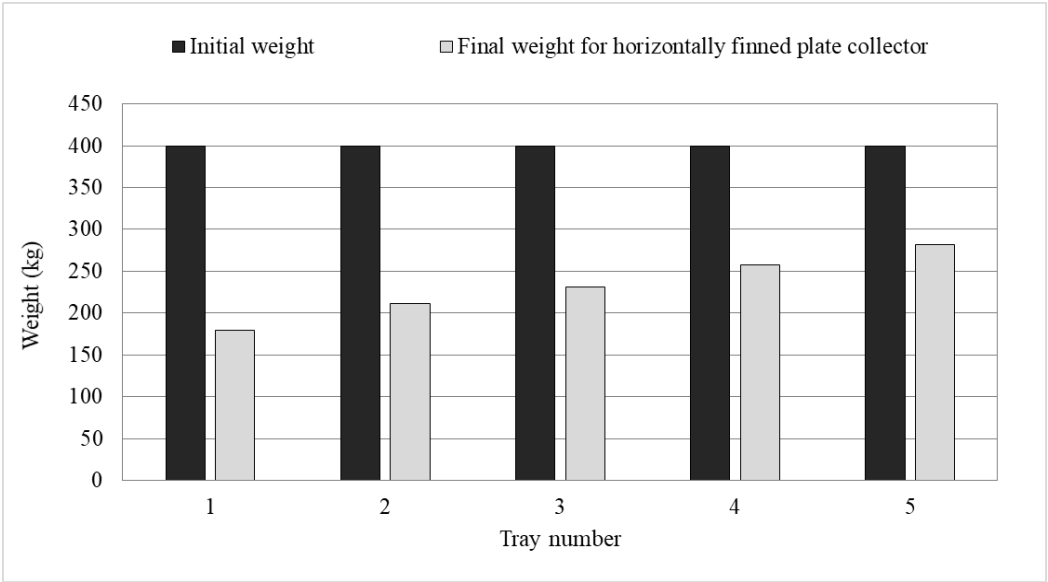

Fig. 4.55. The final weight of dried product in drying chamber trays by using horizontally finned plate double-pass solar air collector

Fig. 4.56 shows the initial and final weights of apple slices in every tray of drying chamber after and before drying process by using a 45° finned plate double-pass solar air collector. The total initial weight of apple slices is divided into 400 g for five trays. The final weight of dried items is 172, 206, 253, 282 and 297 g from the first to the fifth tray respectively.

The lost water content is more than the lost weight by using single-pass solar air collector and flat plate double-pass solar air collector. The changing of fins direction by 45° decreased the amount of lost water from the dried product as well the thermal efficiency of the solar collector.

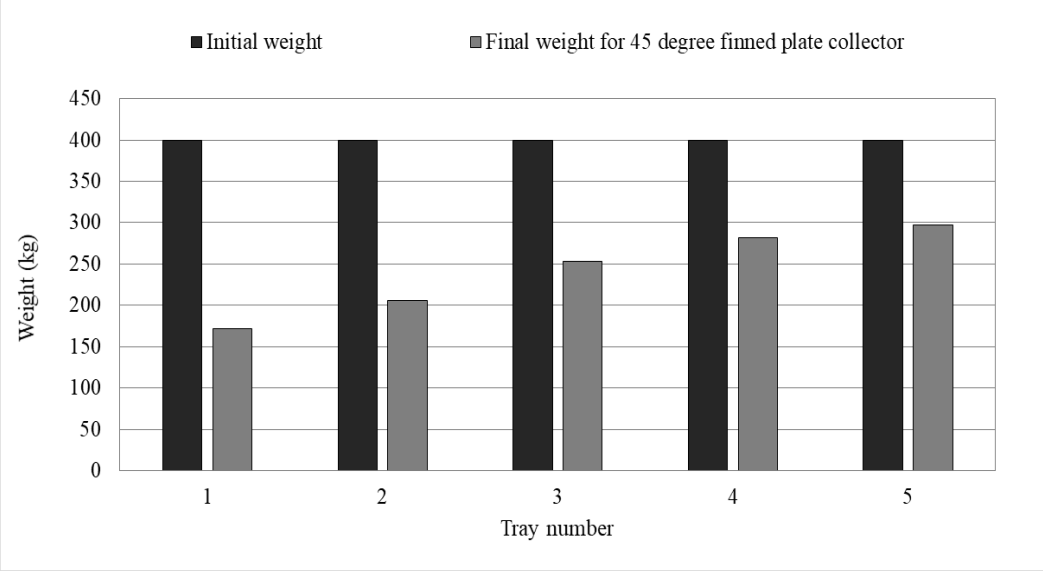

Fig. 4.56. The final weight of dried product in drying chamber trays by using 45° finned plate double-pass solar air collector

Fig. 4.57 shows the initial and final weights of apple slices by integrating a vertical finned plate double-pass solar air collector. As shown, the changing of fins direction to the vertical form has an adverse effect on the amount of evaporated water from the product as well thermal efficiency of the solar collector. The final weights of apple slices are 188, 231, 284, 322 and 348 g for every tray respectively.

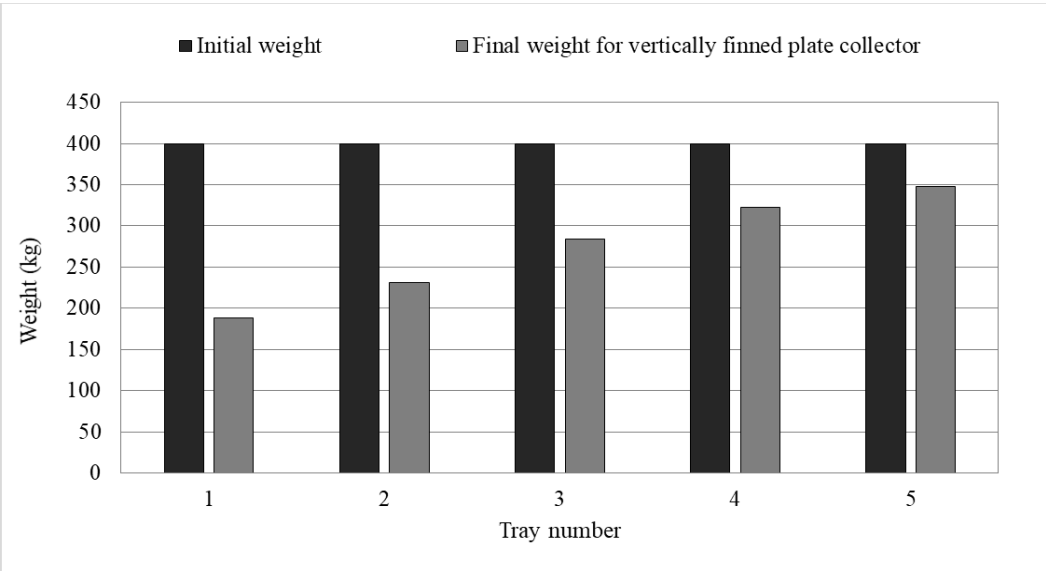

Fig. 4.57. The final weight of dried product by using vertically finned double-pass collector

The final weights of items are more than the recorded weights by using horizontal and 45^{o} finned plate solar collectors. The attaching helical fins to absorbing surface of double-pass solar air collector has a very significant improvement of evaporated water increasing from product items. As shown in Fig. 4.58, the final weights of slices are 158, 177, 189, 206 and 223 g from the first to the fifth tray respectively. As noted, the amount of evaporated water during drying process much more than the lost water content by using flat plate solar air collector.

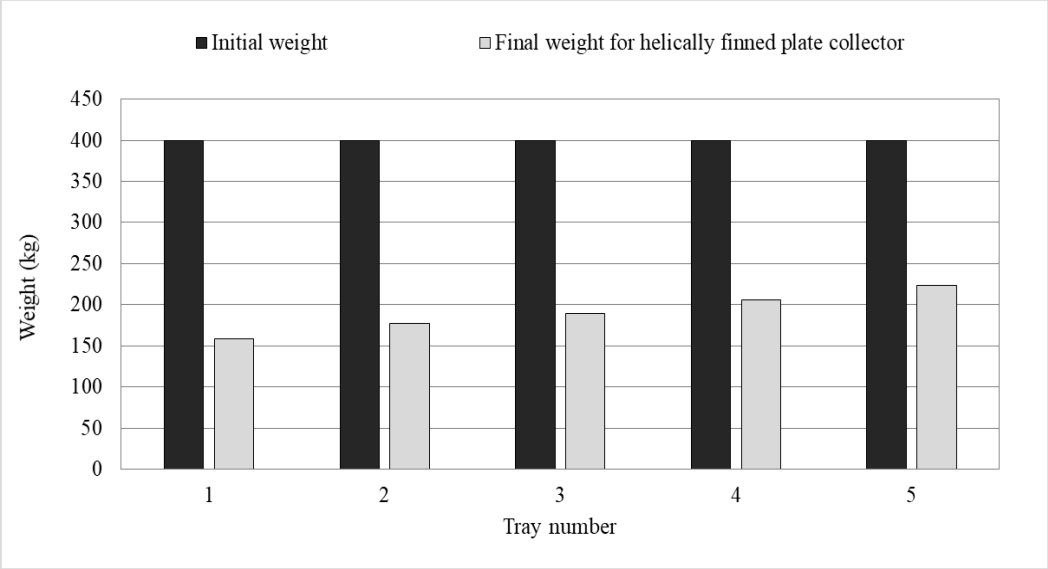

Fig. 4.58. The final weight of dried product in drying chamber trays by using helically-finned plate double-pass solar air collector

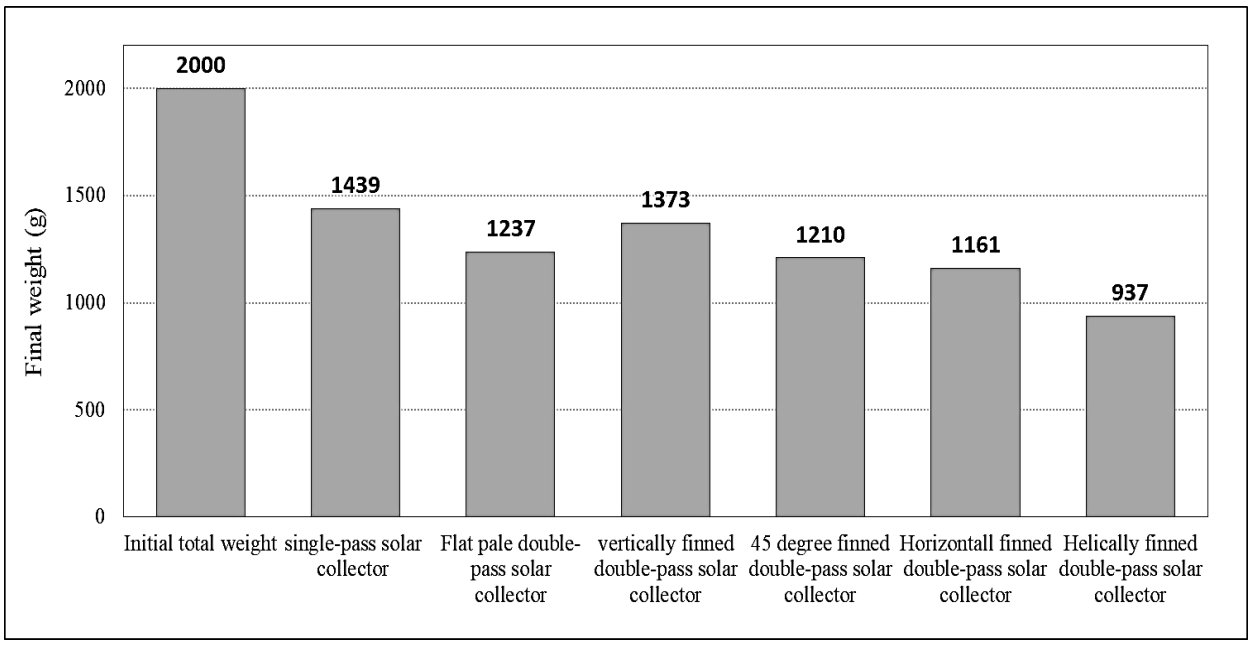

Fig. 4.59. The final total weight of dried product by using different solar air collectors

The total final weight of dried product by using different types of solar collectors is shown in Fig. 4.59. The experimental deviation of these measurements were about ± 3 to ±5% of the measured values. Apple selected as a sample because of its high initial moisture content and its high maximum allowable temperature. The initial moisture content and maximum allowable temperature for an apple during drying process are 80% (wet base) and 70 ^{o}C respectively (Sharma

et al., 2009). The total initial weight of the dried product is 2000 g which scaled by a laboratorian weight scale and average initial moisture content 80%. The average diameter of slices is 65mm with 4 mm as an average thickness. The product (apple) are cut into approximately equal thicknesses slices and divided into five sets with 400 g.

The best result was with using a helically-finned plate double-pass solar air collector with final weight 937 g (lost about 53% of its initial weight). The using of double-pass solar air collector enhanced water content missing from 28% to 38% compared d with single-pass solar air collector. The attaching of horizontal fins to the double-pass solar collector enhanced the process from 38% to 42% compared with flat plate double-pass solar collector. The changing of fins direction affected on the final weight of the dried product. As shown, the vertical and 45^{o} finned plate solar collectors were less efficient than horizontal finned solar collector as well the thermal efficiencies which mentioned in the previous sections.

The shape and size of dried apple slices are much changed after drying process as shown in Fig. 4.60. The colour of slices became darker than the fresh slices due to the missed moisture content of product items. The final moisture contents for apple slices were approximately between 40 and 50% for the different types of tested solar air collectors.

The final moisture content showed a good agreement for the short time of drying process (5 hours) and compared with 24% as a desired final moisture contents for apple (Sharma et al., 2009). Actually, the drying process for any product leads to a physical and chemical changes in the product items. The high working temperature is damaging some products like meat and fish, so the temperature must be controlled for some types of products.

Fig. 4.60. The product items after and before the drying process

4.7. New scientific results

In this section the unique scientific results investigated in my study are shown as following:

1. Air passes number of solar air collector

Based on experimental results, I enhanced the instantaneous thermal efficiency of solar air collector by increasing the number of air passes from one to two passes. For justification of

enhancement I developed a linear mathematical model can be applied for single and double passes types of solar collectors as:

$$\eta = a \frac{T_{av,s} - T_a}{I} + b.$$

I have identified the parameters of the model, *a* and *b*, for the ranges of experimental cases for single and double-pass solar collectors groups as following:

$a = -3308.3$ *and* $b = 168.8$ for single-pass solar collector group,

$a = -1881.8$ *and* $b = 63.09$ for double-pass solar collector group.

During the approximation the correlation coefficients were 0.42 and 0.335 along with the standard deviations of 7.76% and 3.62% for single and double-pass solar collectors, respectively. The models represent the closest expression of the relationship between temperature difference, solar radiation intensity and thermal instantaneous efficiency.

Consequently, I proved the improvement of the amount of evaporated moisture by using double-pass solar collector from dried product items (apple slices), and also that the temperature of air and relative humidity stratification curves of drying chamber trays are much influenced by useful heat and absorbing temperature curves.

2. Direction and shape of extended surfaces

I improved the experimental thermal efficiency of solar collector by using different shapes and directions of attached fins. Accordingly, I justified that the thermal efficiency of these types of solar collectors is related to the angle of attached fins introducing the following second order polynomial model:

$$\eta = a\,\psi^2 + b\,\psi + c.$$

I have identified the *a*, *b* and *c* parameters of rectangular finned double-pass solar air collectors groups as a=-0.0006, b=-0.0536 and c=55.975, respectively. During the approximation the correlation coefficient was 0.99 along with the standard deviation of 3.9%.

Based on the experimental and modelling results, I proved that the horizontal direction of rectangular extended surfaces (fins) attachment is the most efficient direction to get the maximum percentage of useful gained heat. I have pointed out that the vertical rectangular fins did not increased the thermal efficiency of solar collector significantly.

I have justified that the lost water content from dried product items by the horizontally finned solar collector was higher than the case of using flat, vertically finned or 45^o inclined finned plate solar air collector, as well the single-pass solar collector.

In other hand, I proved that a solar air collector with aluminium helical fins attachment has a significant thermal improvement in its instantaneous thermal efficiency and drying process time.

3. Solar air collector overall daily performance

I introduced the daily efficiency to evaluate the thermal performance of solar air collectors. Based on integrated daily experimental results I justified the overall enhancement of the solar collector's thermal behaviour by 7.3% caused by applying air passes duplication. Additionally, I have determined also the enhancements caused by changing the directions of extended surfaces (fins)

which attached to the absorber surface, as follows: 11% for horizontal, 7% for 45 degree and 1% for vertical fins

I proved that the helically finned plate double air pass solar collector achieved the highest thermal daily efficiency (63.3%) compared to the other tested solar air collectors. The enhancement of thermal efficiency compared with flat plate solar collector (reference collector) was about 18%.

4. Forced and natural air mass flow rate

In case forced air movement, I proved that the thermal daily efficiency of solar air collector varies indirectly with variation of air mass flow rate of inline blower. The thermal performance of solar air collector investigated under four values of air mass flow rate, then I justified that the highest value of thermal efficiency was at highest air mass flow rate, while the lowest was at the lowest air flow rate.

In case of natural air movement, I justified the increase of air speed with using circular shape of solar chimney. For that purpose, I have developed a second order polynomial model in order to determine the relation between the speed of air stream in circular chimneys versus solar radiation intensity in the operational range of 600 W/m^2 and 1100 W/m^2:

$$V_{ch} = 10^{-6}\, I^2 - 0.002\, I + 1.3806.$$

During the approximation the correlation coefficient was 0.96 along with the standard deviation of 0.075 m/s.

Additionally, I developed a linear model to estimate the speed of air in circular of chimneys in term of average temperature of absorbing surface for absorber temperature range between 70 and 83 ^{o}C as following:

$$V_{ch} = 0.016\, T_{s,av} - 0.4709.$$

During the approximation the correlation coefficient was 0.57 along with the standard deviation of 0.082 m/s. I proved that the increasing of absorbing surface temperature leads to rise the temperature of air which resulted increasing of bouncy force. The little slope which done in the top of drying chamber leads to smooth movement of air flow.

5. Final weight of dried product

I evaluated and justified the enhancement of drying process in term of final weight by increasing number of air passes and using different shapes and directions of attached fins. I proved that using attached helical fins to absorber surface of double-pass solar air collector provides the lowest final weight of dried product items. After 5 hour drying period the product lost about 53% of its initial weight.

The changing of fins direction affected on the final weight of the dried product. I elaborated that in case of using the double-pass solar air collector the weight loss of material to be dried enhanced from 28% to 38% compared with single-pass solar air collector after 5 hour drying period. Attaching horizontal fins to the double-pass solar collector enhanced weight loss from 38% to 42% compared with flat plate double-pass solar collector for the same drying period.

5. CONCLUSIONS AND SUGGESTIONS

In conclusion, an experimental study has been carried out to investigate the performance of various types of solar air collectors for drying processes objectives. In this study, the effect of air pass number have been studied by a ccomparison between single-pass solar air collector and double-pass solar air collector. The results showed the single and double-pass solar air collector inlet, outlet and second pass temperatures are directly proportioning with the solar radiation intensity and ambient temperature. The high absorbing surface temperates lead to increasing of solar collector heat losses and useful heat gained at the same time. Additionally, the useful heat gained by using double-pass solar air collector much higher than the gained useful heat by using single-pass solar air collector which leads to higher thermal efficiency and drying rates.

The direction and shape of extended surfaces (fins) are played a significant factor to improve the thermal performance of solar air collectors and drying process. The horizontal direction of rectangular extended surfaces (fins) attachment is the most efficient direction to get the maximum percentage of useful gained. The vertical rectangular fins did not increase the thermal efficiency of solar collector significantly. The vertical direction of extended surfaces does not produce high air turbulence as noticed with horizontal fins or 45^{o} inclined fins which leads to highest air temperatures. The lost water content from dried product items by the horizontally finned solar collector was more than the evaporated water by using flat, vertically finned or 45^{o} inclined finned plate solar air collector, as well the single-pass solar collector. In case of attaching the aluminium helical fins, it has a significant thermal improvement of solar air collector by about 18% of daily thermal efficiency and gained useful heat. The drying process enhanced by using the helically-finned solar air collector. The evaporated water from the dried product (apple slices) was much higher than the collected experimental measurements by using the other types of tested solar air collectors. The helically-finned solar collector showed a significant enhancement of drying process due to increasing the evaporated water from the dried product with initial weight 2000 g.

The air temperature stratification curves of drying chamber five trays are much affected by useful heat and absorbing temperature curves. Also, the relative humidity stratification of air in the drying chamber trays are high at the beginning of experiments due to the high moisture content of dried product items, then decrease exponentially with the time of experiments and ambient relative humidity.

The effect of air mass flow rate had been invisigted. In case of forced air circulation, the thermal efficiency of solar collector proportions indirectly with the mass flow rate of air. The efficiency of double-pass solar collector increased signifigntly by increasing the flow rate of air. In case of natural air circulation, the speed of air is much affected by solar radiation and absorbing surface temperature by circular chimney integration.

For the future works, many ideas can be suggested to improve this work. The tested solar air collectors and dryer can be simulated by using one of the standard simulation software like Matlab or ANSYS. The changing of the shape of absorbing surface from rectangular to other shapes can improve the thermal efficiency of solar air collector such as twisted, perios fins, holed, circular fins, etc. The investigation of the performance of the tested solar collectors for other products drying can be suggested for the future projects. Additionally, the investigation of the thermal efficiency of the double-pass solar collector by the holed absorbing surface. The studied drying system can be developed to be controlled temperature and humidity.

6. SUMMARY

PERFORMANCE ENHANCEMENT OF SOLAR AIR COLLECTORS APPLIED FOR DRYING PROCESSES

In this work, a comprehensive experimental investigation carried out to evaluate the thermal enhancement of solar air collector performance for drying purposes. The tested system consists of many essential parts: solar air collector, drying chamber, blower, and chimney. To achieve the aims of this research a six solar collectors are tested experimentally in the laboratory of Szent István University in Hungary. The first collector is a flat plate single-pass solar air collector while the second is a flat plate double-pass solar air collector. The third, fourth and fifth collector are horizontal, 45 degrees and vertically finned plate double-pass solar air collector respectively. The sixth collector is helically-finned plate double-pass solar air collector. The external dimensions of every collector are 50× 120×15 cm width, length, and depth respectively. The drying chamber has been made from 5 cm thick of polystyrene with 50×50×100 cm length, width, and height respectively. The chamber carried five trays where the dried product (apple slices) items must be put. To show the effect of forced and natural air mass flow rate, an inline air blower and 1.5 m circular section chimney are integrated with the solar system. The inline blower connected to PV module by a power supply regulator. The system is tested on many days and under different conditions of weather and air mass flow rates. The collected data such as humidity, temperature, radiation and flow speed are measured by using a calibrated instruments.

The results showed good agreements with previous studies. The results obtained that the useful heat gained by using double-pass solar air collector much higher than the gained useful heat by using single-pass solar air collector. The double-action of air pass number increased the daily thermal efficiency of solar air collector from 38.25% to 45.56%. The experimental results proved that the horizontal direction of attached fins is more efficient than the vertical and 45-degree direction. The experiments showed that the daily thermal efficiencies of flat, vertically finned, horizontally finned, 45 degrees finned, and helically-finned plate double-pass solar air collector are 45.56%, 46.53%, 56.01%, 52.84% and 63.3% respectively. The thermal efficiency of solar collector proportions indirectly with the mass flow rate of air. The efficiency of double-pass solar collector increased from 45.5% to 59% by increasing the flow rate from 0.0175 kg/s to 0.0251 kg/s. The speed of air is much affected by solar radiation and absorbing surface temperature by circular chimney integration.

The air temperature stratification curves of drying chamber five trays are much influenced by useful heat and absorbing temperature curves. Air relative humidity stratification of drying chamber trays are high at the beginning of experiments due to the high moisture content of dried product items, then decrease exponentially with the time of experiments and ambient relative humidity. The shape and size of dried apple slices are much changed after drying process. The color of slices became darker than the fresh slices due to the missed moisture content of product items.

The helically-finned solar collector showed a significant enhancement of drying process due to increasing the evaporated water from the dried product with original weight 2000 g. The final total weight of product items by using helically-finned collector was much less that final rcorded weights of propuct by using single-pass, flat plate double-pass, vertically finned, 45 degrees finned and horizontally finned plate solar air collector respectively.

7. ÖSSZEFOGLALÁS (SUMMARY IN HUNGARIAN)

SZÁRÍTÁSI CÉLÚ LEVEGŐS NAPKOLLEKTOROK TELJESÍTMÉNYÉNEK NÖVELÉSE

A dolgozatban a szárítási célú levegős napkollektorok teljesítményének növelése érdekében egy átfogó kísérleti vizsgálatot végeztem. A vizsgált rendszer az alábbi részekből állt: levegős napkollektor, szárító kamra, ventilátor és kémény. A vizsgálatokhoz 6 különböző napkollektort vizsgáltam a Szent István Egyetem laboratóriumában. Ez első egy egyjáratú síkkollektor, a második egy kétjáratú síkkollektor. A harmadik, negyedik és ötödik kollektor rendre vízszintes, 45 fokban döntött és függőleges bordákkal ellátott, a hatodik pedig egy spirálisan bordázott kétjáratú napkollektorok voltak. A kollektorok befoglaló méretei egységesen 50×120×15 cm volt. A szárító kamra 5 cm vastagságú polisztirolból készült és 50×50×100 cm-es befoglaló mérettel rendelkezik. A kamrában 5 tálca található a szárítandó anyagok (almaszeletek) tárolására. A kényszerített és a természetes légáramlás vizsgálatához egy ventilátor és egy 1.5 m átmérőjű kémény lett beépítve a rendszerbe. A ventilátor egy feszültségszabályozó tápegység segítségével napelemhez van kötve. A rendszer különböző időjárási és légáramlási viszonyok között lett tesztelve több napos időintervallumokban. A vizsgált jellemzőket (levegő nedvességtartalom, hőmérséklet, napsugárzás intenzitás és áramlási sebesség) kalibrált mérőműszerek segítségével mértük.

Az eredmények összevetésre kerültek a korábbi vizsgálatokkal is. A kapott eredmények alapján megállapítható volt, hogy a kétjáratú napkollektorokból kinyerhető hasznos hő jelentősen nagyobb, mint az egyjáratú napkollektorok esetében. A kettős légáram hatására a kollektor napi termikus hatásfoka 38.25%-ról 45.25%-ra növekedett. A kisérletek igazolták, hogy a vízszintes bordázottság hatékonyabb, mint a 45 fokban döntött vagy a függőleges. Az eredmények alapján a napi átlagos termikus hatásfok az kétjáratú síkkollektor, a függőlegesen bordázott, a vízszintesen bordázott, a 45 fokban bordázott, és a spirálisan bordázott kétjáratú napkollektorok esetén 45.56%, 46.53%, 56.01%, 52.84% és 63.3%. A napkollektor termikus hatásfoka arányos a levegő tömegáramával is. A kétjáratú napkollektor hatásfoka 45.5%-ról 59%-ra növekedett a tömegáram 0.0175 kg/s-ról 0.0251 kg/s-ra történő változtatásával. A levegő sebességét nagyban befolyásolja a napsugárzás és a beépített kémény felületi hőelnyelése is.

Az öt szárító tálca léghőmérséklet rétegződési görbéit nagyban befolyásolták a hasznos és elnyelt hőmennyiségek értékei. A tálcákhoz tartozó relatív nedvességtartalom rétegződése magas volt a kisérletek kezdetén az anyagok magas nedvességtartalma miatt, ami exponenciálisan csökkent az idő és a környezet levegője relatív nedvességének változásával. A vizsgált szárított almaszeletek mérete és formája megváltozott a szárítási folyamat során. A szeletek színe sötétebb lett, mint amilyen friss állapotukban volt, az elvitt nedvesség miatt.

A spirálisan bordázott napkollektor esetén mutatkozott a legjelentősebb hatékonyság javulás a szárítási folyamatban, tekintettel a szárítandó anyagból elpárolgó víz mennyiségének növekedése miatt. Következésképpen a szárított anyag végső tömege ebben az esetben volt a legalacsonyabb összevetve az egyjáratú síkkollektor valamint a kétjáratú síkkollektor és annak függőlegesen, vízszintesen és 45 fokban bordázott esetekre.

8. APPENDICES

A1. Bibliography

1. Abdullah, A.S., El-Samadony, Y.A.F, Omara, Z.M. (2017): Performance evaluation of plastic solar air heater with different cross sectional configuration, Applied Thermal Engineering, 121, pp. 218-223.
2. Aboul-Enein, S., El-Sebaii, A.A., Ramadan, M.R.I., El-Gohary, H.G. (2000): Parametric study of a solar air heater with and without thermal storage for solar drying applications, Renewable Energy Journal, 21, pp. 505–522.
3. Adelaja, A.O., Ogunmola, B.Y., Akolade P.O. (2009): Development of a photovoltaic powered forced convection solar dryer, Advanced Materials Research Journal, 2009, 62-64, pp. 543-548.
4. Afriyie, J.K., Nazha, M.A.A., Rajakaruna, H., Forson, F.K. (2009): Experimental investigations of a chimney-dependent solar crop dryer, Renewable Energy Journal, 34, pp. 217–222.
5. Afriyie, J.K., Plange, A.B. (2012): Performance investigation of a chimney-dependent solar crop dryer for different inlet areas with a fixed outlet area, International scholarly research network, Renewable Energy Journal.
6. Aghbashlo, M., Müller, J., Mobli, H., Madadlou, A., Rafiee, S. (2015): Modeling and simulation of deep-bed solar greenhouse drying of chamomile flowers, Drying Technology: An International Journal, 33(6), pp. 684-695.
7. Ahn, J.G., Kim, J.H., Kim, J.T. (2015): A study on experimental performance of air-type PV/T collector with HRV, Energy Procedia Journal, 6th International Building Physics Conference, 78, pp. 3007 – 3012.
8. Aissa, W., El-sallak, M., Elhakem, A. (2014): Performance of solar dryer chamber used for convective drying of spong-ecotton, Thermal Science Journal, 18(2), pp. S451-S462.
9. Ajiwiguna, T.A., Hamonangan, T., Kirom, M.R. (2016): Experimental study of thermal efficiency on plate-fin solar thermal collector, ARPN Journal of Engineering and Applied Sciences, 11(2), pp. 809-811.
10. Akpinar, E.K., Koçyiğit, F. (2010): Energy and exergy analysis of a new flat-plate solar air heater having different obstacles on absorber plates, Applied Energy Journal, 87, pp. 3438–3450.
11. Aldabbagha, L.B.Y., Egelioglu, F., Al-Khawajah, M.F. (2010): the effect of partitioning single pass mesh wire packed bed solar air heater, 7th international conference on heat transfer, fluid mechanics and thermodynamics, 19-21 July, Antalya, Turkey.
12. Ali, S. Y., Desmons, J. Y (2005): Simulation of a new concept of an indirect solar dryer equipped with offset rectangular plate fin absorber plate, International Journal of Energy Research, 29, pp. 317–334.
13. Al-Juamily, K.E.J., Khalifa, A.J.N., Yassen, T.A. (2007): Testing of performance of fruit and vegetable solar drying system in Iraq, Desalination Journal, 209, pp. 163–170.
14. Al-Neama, M.A., Farkas, I. (2016): Modelling of a modular indirect natural convection solar dryer, 11th International Conference on Solar Energy for Buildings and Industry, EuroSun2016, Palma (Mallorca), Spain, October 11-14, pp. 660-669.
15. American society of heating refrigeration & air conditioning engineers (1999); ASHRAE HVAC applications Handbook, Chapter 33.

16. Anyanwu, C.N., Oparaku, O.U., Onyegegbu, S.O., Egwuatu, U., Edem, N.I., Egbuka, K., Nwosu, P.N., Sharma, V. K. (2012): Experimental investigation of a photovoltaic-powered solar cassava dryer, Drying Technology Journal, 30, pp. 398-403.
17. Bayrak, F., Oztop, H. F. (2015): Experimental analysis of thermal performance of solar air collectors with aluminum foam obstacles, Journal of Thermal Science and Technology, 35(1), pp. 11-20.
18. Bhushan, C., Singh, S.N. (2014): Experimental investigation of double-pass solar air heater, ELK Asia Pacific Journals, Special Issue.
19. Bennamoun, L. (2012): An Overview on Application of Exergy and Energy for Determination of Solar Drying Efficiency, International Journal of Energy Engineering, 2012, 2(5), pp. 184-194.
20. Bennamoun, L. (2013): Integration of photovoltaic cells in solar drying systems, Drying Technology Journal, 31, pp. 1284-1296.
21. Bimbenet, J. J, Bonazzi, C. and Dumoulin, E. (2002): Drying of foodstuffs, proceeding of the 13th International Drying Symposium, A, pp. 64-80.
22. Bolaji, BO. (2005): Development and performance evaluation of box-type absorber solar air collector for crop drying, Journal of Food Technology, 3(4), pp. 515–600.
23. Budijono, A.P., Habib, B.N., Setiyawan, N. (2016): The effect of angle slope variation and dark light chimney for humidity and temperature full transparent walled dryer chamber, AIP Conference Proceedings, 1778, pp.1-11.
24. Can, A. (2000): Drying kinetics of pumpkinseeds, International Journal of Energy Research, 24, pp. 965-975.
25. Ceylan, I., Kaya, M., Gürel, A.E., Ergun, A. (2013): Energy analysis of a new design of a photovoltaic cell-assisted solar dryer, Drying Technology Journal, 2013, 31, pp. 1077-1082.
26. Chabane, F., Moummia, N., Benramache, S. (2013): Experimental analysis on thermal performance of a solar air collector with longitudinal fins in a region of Biskra, Algeria, Journal of Power Technologies, 93 (1), pp. 52–58.
27. Chabane, F., Moummi, N., Benramache, S., Bensahal, D., Belahssen, O. (2013): Collector efficiency by single pass of solar air heaters with and without using fins, Engineering Journal, 17(3), pp. 43-55.
28. Collins, M.R., Abulkhair, H. (2014): An evaluation of heat transfer and effectiveness for unglazed transpired solar air heaters, Solar Energy Journal, 99, pp. 231-245.
29. Chauhan, P. S., Kumar, A., Tekasakul, P. (2015): Applications of software in solar drying systems: A review, Renewable and Sustainable Energy Reviews, 51, pp. 1326–1337.
30. Chen, Z.D, Bandopadhayay, P., Halldorsson, J., Byrjalsen, C., Heiselberg, P., Li, Y. (2003): An experimental investigation of a solar chimney model with uniform wall heat flux, Building and Environment Journal 38, pp. 893-906.
31. Dissa, A.O., Bathiebo, J., Kam, S., Savadogo, P.W., Desmorieux, H., Koulidiati, J. (2009): Modeling and experimental validation of thin layer indirect solar drying of mango slices, Renewable Energy Journal, 34, pp. 1000-1008.
32. Duffie, J. and Beckman, W. (2013), Solar Engineering of Thermal Processes, Fourth edition, John Wiley & Sons, New Jersey, USA.
33. Ekechukwu, O.V., Norton, B. (1997): Design and measured performance of a solar chimney for natural-circulation solar-energy dryers, Renewable Energy Journal, 10(1), pp. 81-90.

34. Ekechukwu, O., Norton, B. (1999): Review of solar-energy drying Systems II: an overview solar drying technology, Energy Conversion & Management Journal, 40, pp. 615-655.
35. Ekechukwu, O.V., Norton B. (1999): Review of solar-energy drying systems III: low temperature air-heating solar collectors for crop drying applications, Energy Conversion & Management Journal, 40, pp. 657–667.
36. Elbreki , A.M., Alghoul, M.A., Al-Shamani, A.N., Ammar, A.A., Yegani, B., Aboghrara A. M., Rusaln, M.H., Sopian, K. (2016): The role of climatic-design-operational parameters on combined PV/T collector performance: A critical review, Renewable and Sustainable Energy Reviews Journal, 57, pp. 602-647.
37. El-Sebaii, A.A., Aboul-Enein, S., Ramadan, M.R.I., Shalaby, S.M., Moharram, B.M. (2011): Thermal performance investigation of double pass-finned plate solar air heater, Applied Energy, 88, pp. 1727-1739.
38. Ertekin, C., Yaldiz, O. (2004): Drying of eggplant and selection of a suitable thin layer drying model, Journal of Food Engineering, 63, pp. 349-359.
39. Farkas, I., Seres, I., Meszaros, C. (1999): Analytical and experimental study of a modular solar dryer, Renewable Energy Journal, 16, pp. 773-778.
40. Ferreira, A.G., Maia, C.B., Cortez, M.F.B., Valle R.M. (2008): Technical feasibility assessment of a solar chimney for food drying, Solar Energy Journal, 82, pp. 198-205.
41. Fudholi (2011): Thermal efficiency of double pass solar collector with longitudinal fins absorbers, American Journal of Applied Sciences, 8(3), pp. 254–260.
42. Ghaffari, A., Mehdipour, R. (2015): Modeling and improving the performance of cabinet solar dryer using computational fluid dynamics, International Journal of Food Engineering, 11(2), pp. 157,172.
43. Ghazanfari, A., Tabil, L., Sokhansanj, S. (2003): Evaluating a solar dryer for shell drying of split pistachio nuts, Drying Technology Journal, 21(7), pp. 1357-1368.
44. Google map, online at: www.google.hu/maps, accessed on 06 May 2018.
45. Hall, C.W. (1980): Drying and storage of agricultural crops, Avi Publishing Co., The University of Wisconsin, Madison, 1980.
46. Hematian A., Bakhtiari, A.A. (2015): efficiency analysis of an air solar flat plate collector in different convection modes, International Journal of Green Energy, 12(9), pp. 881-887.
47. Hii, C.L., Jangnam, S.V., Ong, S.P., Mujumdar, A.S. (2012): Solar Drying: Fundamental, Applications and Innovations, Authors of individual chapter.
48. Ibrahim, Z., Ibarahim, Z., Yatim, B., Ruslan M.H. (2013): Thermal efficiency of single-pass solar air collector, AIP Conference Proceedings, 1571, pp. 90-94.
49. Jain, D. (2007): Modeling the performance of the reversed absorber with packed bed thermal storage natural convection solar crop dryer, Journal of Food Engineering, 78, pp. 637-647.
50. Kareem, M.W., Habib, K., Sulaiman, S.A. (2013): Comparative study of single pass collector and double pass solar collector filled with porous media, Asian Journal of Scientific Research, 6(3), pp. 445-455.
51. Karim, M. A., Perez, E., Amin, Z.M. (2013): Mathematical Modelling of Counter Flow v-Grove Solar Air Collector, Renewable Energy, 67, pp. 192–201.
52. Kumar, A., Tiwari, G.N. (2006): Thermal modeling of a natural convection greenhouse drying system for jaggery: An experimental validation, Solar Energy Journal, 80, pp. 1135-1144.
53. Kumar, M., Sansaniwal, S.K. and Khatak, P. (2016): Progress in solar dryers for drying various commodities, Renewable and Sustainable Energy Reviews Journal, 55, pp 346-360.

54. Koca, A., Oztop, H.F., Koyun, T., Varol, Y. (2008): Energy and exergy analysis of a latent heat storage system with phase change material for a solar collector, Renewable Energy Journal, 33, pp. 567–574.
55. Kurtbas, I., Turgut, E. (2006): Experimental investigation of solar air heater with free and fixed fins: efficiency and exergy loss, International Journal Of Science & Technology, 1(1), pp. 75-82.
56. Leon, M.A., Kumar, S., Bhattacharya, S.C. (2002): A comprehensive procedure for performance evaluation of solar food dryers, Renewable and Sustainable Energy Reviews, 6, 367-393.
57. Madhlopa, A., Jones, S.A., Saka, J.D.K. (2002): A solar air heater with composite-absorber systems for food dehydration, Renewable Energy Journal, 27, pp. 27-37.
58. Madhukeshwara, N., Prakash, E.S. (2012): investigated the performance characteristics of solar flat plate collector with different selective surface coating, International Journal of Energy and Environment, 3(1), pp. 99-108.
59. Mahapatra, A. K., Imre, L., Barcza, J., Bitai, A., Farkas, I. (1994): Simulation of a directly irradiated solar dryer with integrated collector, International Journal of Ambient Energy, 15(4), pp. 195-204.
60. Mahboub, C., Moummi N., Brima, A.. Moummi A. (2016): Experimental study of new solar air heater design, International Journal of Green Energy, 13(5), pp. 521-529.
61. Mahendra, S., Narendra, K., Kumar, A., Pradeep, K. and Malik, M.A.S. (1987): Solar crop drying, CRC press, Florida, USA, 1987.
62. Marathe, A. P., Joshi S. M., Thokal, G. N. (2013): Mathematical Modelling of Solar Air Heater, Research and Applications (IJERA), 3(3), pp. 1000-1010.
63. Messenger, R.A., Ventre, J. (2004): Photovoltaic Systems Engineering, CRC Press Technology and Industrial, Second edition, US.
64. Mohanraj, M., Chandrasekar, P. (2009): Performance of a solar drier with and without heat storage material for copra drying, International Journal Global Energy Issues, 31(2), pp. 112-121.
65. Ong, K. S. (1995): Thermal Performance of Solar Air Heaters: Mathematical Model and Solution Procedure, Solar Energy, 55(2), pp. 93–109.
66. Othman, M.Y., Yatim, B., Sopian, K., Zaharim A., Abu Bakar, M.N. (2008): Studies of a photovoltaic-thermal solar drying system for rural applications, 2nd WSEAS/IASME International conference on renewable energy sources (RES'08), Corfu, Greece, 26-28 October, pp. 132-136.
67. Öztürk, H.H., Demirel, Y. (2004): Exergy-based performance analysis of packed-bed solar air heaters, International Journal of Energy Research, 28, pp. 423-432.
68. Perez, R., Marc, P. (2009): A fundamental look at energy reserves for the planet, Report, The IEA/SHC solar update, January 2009.
69. Prasartkaewa, B., Kumar, S. (2014): Design of a renewable energy based air-conditioning system, Energy and Building, 68, pp. 156-164.
70. Rai, S., Chand, P., Sharma, S.P. (2016): Investigation of an Offset Finned Solar Air Heater Based on Energy and Exergy Performance, Iranica Journal of Energy and Environment, 7 (3), pp. 212-220.

71. Rai, S., Chand, P., Sharma, S.P. (2017): An analytical investigations on thermal and thermohydraulic performance of offset finned absorber solar air heater, Solar energy, 153, pp. 25-40.
72. Romero, V.M., Cerezo, E., Garcia, M.I., Sanchez, M.H. (2014): Simulation and validation of vanilla drying process in an indirect solar dryer prototype using CFD Fluent program, Energy Procedia Journal, 2013 ISES Solar World Congress, 57, pp. 1651-1658.
73. Russon, J. K., Dunn, M. L.,Steele, F. M. (2009): Optimization of a convective air flow solar food dryer, International Journal of Food Engineering, pp. 1-11.
74. Scheid, F. (1968): Numerical analysis, First edition, McGraw-Hill Book Company, USA.
75. Sencan, A., Özdemir, G. (2007): Comparison of thermal performances predicted and experimental of solar air collector, Journal of Applied Sciences, 7(23), pp. 3721-3728.
76. Seveda, M. S, Jhajharia, D. (2012): Design and performance evaluation of solar dryer for drying of large cardamom (Amomum subulatum), Journal of Renewable and Sustainable Energy, 4, pp. 1-11.
77. Sharma, A., Chen, C.R., Lan, N.V. (2009): Solar-energy drying systems: A review, Renewable and Sustainable Energy Reviews Journal, 13, pp. 1185-1210.
78. Sharma, S. P., Saha, S.N. (2017): Thermohydraulic performance of double flow solar air heater with corrugated absorber, International Journal of Energy and Power Engineering, 11(7), pp. 855-861.
79. Shojaee, S.M.N., Moradian, M.A., Mashhoodi, M. (2015): Numerical investigation of wind flow around a cylindrical trough solar collector, Journal of Power and Energy Engineering, 3, pp. 1-10.
80. Sigge, G.O., Hansmann, C.F., Joubert, E. (2007): Effect of temperature and relative humidity on the drying rates and drying times of green bell peppers (capsicum annuum l), Drying Technology Journal, 16(8), pp. 1703-1714.
81. Simate, I.N. (2003): Optimization of mixed-mode and indirect-mode natural convection solar dryers, Renewable Energy Journal, 28, pp. 435-453.
82. Sundari, AR.U., Neelamegam, P., Subramanian, C.V. (2013): An experimental study and analysis on solar drying of bitter ground using an evacuated tube air collector in Thanjavur, Tamil Nadu, India, International conference on solar energy photovoltaic.
83. Tan, A.Y.K., Wong, N.H. (2013): Parameterization studies of solar chimneys in the tropics, Energies Journal, 6, pp. 145-163.
84. Tashtosh, G. M., Jaradat, M., Zuraiakt, S., Aljarah, M. (2014): A mathematical model of indirect solar drying of dairy products, 2(1), pp. 1-13.
85. Tiwari, S., Tiwari, G.N., Al-Helal, I.M. (2016): Performance analysis of photovoltaic–thermal (PVT) mixed mode greenhouse solar dryer, Solar Energy Journal, 133, pp. 421-428.
86. Toshniwal, U., Karale, S.R (2013): A review paper on Solar Dryer, International Journal of Engineering Research and Applications (IJERA), 3(2), pp. 896-902.
87. Umayorupagam, P.A., Edwin, M. (2017): Experimental investigations on thermal performance of solar air heater with different absorber plates, International Journal of Heat And Technology, 35(2), pp. 393-397.
88. Umar, S., Kangiwa. U. M., Garba, M. M., Yahya H. N. (2014): Effects of atmospheric variables on the performances of parabolic trough concentrating collector, American Journal of Energy Engineering, 2(1), pp. 23-26.

89. Umogbai, V.I., Iorter, H.A. (2013): Design, construction and performance evaluation of a passive solar dryer for maize cobs, African Journal of Food Science and Technology, 4(5), pp. 110-115.
90. Velmurugan, P., Kalaivanan, R. (2013): Effect of diverse stream patterns on the performance of solar air heater, International Journal of Mechanical Engineering and Robotics Research, 2(1), pp. 65-70.
91. Vlachos, N.A., Karapantsios, T. D., Balouktsis, A.I., Chassapis, D. (2002): Design and testing of a new solar tray dryer, Drying Technology Journal, 20(6), pp. 1243-1271.
92. Vyas, S., Punjabi, S. (2014): Thermal performance testing of a flat plate solar air heater using optical measurement technique, International Journal of Recent advances in Mechanical Engineering (IJMECH), 3(4), pp. 69-84.
93. Waziri, N. H., Usman, A. M., Enaburekhan, J. S., Babakano, A. (2014): Determination of optimum tilt angle and orientation of a flat plate solar collector for different periods in kano, Scientific Research Journal (SCIRJ), 2(2), pp. 34-40.
94. Wikipedia: Solar dryer, online at: https://en.wikipedia.org/wiki/Solar dryer, accessed on 07 September, 2017.
95. Yang, M., Yang, X., Li, X., Wang, Z., Wang, P. (2014): Design and optimization of a solar air heater with offset strip fin absorber plate, Applied Energy Journal,113, pp. 1349-1362.
96. Yang, M., Wang, P., Yang, X., Shan, M. (2012): Experimental analysis on thermal performance of a solar air collector with a single pass, Building and Environment Journal, 56, pp. 361-369
97. Yousef, A.A.B.,Adam, N.M. (2012): Performance and cost analysis of double duct solar air heater, International Journal of Scientific & Technology Research, 1(6), pp. 108-116.
98. Zahed, A.H., Elsayed, M.M. (1989): Mathematical modeling of a solar kiln, Solar and Wind Technology Journal, 6(1), pp. 19-27.
99. Zambrano, W., Alvarado, S. (1984): Design, construction and testing of a chimney that reduces dangerous temperatures in a radiative convective solar dryer, Solar Energy Journal, 32(5), pp. 581-584.

A2. Publications related to the thesis

Refereed papers in foreign languages:

1. **Al-Neama, M.A.,** Farkas, I. (2016): Influencing of solar drying performance by chimney effect, Hungarian Agricultural Engineering, Gödöllő, Hungary, Vol. 30, pp. 11-16. HU ISSN 0864-7410
2. **Al-Neama, M.A.,** Farkas, I. (2017): Investigation of finned solar air collector performance for drying purposes, R&D in Mechanical Engineering Letters, Gödöllő, Hungary, 2017, Vol. 16, pp. 64-72. HU ISSN 2060-3789
3. **Al-Neama, M.A.,** Farkas, I. (2018): Utilization of solar air collectors for product's drying processes, Journal of Scientific and Engineering Research, Vol. 5., No 2., 2018, pp. 40-56, ISSN 2394-2630
4. **Al-Neama, M.A.**, Farkas, I. (2018): Thermal efficiency of vertical and horizontal-finned solar collector integrated with forced air circulation dryer for apple as a sample, Drying Technology Journal, online version, ID: 1488260, DOI:10.1080/07373937.2018.1488260 (IF=2.219*)
5. **Al-Neama, M.A.,** Farkas, I. (2018): Evaluation of temperature and relative humidity stratifications in a solar drying chamber, Journal of Scientific and Engineering Research, ID: JSAER2018574. ISSN 2394-2630. (Accepted)
6. **Al-Neama, M.A.,** Farkas, I. (2018): Investigation of finned and un-finned solar air collector thermal performance for drying processes, Electrotehnica, Electronica, Automatica Journal. (Submitted)
7. **Al-Neama, M.A.,** Farkas, I. (2018): Manufacturing and thermal efficiency estimation of finned and un-finned double-pass solar air heaters, Technical Gazette Journal (IF=0.686*). (Submitted)

International conference proceedings:

8. **Al-Neama, M.A.,** Farkas, I. (2015): Study of solar energy drying system performance, Proceedings of the 5th European Drying Conference (EuroDrying'2015), Budapest, Hungary, October 21-23, 2015, pp. 22-27. ISBN 978-963-9970-62-5
9. **Al-Neama, M.A.**, Farkas, I.: Modeling of solar drying system with natural convection air flow, Proceedings of IDS 2016, 20th Internatinal Drying Symposium, Gifu, Japan, August 7-10, 2016, Paper No D-4-4, pp. 1-5.
10. **Al-Neama, M.A.,** Farkas, I. (2016): Modelling of a modular indirect natural convection solar dryer, Proceedings of EuroSun 2016 Conference, Palma, Spain, October 11-14, 2016, pp. 660-669, ISBN 978-3-9814659-6-9
11. **Al-Neama, M.A.,** Farkas, I. (2016): Energy analysis of active solar drying system connected with photovoltaic modules, Energy and the Environment, Croatian Solar Energy Association, Opatija, Croatia, October 26-28, 2016. pp. 187-196. ISBN 978-953-6886-23-4
12. **Al-Neama, M.A.,** Farkas, I. (2018): Flat plate solar air heater with helical integrated fins for drying processes, Proceedings of IDS 2018, 21st Internatinal Drying Symposium, Valencia, Spain, September 11-14, 2018, pp. 489-496. ISBN 978-84-9048-688-7

Book chapter in foreign languages:

13. **Al-Neama, M.A.**, Farkas, I. (2017): Design aspects of flat plate solar collectors used for drying applications, Towards sustainable agricultural and biosystems engineering, /ed. by A. Nyéki, A.J., Kovács, G. Milics/, Universitas-Győr Nonprofit Ltd, 2017, pp. 391-407, ISBN 978-615-5776-03-8

International conference abstracts:

14. **Al-Neama, M.A.**, Farkas, I. (2015): Performance enhancement of solar air collectors, Book of Abstracts, 14th International Workshop for Young Scientists (BioPhys Spring 2015), Gödöllő, Hungary, May 27-29, 2015, pp. 40-41. ISBN 978-83-89969-37-8
15. **Al-Neama, M.A.,** Farkas, I. (2015): Chimney effect on a solar drying system, Abstracts, IV. Synergy International Conference, Gödöllő, Hungary, October 12-15, 2015, p. 34. ISBN 978-963-269-505-1
16. **Al-Neama, M.A.,** Farkas, I. (2015): Performance enhancement methods of solar air heaters, 21th Workshop on Energy and Environment, Gödöllő, Hungary, December 3-4, 2015, p. 11, ISBN 978-963-269-511-2
17. **Al-Neama, M.A.,** Farkas I. (2016): Modelling of solar air heater integrated with dryer chamber, Book of Abstracts, 15th International Workshop for Young Scientists (BioPhys Spring 2016), Prague, Czech Republic, May 5-6, 2016, pp. 52-53. ISBN 978-83-89969-42-2
18. **Al-Neama, M.A.,** Farkas, I. (2016): Energy characteristics of passive indirect solar drying for agricultural products, Book of Abstracts, 11st International Conference on Agrophysics (ICA 2016), Lublin, Poland, September 26-28, 2016. p. 51. ISBN 978-83-89969-43-9
19. **Al-Neama, M.A.,** Farkas, I. (2016): Design characteristics of solar air collectors with different absorbers plates, Book of Abstracts, 22th Workshop on Energy and Environment, Gödöllő, Hungary, December 1-2, 2016, p. 9, ISBN 978-963-269-579-2
20. **Al-Neama, M.A.,** Farkas I. (2017): Thermal analysis of single and double-pass solar air collectors, Book of Abstracts, 16th International Workshop for Young Scientists (BioPhys Spring 2017), Lublin, Poland, June 1-3, 2017, pp. 22-23. ISBN 978-83-89969-47-7
21. **Al-Neama, M.A.,** Farkas, I. (2017): Thermal analysis of single and double pass solar air collectors used for drying, Book of Abstracts, 6th European Drying Conference (EuroDrying'2017), Liége, Belgium, June 19-21, 2017, pp. 216-217.
22. **Al-Neama, M.A.,** Farkas, I. (2017): Daily efficiency estimation of forced convection solar air heater, Book of Abstracts, 23th Workshop on Energy and Environment, Gödöllő, Hungary, November 30-December 1, 2017, p. 16, ISBN 978-963-9483-91-0
23. **Al-Neama, M.A.,** Farkas I. (2018): Designing and evaluation of a drying chamber, Book of Abstracts, 17th International Workshop for Young Scientists (BioPhys Spring 2018), Nitra, Slovakia, May 15-18, 2018, p. 10. ISBN 978-83-89969-57-6

9. ACKNOWLEDGMENTS

This thesis work was supported by the Stipendium Hungaricum Scholarship Program and Mechanical Engineering Doctoral School at the Szent István University, Gödöllő, Hungary, between February 2015 and July 2018.

First of all, I would like to express my sincere gratitude and thanks to my God for the guidance through this work and for all the blessings bestowed upon me.

I am genuinely thankful to my supervisor, Prof. István Farkas, for the guidance, encouragement, and valuable advice he has provided throughout my time as his student. I have been fortunate to have a supervisor who cared so much about my work, and who responded to my questions and queries so promptly.

My most profound gratitude goes to my beloved my father Ali Jasim Al-Neama and my mother Sawsan Shakir, without whom this project would never have been possible, thank you so much for your love and patience all along.

I would like to express my thanks to the staff who helped me in Mechanical Engineering Doctoral school- Szent István University.

Furthermore, I would like to thank all kind, helpful and lovely people who helped me directly and indirectly to complete this work, and I apologize to those for being unable to mention them by name here.

Maytham Ali Al-Neama

Gödöllő, 2018